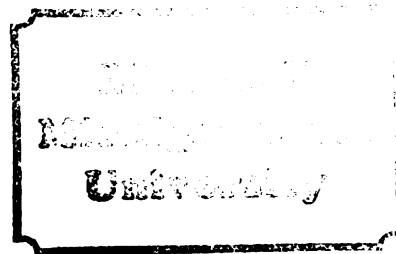


THESIS



This is to certify that the

dissertation entitled

VITAMIN B₆ MODEL COMPOUNDS AND THEIR

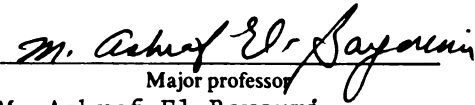
INTERACTIONS WITH METAL IONS

presented by

Kamal Zaki Ismail

has been accepted towards fulfillment
of the requirements for

Ph.D. degree in Chemistry


Major professor
M. Ashraf El-Bayoumi

Date April 23, 1982



RETURNING MATERIALS:
Place in book drop to
remove this checkout from
your record. FINES will
be charged if book is
returned after the date
stamped below.

--	--	--

VITAMIN B₆ MODEL COMPOUNDS AND THEIR
INTERACTIONS WITH METAL IONS

By

Kamal Zaki Ismail

A DISSERTATION

Submitted to
Michigan State University
in partial fulfillment of the requirements
for the degree of

DOCTOR OF PHILOSOPHY

Department of Chemistry

1982

ABSTRACT

VITAMIN B₆ MODEL COMPOUNDS AND THEIR INTERACTIONS WITH METAL IONS

By

Kamal Zaki Ismail

Nearly all reactions concerned with amino acid transformations are catalyzed by pyridoxal phosphate (PLP). Such reactions involve racemization, transamination, decarboxylation, α,β -elimination, β, γ -elimination and dealdolization. Pyridoxal phosphate, PLP, (vitamin B₆) is a substituted pyridine derivative with a hydroxyl group in position 3- and an aldehyde group in position 4-. The biologically active form of pyridoxal phosphate, PLP, is its Schiff base with an ϵ -amino group of a lysine residue in the active site of the enzyme. Salicylaldehyde derivatives have been used as model compounds of PLP since they contain its essential chromophore. We have studied both absorption and emission properties of four model compounds namely: salicylaldehyde, 2-methoxybenzaldehyde, 2-hydroxyacetophenone, and 4,6-dimethyl-2-hydroxyacetophenone and their corresponding Schiff bases with an aliphatic amine, n-butylamine, and an amino acid, DL-valine, in different media and at both room

temperature and 77°K. Intermolecular and intramolecular excited-state proton-transfer have been observed. The steric hindrance in 4,6-dimethyl-2-hydroxyacetophenone model compound and its Schiff base clearly manifested itself in their spectral properties.

The presence of monovalent cation is very essential for activity in some PLP-enzymatic reactions. In tryptophanase both NH_4^+ and K^+ are good activators whereas, Na^+ and Li^+ are not. Different techniques have been used extensively to study monovalent cation interactions with different enzymes. We have studied both absorption and emission spectra of some monovalent cation (e.g., Li^+ , Na^+ , K^+ and Tl^+) salts of salicylaldehyde and three other para-substituted phenols in THF and in other solvents. Stronger cation-anion interaction (tighter ion-pair formation) was observed in salicylaldehyde salts. Even in polar solvents, e.g., ethanol and DMSO an equilibrium between ion pairs and free ions was observed.

Because of their intense and narrow emission, lanthanide ions, Ln(III) , have been extensively used to probe the microenvironment at the active site in proteins. The number of coordinated water molecules in the first shell of Eu(III) are determined by following the fluorescence decay of the metal ion in $\text{H}_2\text{O}/\text{D}_2\text{O}$ mixtures. Energy transfer in Ln(III) bound protein, substituting Ca^{2+} or Mg^{2+} , is used to measure the distances between different sites in proteins.

To explore the potential of use of europium (III) in probing PLP-enzymes active sites we have prepared the europium chelate of salicylidenevalinate Schiff base and studied its magnetic and optical properties. The complex seems to be in an octahedral configuration. Energy transfer from ligand to metal was observed and an energy level diagram revealing both absorption and emission properties of the complex was constructed.

*To my Mother,
My Wonderful Wife,
and my Son*

ACKNOWLEDGMENT

I would like to express my deep appreciation to my advisor, Dr. M. Ashraf El-Bayoumi for his guidance, encouragement, and friendship during the course of this study. I also thank the members of my committee, Dr. Carl Brubaker, Dr. Thomas Pinnavaia, and Dr. Andrew Timnick.

My thanks also go to Mr. Ernest Oliver for the mass spectroscopic measurements, Ms. Jo Kotarski for patiently drawing all the figures, and Ms. Peri-Anne Warstler for doing an excellent job in typing this Dissertation.

I thank my former colleagues, Dr. Khader Al-Hassan and Ms. Nahid Shabestary, for their friendship and support.

My thanks are extended to my beloved country, Egypt, and to Alexandria University. I also extend my gratitude to all my friends in the Egyptian Club in East Lansing for making me feel at home with their friendship and brotherhood.

Last, but not least, I would like to thank my wife, Eman, for her continuous encouragement and endless patience throughout this work. To my son, Kareem, I give my everlasting gratitude for waiting one entire week after my oral defense to be born, on Friday, April 30, 1982, thus allowing me a recovery period.

TABLE OF CONTENTS

Chapter	Page
LIST OF TABLES	vii
LIST OF FIGURES	viii
CHAPTER I - INTRODUCTION	1
CHAPTER II - EXPERIMENTAL	7
I. Systems Studied	7
A. Model Compounds	7
a. Aldehydes	7
b. Schiff bases	8
Preparation and Purification of Compounds	8
B. Monovalent-cation Salts	9
C. Potassium bis(salicylidene-DL- valinato) Europium(III) Chelate	10
II. Materials	11
A. Purification of Solvents	11
1. Ethanol	11
2. 3-Methylpentane (3MP)	11
3. Water	12
4. Acetonitrile, P-Dioxane and N,N-Dimethylformamide (DMF)	12
5. Dimethylsulfoxide (DMSO)	12
6. Tetrahydrofuran (THF)	12
B. Spectral Measurements	13
1. Absorption Spectra	13
2. Emission Spectra	13
3. 77°K Emission Spectra	13
4. Infrared Spectra	14
5. Mass Spectra	14

Chapter	Page
CHAPTER III - OPTICAL SPECTRA OF SALICYLALDEHYDE MODEL COMPOUNDS	15
I. Introduction.	15
II. Room Temperature Absorption Spectra.	16
III. Emission Spectra and Excited-State Proton-Transfer in Salicylaldehyde Model Compounds	38
CHAPTER IV - ABSORPTION AND EMISSION STUDY OF THE ASSOCIATION OF MONOVALENT CAT- IONS WITH PHENOXIDE AND SALICYL- ALDEHYDE ANIONS.	67
I. Introduction.	67
Monovalent Cation Interactions.	68
II. Spectroscopic Studies of Ion-Pair Formation.	71
A. Ultraviolet-Visible	73
B. Infrared and Raman.	89
C. Electron Spin Resonance (ESR)	93
D. Nuclear Magnetic Resonance (NMR). . .	95
E. Luminescence.	97
III. Results and Discussion.	98
CHAPTER V - EUROPIUM (III) CHELATE WITH SALICYLIDENE-VALINATE SCHIFF BASE.	125
I. Lanthanide Ions as Luminescence Probes of the Structure of Biological Macromolecules.	125
A. Decay Lifetimes as a Measure of the Number of Metal Co- ordinated Water Molecules	132

Chapter	Page
B. Characterization of Individual Binding Sites	136
C. Inter Metal Ion Energy Transfer Distance Measurements	138
II. Energy Transfer in Rare-Earth Metal Chelates	140
A. Paths of Energy Migration	141
B. Rate of Energy Transfer	145
C. Mechanism of Energy Transfer.	146
III. Europium Complex with Salicylidene-DL-Valinate Schiff Base	147
A. Introduction.	147
B. Results and Discussion.	151
CHAPTER VI - CONCLUSION AND FUTURE WORK	160
REFERENCES.	163

LIST OF TABLES

Table		Page
1	Solvent Effect on the Absorption Spectra of Compounds I-IV	23
2	Absorption Spectra of Schiff base Model Compounds in Different Solvents .	33
3	Emission Spectra of Compound I in Different Media.	45
4	Emission Spectra of Compounds (I-IV) in Ethanol and 3MP	53
5	Emission Spectra of Compounds (I-IV) in Water	53
6	Log K, ΔH , and $T\Delta S$ for the Formation of 18-Crown-6 Complexes with Metal Ions in H_2O at $25^\circ C$	87
7	Rate Constants for Reaction at $25^\circ C$ in H_2O , $\mu=0.3$: $M^+ + 18\text{-Crown-6} \xrightleftharpoons[k_d]{k_f} M\text{-Crown}^+$. .	87
8	Absorption Bands of Alkali Metal Salts in Dimethylsulfoxide.	91
9	Room Temperature Absorption and Emission Maxima of Para-Substituted Phenols in THF	123

LIST OF FIGURES

Figure		Page
1	Pyridoxal phosphate (vitamin B ₆) related compounds	1
2	The effect of pH on the spectrum of holotryptophanase.	4
3	Room temperature absorption spectra of dilute solutions (5×10^{-5} M) of compound I (—), II (-.-.-.-), III (-.-.-.-) and IV (----) all in ethanol.	17
4	Room temperature absorption spectra of dilute solutions (5×10^{-5} M) of compound I (—), II (-.-.-.-), III (-.-.-.-) and IV (----) all in 3MP	22
5	Room temperature absorption spectra of dilute alkaline solutions (5×10^{-5} M) of compound I (—), II (-.-.-.-), III (-.-.-.-) and IV (----) in ethanol	25
6	Room temperature absorption spectra of dilute solutions (5×10^{-5} M) of compound I-b (—), II-b (-.-.-.-) and IV-b (----) all in 3MP.	28

Figure	Page
7	Room temperature absorption spectra of dilute solutions (5×10^{-5} M) of compound I-b in different solvents: ethanol (—), dioxane (----) and DMSO (-.-.-) 29
8	Room temperature absorption spectra of dilute solutions (5×10^{-5} M) of compound II-b in ethanol (-.-.-), acidic ethanol (----), dioxane (....) and 3MP (—). 30
9	Room temperature absorption spectra of dilute solutions (5×10^{-5} M) of compound I-v in different solvents: ethanol (----), dioxane (—) and DMSO (-.-.-). 32
10	Room temperature absorption spectra of dilute solutions (5×10^{-5} M) of compound I-b in: ethanol (—), acidic ethanol (----), and alkaline ethanol (-.-.-) 34
11	Room temperature absorption spectra of dilute solutions (5×10^{-5} M) of compound I-v in ethanol (----), acidic ethanol

Figure	Page
11	solution (—) and alkaline ethanol solution (-·-·-·) 35
12	Room temperature absorption spectra of dilute solutions (5×10^{-5} M) of compound II-v in ethanol (----), and in acidic ethanol solution (—). 36
13	Room temperature absorption spectra of dilute solutions (5×10^{-5} M) of compound IV-b in: ethanol (----), acidic ethanol solution (—) and alkaline ethanol solution (-·-·-) 37
14	Room temperature emission spec- tra of a dilute solution (5×10^{-5} M) of compound I in ethanol at dif- ferent excitation wavelengths, $\lambda_{exc} = 330$ nm (—) and $\lambda_{exc} =$ 380 nm (----) 39
15	Emission spectra of a dilute alkaline solution (5×10^{-5} M) of compound I in ethanol, $\lambda_{exc} =$ 380 , at room temperature (—), and at 77°K (----). 40

Figure		Page
16	Room temperature emission spectra of a dilute solution (5×10^{-5} M) of compound I in water at different excitation wavelengths, $\lambda_{exc} = 320$ nm (—) and $\lambda_{exc} = 380$ nm (----).	42
17	Room temperature emission spectra of dilute solution (5×10^{-5} M) of compound I in 3MP $\lambda_{exc} = 320$ nm. . .	44
18	Room temperature emission spectra of dilute solutions (5×10^{-5} M) of compound II, $\lambda_{exc} = 320$ nm in 3MP (-·-·-·-·-·-), ethanol (----) and water (—).	46
19	Emission spectra of dilute solutions (5×10^{-4} M) of compound III in ethanol; neutral solution ($\lambda_{exc} = 320$ nm) at room temperature (-·-·-·-·-·-) and 77°K (----); alkaline solution ($\lambda_{exc} = 380$ nm) at room temperature (—) and 77°K (-·-·-·-·-·-)	47
20	Room temperature emission spectra of dilute solutions (5×10^{-5} M) of compound III, in aqueous solution	

- acidic solution $\lambda_{\text{exc}} = 330\text{-}380$ nm
at room temperature (—) and at
77° (-·-·-·). 59
- 26 Room temperature emission spectra
of dilute solutions (5×10^{-5} M)
of compound I-v in ethanol: in
neutral solution $\lambda_{\text{exc}} = 320$ nm
(—) and $\lambda_{\text{exc}} = 400$ nm (-·-·-·),
in acidic solution $\lambda_{\text{exc}} = 365$ nm
(----), and in alkaline solution
 $\lambda_{\text{exc}} = 360$ nm (-·-·-·) 61
- 27 Room temperature emission spectra
of dilute solution (5×10^{-5} M) of
compound II-b in ethanol $\lambda_{\text{exc}} = 330$
nm (—) and in acidic ethanol
 $\lambda_{\text{exc}} = 350$ nm (----). 62
- 28 Room temperature emission spectra
of dilute solutions (5×10^{-5} M)
of compound II-v in dioxane
(-·-·-·) and in ethanol (—)
 $\lambda_{\text{exc}} = 320$ nm 64
- 29 Room temperature emission spectra
of dilute solutions (5×10^{-4} M)
of compound IV-b in ethanol:
neutral solution, $\lambda_{\text{exc}} = 320$ nm

Figure	Page
	(—), acidic solution $\lambda_{exc} = 320$ nm (----) and alkaline solution $\lambda_{exc} = 360$ nm (-·-·-·) 65
30	Room temperature emission spectra of dilute solutions (5×10^{-4} M) of compound IV-v, $\lambda_{exc} = 320$ nm: in ethanol (-·-·-·-), alkaline ethanol (-·-·-·), acidic ethanol (—) and in dioxane (----). 66
31	Comparative effects of monovalent cations on the spectrum of holotryptophanase at 21°. Samples contained 2.0 mg of enzyme per 1.0 ml of 0.02 M imidazole-HCl buffer (pH 8.0), 2 mM mercaptoethanol, and ether 0.1 M NaCl, 0.1 M KCl, or 0.1 M imidazole-HCl (Im), as indicated. 70
32	Correlation between wave number and the inverse of the cationic radius for contact fluorenyl ion pairs in THF at 25°C. 76
33	Absorption spectra of fluorenyl salts in THF at -30°C for various counterions 76

Figure		Page
34	Optical spectrum of contact and separated ion pairs of fluorenyllithium at 25°C in 3,4 dihydropyran,; 3-methyltetrahydrofuran, ----; 2,5 dihydrofuran, —; and hexamethylphosphoramide, -·-·-.	77
35	Optical absorption spectrum of fluorenylsodium in THF at 25, -30, and -50°C.	80
36	Temperature dependence of the contact-solvent-separated ion-pair equilibrium of 9-(2-hexyl)fluorenyllithium in 2,5-dimethyltetrahydrofuran.. . . .	80
37	Pressure dependence of the contact-solvent-separated ion-pair equilibrium of fluorenylsodium in THF at 25°C.	81
38	(I) Dibenzo-18-crown-6. (II) Dicyclohexyl-14-crown-4; (III) monobenzo-15-crown-5.	83
39	Selectivity of 18-crown-6: log K values for reaction of 18-crown-6 with metal cations in H ₂ O vs. ratio of cation diameter to 18-crown-6	

Figure	Page
	cavity diameter. Value for Ca ²⁺ reported <0.5. 85
40	Optical absorption spectrum of barium fluorenyl and its 1:1 complex with dimethyldibenzo-18- crown-6 between 320 and 400 nm in THF at 25°C. 88
41	Possible structure of the barium fluorenyl-dimethyldibenzo-18- crown-6 complex in THF or pyridine. . . . 88
42	Room temperature absorption spec- tra of dilute solutions (5 x 10 ⁻⁵ M) of Na ⁺ salt of salicylaldehyde in DMSO (----) and in DMSO in the presence of 2 x 10 ⁻² M NaBF ₄ (——). 99
43	Room temperature absorption spectra of dilute solutions (5 x 10 ⁻⁵ M) of Tl(I) salt of salicyl- aldehyde in DMSO (----) and in DMSO in the presence of 5 x 10 ⁻³ M TlNO ₃ (——). 101
44	Potential energy of ion-pair formation as a function of the interionic distance 102

Figure	Page
45	Room temperature absorption spectra of dilute solution of Na ⁺ salt of salicylaldehyde: (4.8 x 10 ⁻⁵ M) in water (----), (4.5 x 10 ⁻⁵ M) in ethanol (-·-·-·-) and (4.5 x 10 ⁻⁵ M) in THF (—). 105
46	Room temperature absorption spectra of dilute solutions of Tl(I) salt of salicylaldehyde: (4.5 x 10 ⁻⁵ M) in water (----), (5.2 x 10 ⁻⁵ M) in ethanol (-·-·-·-) and (4.5 x 10 ⁻⁵ M) in THF (—) 106
47	Room temperature absorption spectra of dilute solutions (4.5 x 10 ⁻⁵ M) in THF of Na ⁺ (----) and Tl ⁺ (—) salts of salicylaldehyde. 107
48	Room temperature emission spectra of dilute solutions of Na salt of salicylaldehyde (5 x 10 ⁻⁵ M) in DMSO: λ _{exc} = 320 nm (----), λ _{exc} = 380 nm (—) and in the presence of NaBF ₄ (2 x 10 ⁻² M), λ _{exc} = 320 (-·-·-·-) 108
49	Room temperature emission spectra of dilute solutions (5 x 10 ⁻⁵ M)

- in DMSO of: Tl(I) salt of salicyl-
aldehyde, $\lambda_{\text{exc}} = 320 \text{ nm}$ (----)
and 420 nm (—); Tl(I) salt
of salicylaldehyde in presence
of $\sim 5 \times 10^{-3} \text{ M TlNO}_3$, $\lambda_{\text{exc}} =$
 320 nm (-·-·-·-). 110
- 50 Room temperature emission spectra
of dilute solutions ($5 \times 10^{-5} \text{ M}$)
of Na^+ and Tl^+ salts of salicyl-
aldehyde in THF. Na^+ salt, $\lambda_{\text{exc}} =$
 320 and 390 nm (—); Na^+ salt
in presence of $\sim 2 \times 10^{-2} \text{ M}$
 NaBF_4 , $\lambda_{\text{exc}} = 320 \text{ nm}$ (----);
Tl(I) salt, $\lambda_{\text{exc}} = 320$ and 390 nm
(-·-·-·-); and Tl(I) salt in
presence of $\approx 5 \times 10^{-3} \text{ M TlNO}_3$,
 $\lambda_{\text{exc}} = 320 \text{ nm}$ (-·-·-·-) 112
- 51 Room temperature absorption spec-
tra of dilute solutions ($5 \times 10^{-5} \text{ M}$)
of alkali-metal salts of p-hydroxy-
benzaldehyde in THF. P-hydroxy-
benzaldehyde (—); Li^+ salt (....);
 Na^+ salt (-·-·-·-) and K^+ salt
(-·-·-·-) 114

- 52 Room temperature emission spectra of dilute solutions (5×10^{-5} M) of alkali-metal salts of p-hydroxybenzaldehyde in THF. Li^+ salt, $\lambda_{\text{exc}} = 335$ nm (-----), K^+ salt, $\lambda_{\text{exc}} = 345$ nm (—) and K^+ salt in presence of 10^{-3} M 18C6, $\lambda_{\text{exc}} = 345$ nm (-·-·-·-·). 116
- 53 Room temperature absorption spectra of dilute solutions (1.8×10^{-4} M) of alkali-metal salts of p-methoxyphenol in THF. P-methoxyphenol (—), Na^+ salt (-·-·-·-·) and K^+ salt (-·-·-·). 118
- 54 Room temperature emission spectra of dilute solutions (1.8×10^{-4} M) of alkali-metal salts of p-methoxyphenol in THF. P-methoxyphenol, $\lambda_{\text{exc}} = 290$ nm (—); Na^+ salt, $\lambda_{\text{exc}} = 320$ nm (-·-·-·-·); Na^+ salt in presence of 10^{-3} M 18C6, $\lambda_{\text{exc}} = 320$ nm (.....); K^+ salt, $\lambda_{\text{exc}} = 335$ nm (-·-·-·-·) and K^+ salt in presence of 10^{-3} M 18C6, $\lambda_{\text{exc}} = 335$ nm (-----). 119

- 55 Room temperature absorption spectra of dilute solutions (2.5×10^{-4} M) of alkali-metal salts of p-methylphenol in THF. P-methylphenol (—), Na⁺ salt (-·-·-·-), K⁺ salt (-·-·-·-·) and K⁺ salt in presence of 10^{-3} M 18C6 (----) 121
- 56 Room temperature emission spectra of dilute solutions (2.5×10^{-4} M) of alkali-metal salts of p-methylphenol in THF. P-methylphenol, $\lambda_{\text{exc}} = 290$ nm (—), Na⁺ salt, $\lambda_{\text{exc}} = 320$ nm (-·-·-·-) and K⁺ salt, $\lambda_{\text{exc}} = 330$ nm (-·-·-·-·) 122
- 57 Electronic energy levels for europium(III) and terbium(III). The two upward-pointing arrows show the transitions which occur upon laser excitation at the wavelengths indicated. The two downward-pointing arrows label the most intense emissive transitions of the two ions. Radiationless

	energy transfer competes with the radiative processes through coupling of the emissive states to the O-H vibrational overtones of coordinated H ₂ O molecules. (The energy level diagram of Tb(III) has been displaced slightly to position the highest electronic acceptor state of the ground ⁷ F term to coincide with the zero-point energies of the vibrational overtone ladders.)	131
58	Plot of the observed reciprocal luminescence lifetimes τ_{obsd}^{-1} , vs. the mole fraction of H ₂ O, $\chi_{\text{H}_2\text{O}}$, in D ₂ O-H ₂ O mixtures of Eu(III) solutions. The effect of the chelating ligands NTA and EDTA is to displace water molecules from the first coordination spheres of the aqua-metal ions to yield the approximate values indicated along the right-hand ordinate	135

- 59 Excitation spectral profiles of the ${}^7F_0 \rightarrow {}^5D_0$ transition obtained during the course of the titration of an aqueous EuCl_3 solution with the sodium salt of the dipicolinate anion (DPA). Eu(III) to ligand ratios are indicated to the left of each trace 137
- 60 Schematic energy level diagram for a rare earth chelate possessing low-lying 4f electronic states: \rightarrow , radiative transitions; \rightsquigarrow , radiationless transitions 142
- 61 Energy level diagram for rare-earth chelates: (----) lowest triplet level for the complexes; (—) rare-earth ion level; (—) rare-earth ion resonance level in chelates. Excited singlet states of the complexes have much higher energies and are not shown. Likewise only the lowest triplet-state energy for a complex is given. 144

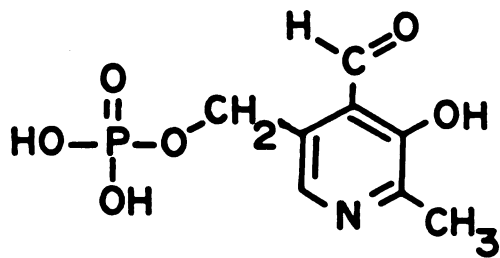
Figure	Page
62	Diagram of Cu(II) complex with: (A) salicylaldehyde-valine Schiff base; (B) PLP-valine Schiff base. 150
63	$K[Eu(C_{12}H_{13}NO_3)_2]$ 153
64	Magnetic behavior of $K[Eu(C_{12}H_{13}NO_3)_2]$ complex 154
65	Absorption spectra of dilute solution (3×10^{-5} M) of $K[Eu(C_{12}H_{13}NO_3)_2]$ in ethanol (----) and DMSO (—) 156
66	Emission spectra of dilute solutions (3×10^{-5} M) of $K[Eu(C_{12}H_{13}NO_3)_2]$ in ethanol at room temperature (----), ethanol at 77°C (- - -), and DMSO at room temperature (—). 157
67	Energy level diagram for $K[Eu-$ $(C_{12}H_{13}NO_3)_2]$ 159

CHAPTER I

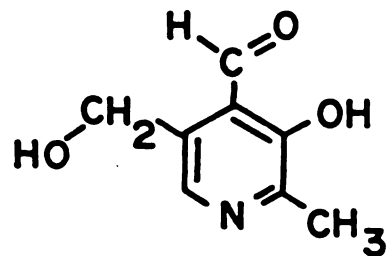
INTRODUCTION

Pyridoxal phosphate (PLP) is the most striking of the known coenzymes in terms of the multiplicity of different enzymatic reactions that are dependent on its presence. Nearly all these reactions are concerned with transformations of amino acids. It is not surprising, then, to learn that numerous nutritional studies in animals and microorganisms have established that a deficiency of pyridoxal (pyridoxine), a biochemical precursor of PLP, results in many irregularities in protein metabolism.⁽¹⁾ Vitamin B₆ is a name presently used to refer to the family of substances of biochemical interest that are structurally related to pyridoxal phosphate, Figure (1).

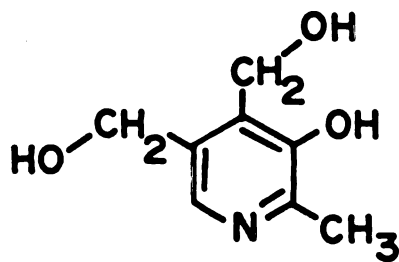
Pyridoxal phosphate-dependent enzymes catalyze a striking variety of distinct reactions such as racemization, transamination, decarboxylation, α,β -elimination, β,γ -elimination and dealdolization. The biologically active form of PLP is its Schiff base with an ϵ -amino group of a lysine residue in the active site of the enzyme. The presence of metal ion as an essential constituent of some enzymes provides an obvious link between enzymatic reactions



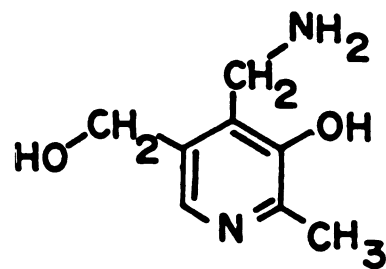
Pyridoxal phosphate
(PLP)



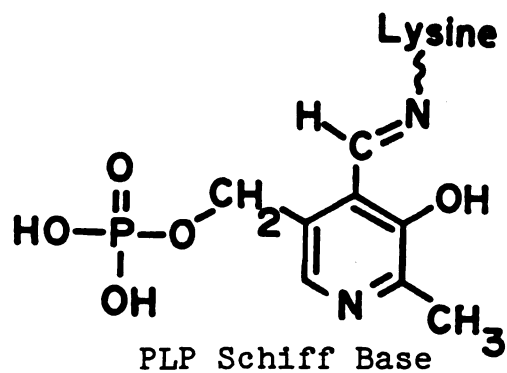
Pyridoxal



Pyridoxol



Pyridoxamine



PLP Schiff Base

Figure 1. Pyridoxal phosphate (vitamin B₆) related compounds.

and coordination chemistry. A good example for the metal ion requirement for activity is that of tryptophanase. All tryptophanases so far examined require NH_4^+ or K^+ , and the concentration required for half-maximum activity is 2-6 mM for NH_4^+ and 8-20 mM for K^+ (2). Na^+ and Li^+ are essentially without activating effects in each case, but they inhibit the E.coli enzyme when added together with NH_4^+ and K^+ (3). At optimal concentrations, NH_4^+ permits a level of activity at least equal to and usually slightly greater than K^+ , Rb^+ also activates but less effectively than K^+ (4). Tl^+ also replaces K^+ for E.coli enzyme and has a greater affinity (0.35 mM gives approximately half-maximum activity). In the presence of K^+ , holoenzyme (tryptophanase-PLP complex) undergoes a pH-dependent change ($\text{pK} = 7.2$) from the protonated form with λ_{max} at 420 nm to the deprotonated form with λ_{max} at 337 nm, Figure (2). Initially, the first band was assigned to the inactive form and the second band to the active form(5). Recent studies,(6,7) however, using rapid-scanning stopped-flow absorption study of the interconversion between the 420 and 337 absorbing species showed that the form absorbing at 337 nm is the inactive form and that absorbing at 420 nm is the active form.

In order to understand the role of monovalent cations and to possibly help in the interpretation of the kinetics data, it became clear that careful spectral assignments of different absorbing species (or conformers) as well as a

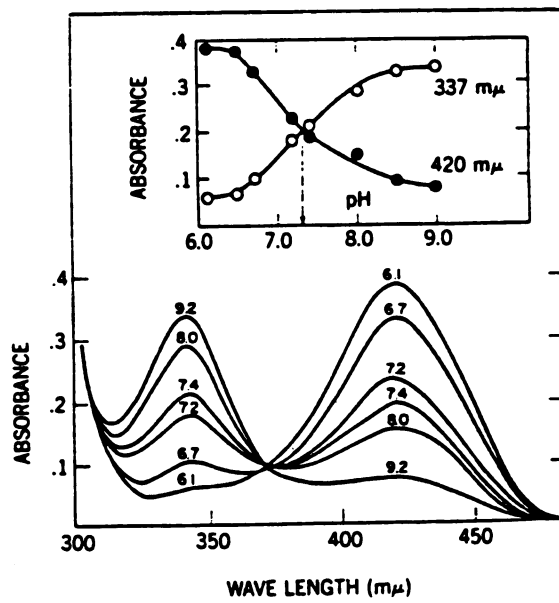


Figure 2. The effect of pH on the spectrum of holotryptophanase. 5

study of the spectral effects of interaction with monovalent cations is important.

Our approach is to study the optical properties (absorption and emission) in different media at both room temperature and 77°K of simple model compounds which maintain the basic electronic structural features of PLP. Substitution at the 2- and 5-positions in PLP ($-\text{CH}_3$ and $-\text{CH}_2-\text{OPO}_3\text{H}_3$) are expected to cause minimal spectral shifts⁽⁸⁾ even though they are important for the PLP activity. Similarly the pyridine nitrogen is an important structural feature for the role of PLP as a cofactor but does not contribute significantly to the spectral properties of PLP. Thus, the study of salicylaldehyde derivatives and their corresponding Schiff bases seem justified. Since the phenolic group may undergo a proton transfer either in the ground or excited electronic states, the corresponding methoxy derivative is also studied as a reference compound. Conformational changes involving the ring-carbonyl group C-C bond seem to play an important role in the enzymatic activity⁽⁹⁾. Thus, two compounds, 2-hydroxyacetophenone and 2-hydroxy-4,6-dimethylacetophenone, were chosen to study the steric effects which remove the coplanarity of the carbonyl group and the benzene ring. The study of the absorption and emission spectra of salicylaldehyde model compounds under different conditions are discussed in Chapter 3. The spectra of the Schiff bases of these model compounds with both n-butylamine

and potassium-DL-valinate were also studied, the results are summarized and discussed in the latter part of Chapter 3.

To investigate the role of monovalent cations, we studied the interaction of salicylaldehyde as well as some simple para substituted phenols, e.g., p-methyl, p-methoxy, and p-formyl phenols, with monovalent cations, such as Li^+ , Na^+ , K^+ , and Tl^+ , in conditions favoring ion-pair formation. Absorption and emission properties of these ion pairs will demonstrate the effect of the approach of a metal ion to the organic moiety in both ground and excited states. The results of our ion-pair study is discussed in Chapter 4, this is preceded by a summary of the use of several spectroscopic techniques in studying ion-pair formation.

Lanthanide ions are very effectively used as probes in biological systems⁽¹⁰⁾ to report microenvironmental changes at the active sites. Eu(III) in particular has been used extensively for this purpose⁽¹¹⁾. Accordingly, we planned to prepare and study Eu(III) complex formation with potassium salicylidene-DL-valinate Schiff base to explore its effectiveness as a probe to report the degree of hydrophobicity or hydrophilicity at the active site of PLP-enzyme systems. The results of our study for Eu(III) complex with salicylaldehyde Schiff base is discussed in Chapter 5, preceded by a short review on the use of lanthanide ions as probes in biological systems. Finally, a conclusion and suggested future experiments are given in Chapter 6.

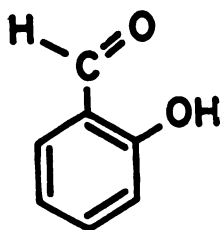
CHAPTER II

EXPERIMENTAL

I. Systems Studied

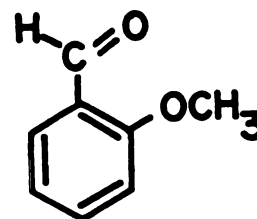
A. Model Compounds

a) Aldehydes



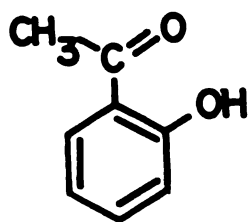
2-hydroxybenzaldehyde
(salicylaldehyde)

I



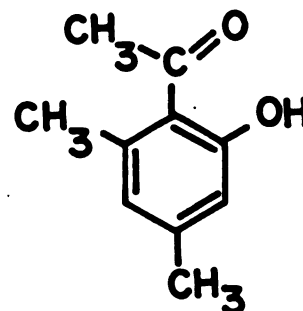
2-methoxybenzaldehyde
(anisaldehyde)

II



methyl-2-hydroxyphenyl ketone
(2-hydroxyacetophenone)

III

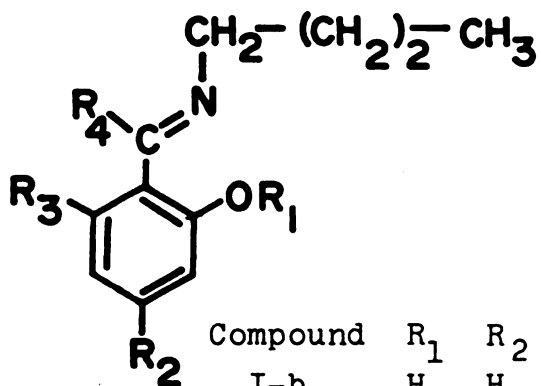


methyl-2-hydroxy-4,6-
dimethyl phenyl ketone
(4,6-dimethyl-2-hydroxy-
acetophenone)

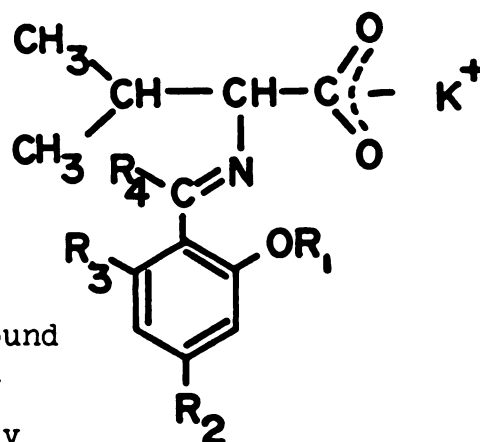
IV

b) Schiff bases

n-butylamine S.B.



potassium valinate S.B.



Compound	R ₁	R ₂	R ₃	R ₄	Compound
I-b	H	H	H	H	I-v
II-b	CH ₃	H	H	H	II-v
IV-b	H	CH ₃	CH ₃	CH ₃	IV-v

Preparation and Purification of Compounds

1. Compound I, II and III were obtained from Fisher Scientific and were purified by vacuum distillation.

2. Compound IV was obtained from Aldrich Chemical and was purified by repeated crystallization from petroleum ether 60-110°C.

3. Compounds I-b and II-b were prepared by refluxing 2 mmoles of the aldehyde with 2 mmoles of n-butylamine in methanol for 30 minutes and the product was obtained and purified by vacuum distillation. Compound I-b was obtained as a yellow liquid and compound II-b as a colorless liquid. Both compounds gave expected mass spectral results. The purity was checked by using gas chromatography.

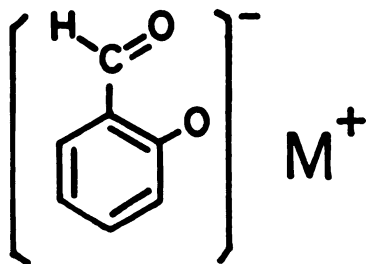
4. Compound IV-b was prepared similarly and was obtained as a creamy white solid which was purified by repeated recrystallization from methanol and ether, m.p. 157-158°C.

5. Compounds I-v, II-v and IV-v were prepared by the method of Heinert and Martell.⁽¹²⁾ Two mmoles of pure DL-valine were added to a solution containing 2 mmoles carbonate-free KOH in dry methanol. After the solid was dissolved completely, the mixture was cooled to 0°C and 2 mmoles of the aldehyde were added. The solution was stirred for 30 minutes between 0 and -10°C. The solid compounds were obtained by evaporating the solvent at low temperatures. Then, the compounds were recrystallized from methanol and ether. Compound I-v was yellow; m.p. 150-152°C, compound II-v was white; m.p. 260-262, and compound IV-v was pale yellow, m.p. 198-200°C. Mass spectra of the prepared Schiff bases confirmed their structure.

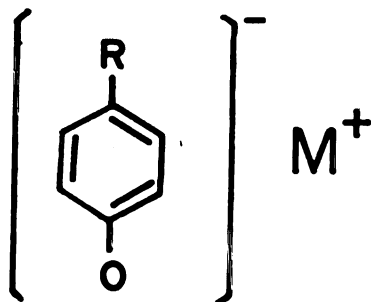
B. Monovalent-cation Salts

i. Preparation of Na⁺ and Tl(I) Salts of Salicylaldehyde - A modified version of the preparation method of Maggio⁽¹³⁾ was used. Two mmoles of ethanolic Na⁺ or Tl(I) ethoxide and 2 mmoles salicylaldehyde were mixed under good stirring conditions. On addition of chloroform and by cooling to 0°C, a yellow solid was obtained in good yield. The solid was recrystallized from boiling ethanol and

washed with ethanol-ether mixture and dried under argon.



ii. Preparation of Li⁺, Na⁺ and K⁺ Salts of P-substituted Phenols⁽¹⁴⁾ - To a dilute solution (10⁻⁴ to 10⁻⁵ M) of p-methyl, p-methoxy, or p-formyl phenol in THF was added an excess amount of the metal hydride. The solution was stirred under dry argon, then, the spectra were measured for a clear solution sample of this mixture.



C. Potassium bis(salicylidene-DL-valinato) Europium(III) Complex

To a clear solution of 2.2 mmoles of the Schiff base was added 2.2 mmoles of carbonate-free KOH in methanol. To this mixture was added 1 mmole of Eu(NO₃)₃·5H₂O solution in methanol and the solution was refluxed for 30 minutes. The complex was obtained by evaporating the solvent under vacuum. On recrystallization of the crude complex from

methanol and ether, yellow crystals were isolated, decomposition temperature $>250^{\circ}\text{C}$ $\text{K}[(\text{C}_{12}\text{H}_{13}\text{NO}_3)_2\text{Eu}] \cdot 2\text{H}_2\text{O}$, analysis, Calcd: C, 43.31; H, 4.54; N, 4.21; Eu, 22.83%. Found: C, 43.17; H, 4.54; N, 4.36; Eu, 22.60%.

II. Materials

A. Purification of Solvents

1. Ethanol

Absolute ethanol was fractionally distilled through a 1 meter vacuum jacket column, at a slow rate (about 5 drops per minute). Portions of about 50 ml were collected, and the absorption spectrum was taken in a 10 ml cell to check for benzene. Distillation was continued until the characteristic benzene UV absorption was no longer apparent. Ethanol was then distilled and used as needed.

2. 3-Methylpentane (3MP)

A modified version of the purification method of Potts⁽¹⁵⁾ was used. 3MP (Phillips Pure Grade) was shaken for 30 minutes with a 50:50 mixture of concentrated sulfuric acid and concentrated nitric acid. It was then shaken 3 times for 30 minutes each with concentrated sulfuric acid. The solution was then treated with sodium carbonate solution until CO_2 production ceased. The 3MP was then washed

several times with water until the water remained clear relative to the yellow color of the first wash. The 3MP was stored over sodium ribbon in a flask overnight. It was refluxed through a vacuum jacketed 1 meter column and distilled for use as needed. Purity was checked by obtaining the absorption spectrum.

3. Water

Was doubly distilled in this laboratory.

4. Acetonitrile, P-Dioxane and N,N-Dimethylformamide (DMF)

Spectroquality solvents from Metheson Coleman and Bell (MC/B) were used without further purification.

5. Dimethylsulfoxide (DMSO)

It was stored overnight over NaOH and distilled at reduced pressure ($\sim 2-3$ mm Hg, b.p. 50°) from NaOH pellets and stored over molecular sieve 4A.

6. Tetrahydrofuran (THF)

Traces of peroxide were removed by refluxing a 0.5% suspension of cuprous chloride for one-half hour, followed by distillation before proceeding. Predried over KOH pellets

and finally refluxed over and distilled from lithium aluminum hydride as needed.

B. Spectral Measurements

1. Absorption Spectra

All reported absorption spectra were recorded by use of a Cary 17 spectrophotometer.

2. Emission Spectra

Fluorescence spectra were recorded by use of a multi-component system consisting of a 500 W xenon light source. 500 mm Bausch & Lomb excitation monochromator (which provides a narrow excitation band width), Spex 1700-II emission Monochromator and EMI Model 9558QA Phototube. Noise reduction and amplification of the PMT signal is achieved by using a Princeton Applied Research Model HR-8-Lock In Amplifier and an appropriate chopping apparatus. Some of the room temperature emission spectra were recorded by using an Aminco-Bowman spectrofluorometer. The phosphorescence spectra were obtained with these instruments equipped with a rotating can phosphoroscope.

3. 77°K Emission spectra

A quartz dewar with flat quartz excitation and emission windows filled with liquid nitrogen, and a narrow glass

tube for the sample were used.

4. Infrared Spectra

Infrared spectra were obtained by using a Perkin-Elmer 457 Grating Infrared Spectrophotometer. Calibration of frequency reading was made by polystyrene film. Samples were examined as KBr disks.

5. Mass Spectra

Mass spectra were obtained with a Finnigan EI-CI gas chromatograph-mass spectrometer.

CHAPTER III

OPTICAL SPECTRA OF SALICYLALDEHYDE MODEL COMPOUNDS

I. Introduction

The purpose of this study is to investigate the absorption and emission properties of four salicylaldehyde model compounds (I, II, III and IV) and their corresponding Schiff bases with n-butylamine (I-b, II-b and IV-b) and with potassium-DL-valinate (I-v, II-v and IV-v) under various conditions. More specifically, we studied:

(i) The absorption and emission properties of possible cations and anions.

(ii) Solvent effects on the absorption and emission spectra of the various possible species.

(iii) The possible occurrence of excited-state proton transfer either intramolecularly (in hydrocarbon solvents, e.g. 3MP) or intermolecularly (in hydrogen bonding solvents e.g., water, alcohol, and dioxane); in the latter case solvent molecules would be involved.

(iv) The steric effects on the spectra, since in compound III and/or IV the carbonyl group may be forced out-of-plane with respect to the benzene ring.

This study should provide relevant information regarding the spectra of enzymes containing similar chromophores and possible transient intermediates occurring as a result of pH changes or during the course of enzymatic reactions. To achieve these goals we have investigated the absorption and emission spectra of the previously mentioned compounds at room temperature as well as at liquid nitrogen temperature (77°K). The spectra were measured in water, dioxane, N,N-dimethylformamide (DMF), dimethylsulfoxide (DMSO), acetonitrile and 3-methylpentane (3MP). In water and ethanol the spectra were measured in both acidic and alkaline solutions. The figures and tables shown in the subsequent pages provide a summary of our results.

II. Room Temperature Absorption Spectra

In Figure (3), room temperature absorption spectra of dilute solutions (5×10^{-5} M) in ethanol are shown for compound I-IV, the electronic absorption spectrum of compound I, salicylaldehyde, exhibits two absorption bands in the near ultraviolet, one at 323 nm with an absorptivity ($\epsilon = 4,000$) and the second at 253 nm ($\epsilon = 12,000$). Considering salicylaldehyde as a disubstituted benzene, its absorption spectrum may be interpreted, in the zeroth-order approximation, as resulting from transitions to either charge-transfer states or to locally-excited states. The locally excited states of benzene are ${}^1B_{2u}$, ${}^1B_{1u}$ and

${}^1E_{1u}$ (16). In salicylaldehyde the absorption bands corresponding to the ${}^1B_{2u}$ benzene transition and carbonyl locally-excited $n \rightarrow \pi^*$ transitions are probably buried under the more intense absorption at 253 nm. Accordingly, the first absorption band at 323 nm corresponds to an electronic transition to an essentially charge-transfer state, where the phenolic group acts as an electron-donor and the carbonyl group acts as an electron-acceptor. Since the two highest filled orbitals in phenol do not differ greatly in energy ($\Delta\epsilon$ is about 4000 cm^{-1}). One may also expect another charge transfer band at higher energies but in the same region. Thus, the second absorption band at 253 nm corresponds also to a transition to a charge-transfer state. In the first order approximation, this charge-transfer state is mixed with the ${}^1B_{1u}$ locally-excited state of benzene. Such assignment is consistent with electronic-energy calculations⁽¹⁷⁾ as well as solvent and steric effects⁽¹⁸⁾. The charge-transfer energies can be calculated using the equation⁽¹⁷⁾,

$$E_{C.T.} = I_D - E_A - C$$

where I_D is the ionization potential of the donor, E_A the electron affinity of the acceptor, and C the coulombic attraction energy between the transferred electron and the hole it left behind.

The use of localized-orbital model⁽¹⁹⁾ as a basis for a perturbation treatment of substituted benzene to calculate the energy of charge-transfer states is very useful because it is easily applied to polysubstituted benzenes, it allows a correlation with the absorption bands of various substituted benzenes and the model can account successfully for steric effects. Although the characterization of absorption band as being charge-transfer (C.T.) or locally excited (L.E.) bands is correct only in the zeroth-order approximation, yet it is very useful in predicting changes in basicities, acidities and dipole moment as a result of excitation. It is known⁽²⁰⁾ that steric effects forcing the carbonyl acceptor group out of plane causes a decrease in the intensity of the charge-transfer band. The intensity of the charge-transfer band depends on the resonance integral across the substituent-hydrocarbon bond which is proportional to $\cos\phi$, ϕ being the angle of twist of the substituent. The intensity of a charge-transfer band diminishes gradually as ϕ increases until it disappears when $\phi = 90^\circ$. For the 90° twisted substituted-benzene molecule the spectrum approximated that of benzene together with low lying absorption bands involving local excitation of the substituent. The substituent in this case may influence the benzene transitions only by inductive perturbation. A charge-transfer state may change only very slightly in energy as a result of twisting the substituent

involved in the charge-transfer transition in question. Such small change is due to the possible variation of the inductive parameter of the substituent with the angle of twist. For example, the spectrum of 4-nitro-N,N-dimethyl aniline approaches that of nitrobenzene when the angle of twist of N,N-dimethylamino group approaches 90°. N,N-dimethylamino group which has (+I_π) effect due to its π-lone pair electrons becomes less π-repelling as a result of twist. The inductive parameter of the nitro group which has (-I_π) effect do not vary much with φ. The angle of twist of the substituent may be calculated from the extinction coefficient of the charge-transfer band using the proportionality $\epsilon \propto \cos^2 \phi$. Steric effects show^(18,20) that the following absorption bands of substituted-benzene spectra are charge-transfer bands: the 322 nm band of p-nitroaniline, the 239 nm of acetophenone, the 233 nm of aniline and the 252 nm of nitrobenzene.

In ethanol two different intermolecular hydrogen bondings may occur between the solvent and solute molecules depending on whether the ethanolic oxygen atom or proton is involved. In compound IV, the first absorption band is blue shifted (shifted to shorter wavelength) and decreased in its intensity showing an absorption at 305 nm ($\epsilon = 2,600$). This blue shift as well as the reduction in absorptivity demonstrate the steric effects due to the interaction between the acetyl methyl group and the ring methyl group in position 6 in compound IV. If

the carbonyl group was completely out of plane with respect to the benzene ring, one should expect compound IV to absorb near 280 nm like methylated phenol (p-methylphenol absorbs at 280 nm).

In 3MP in dilute solutions, only intramolecular hydrogen bonding is expected between the phenolic and the carbonyl oxygen through the phenolic proton. Compound II without phenolic proton (methylated phenolic group) shows a blue shifted absorption band at 307 nm, Figure (4), compared to the rest of the compounds. The intramolecular hydrogen bond in compound I, III and IV caused the red shift in the first absorption band in 3MP. Contrary to its behavior in ethanol, compound IV, shows an intense absorption band at 335 nm reflecting the coplanarity of the carbonyl group with the benzene ring in 3MP. This implies that the energy gained through the formation of the hydrogen bond outweighs the repulsion energy between the sterically hindered methyl groups. The small red shift of the absorption band in compound IV relative to that of compound III is due to the methyl substitution in position 4 and 6.

In Table (I), the solvent effect on the first absorption band of the four model compounds is summarized. The band maximum for compound IV in dioxane lies at a much longer wavelength compared to the band maximum in ethanol and in water; one may conclude that in dioxane the carbonyl group is relatively more coplanar compared to the situation

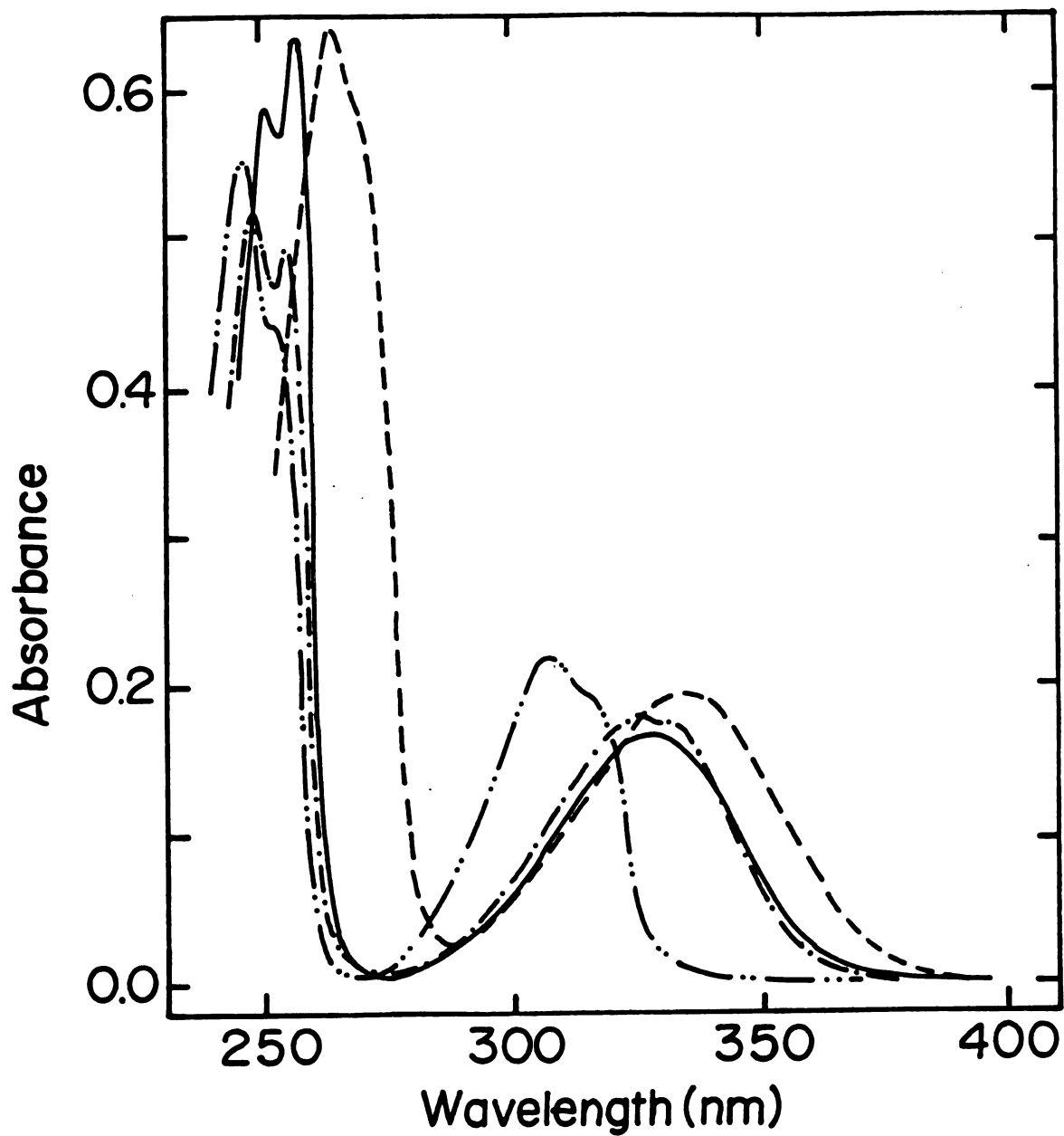


Figure 4. Room temperature absorption spectra of dilute solutions (5×10^{-5} M) of compound I (—), II (-·-·-·-), III (·····) and IV (---) all in 3MP.

Table 1. Solvent Effect on the Absorption Spectra of Compounds I-IV.

Solvent	Compd. (I)			Compd. (II)		
	λ (nm)	$\nu \cdot 10^{-3}$ (cm ⁻¹)	* $\Delta\nu \cdot 10^{-3}$ (cm ⁻¹)	λ (nm)	$\nu \cdot 10^{-3}$ (cm ⁻¹)	* $\Delta\nu \cdot 10^{-3}$ (cm ⁻¹)
3MP	328	30.5	0.0	307	32.06	0.0
Dioxane	323	30.9	+0.4	314	31.8	-0.8
Ethanol	323	30.9	+0.4	318	31.4	-1.2
Water	323	30.9	+0.4	322	31.1	-1.5

Solvent	Compd. (III)			Compd. (IV)		
	λ (nm)	$\nu \cdot 10^{-3}$ (cm ⁻¹)	* $\Delta\nu \cdot 10^{-3}$ (cm ⁻¹)	λ (nm)	$\nu \cdot 10^{-3}$ (cm ⁻¹)	* $\Delta\nu \cdot 10^{-3}$ (cm ⁻¹)
3MP	325	30.8	0.0	335	29.8	0.0
Dioxane	321	31.2	+0.4	325	30.8	+1.0
Ethanol	324	30.9	+0.1	307	32.6	+2.8
Water	323	30.9	+0.1	3-5	32.8	+3.0

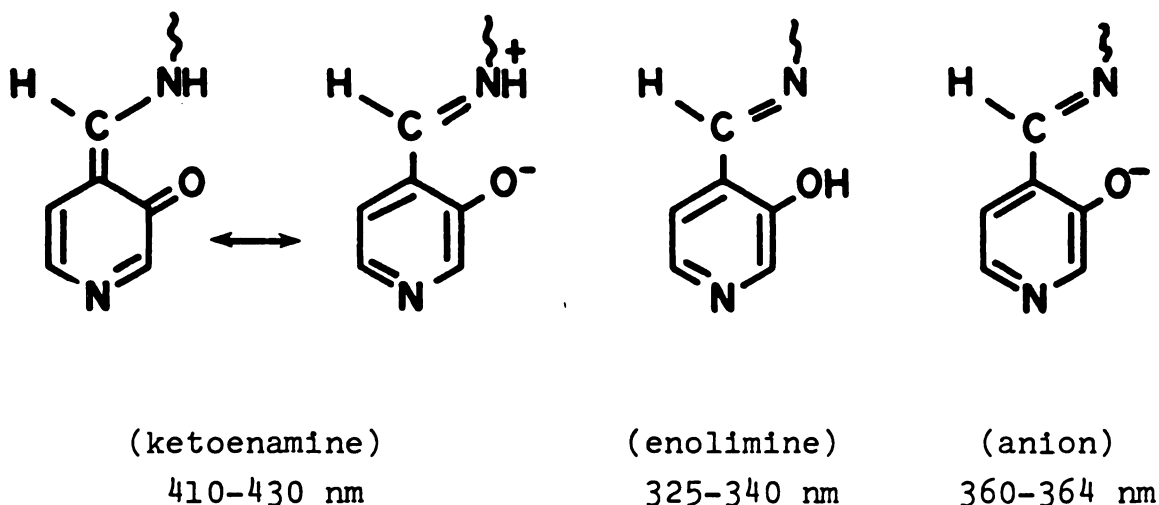
$$*\Delta\nu = \nu_{\text{solv.}} - \nu_{3\text{MP}}$$

in protic solvents. Dioxane can form only an intermolecular hydrogen bond with the phenolic proton.

In an alkaline aqueous and ethanolic solution the absorption spectra of compound I, III and IV are shown in Figure (5). The first absorption band of the anion is red shifted compared to the corresponding first absorption band in neutral solutions. In the case of compound II no change was observed as expected. Due to a smaller ionization potential energy of the phenolate compared with phenol one should expect the anion to absorb at longer wavelengths. The increase in the intensity of this band in the anion is a result of a relatively greater charge migration in the charge-transfer state of the anion. The relative intensities of this band in compounds I, III and IV reflects the steric effect which is more dominant in the case of compound IV.

In pyridoxal phosphate enzymes so far studied, the carbonyl group of the coenzyme is combined with the ϵ -amino group of lysine residue to form a Schiff base⁽²¹⁾. A number of PLP-enzymes have an absorption band at 410-430 nm. In addition to this band, most PLP-enzymes have a peak at 325-340 nm. Some enzymes display an absorption at 360-364 nm at high or at all pH values⁽²¹⁾. These absorption bands can be related to specific species in the acid-base equilibria of the Schiff base of PLP. The 410-430 nm band is assigned to the Schiff base with a protonated

azomethine nitrogen and phenolate group (ketoenamine species), the 325-340 nm band to that of a phenol group without a proton on the azomethine nitrogen (enolimine species), and the 360-364 nm band to that with phenolate group and unprotonated azomethine nitrogen (anionic species). The basis of this currently accepted assignment was provided by Heinert and Martell⁽²²⁾ who studied the absorption spectra of the Schiff bases of 3-hydroxy-4-formylpyridine and related compounds.



It is important here to note that there were no profound effects on the spectra of those model compounds when compared with the spectra of PLP Schiff bases as a result of the 2- and 5-position substituents in PLP. A number of arguments for this conclusion have been presented from the spectral studies on solution equilibria of Schiff bases of pyridoxal and related compounds and on PLP-enzymes and from other physicochemical studies^(21,23).

Figure (6) shows the room temperature absorption of compound I-b, II-b and IV-b in 3MP. In this solvent, intramolecular hydrogen bond between the phenolic group and the azomethine nitrogen gives rise to an absorption at 317 nm in the case of Schiff base I-b. This absorption band can be assigned to the neutral nonpolar form of the Schiff base namely, enolimine form. Again if we treat these model compound Schiff bases as substituted benzene derivatives one should consider the smaller electron affinity of the azomethine group when compared with the carbonyl group in the model compounds. This explains the blue shift ($1,060\text{ cm}^{-1}$) of the first absorption band of these Schiff bases in 3MP compared with the corresponding model compounds in the same solvent.

In polar solvents, Figure (7), a new absorption band is developed at 410 nm, the intensity of this band depends upon the polarity of the solvent. In DMSO, for example, the absorption band at 410 nm is assigned to an absorption by the neutral bipolar form of the Schiff base, keto-enamine form, this band does not exist in the absorption spectrum of the methoxy compound II-b in DMSO, ethanol or dioxane, Figure (8), because of the absence of the phenolic proton and accordingly no ketoenamine formation. The observation that salicylaldehyde, compound I, does not absorb at ~ 410 nm in DMSO demonstrates the lack of intramolecular proton transfer in the ground state in polar solvents,

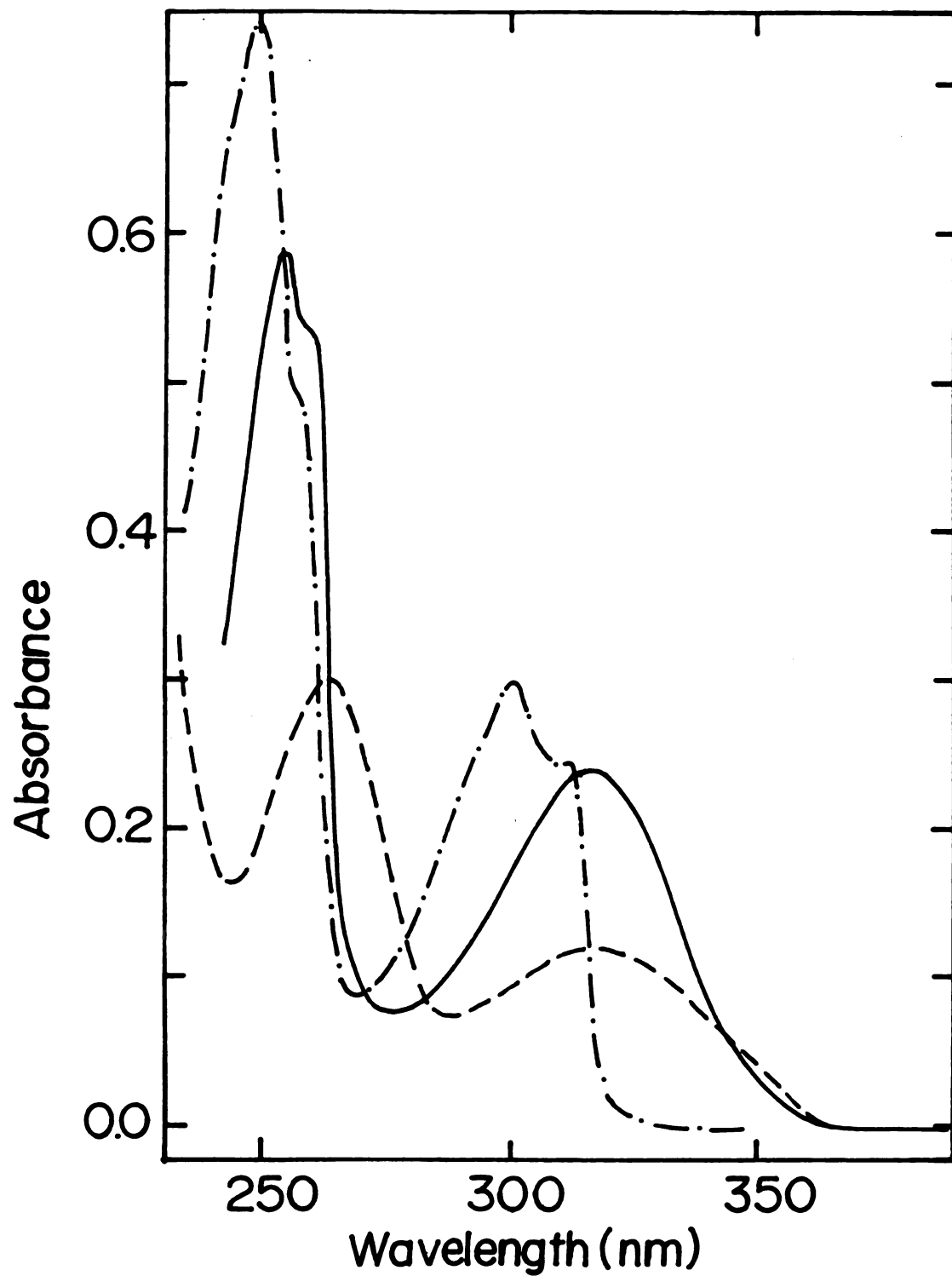


Figure 6. Room temperature absorption spectra of dilute solutions (5×10^{-5} M) of compound I-b (—), II-b (-·-·-·) and IV-b (----) all in 3MP.

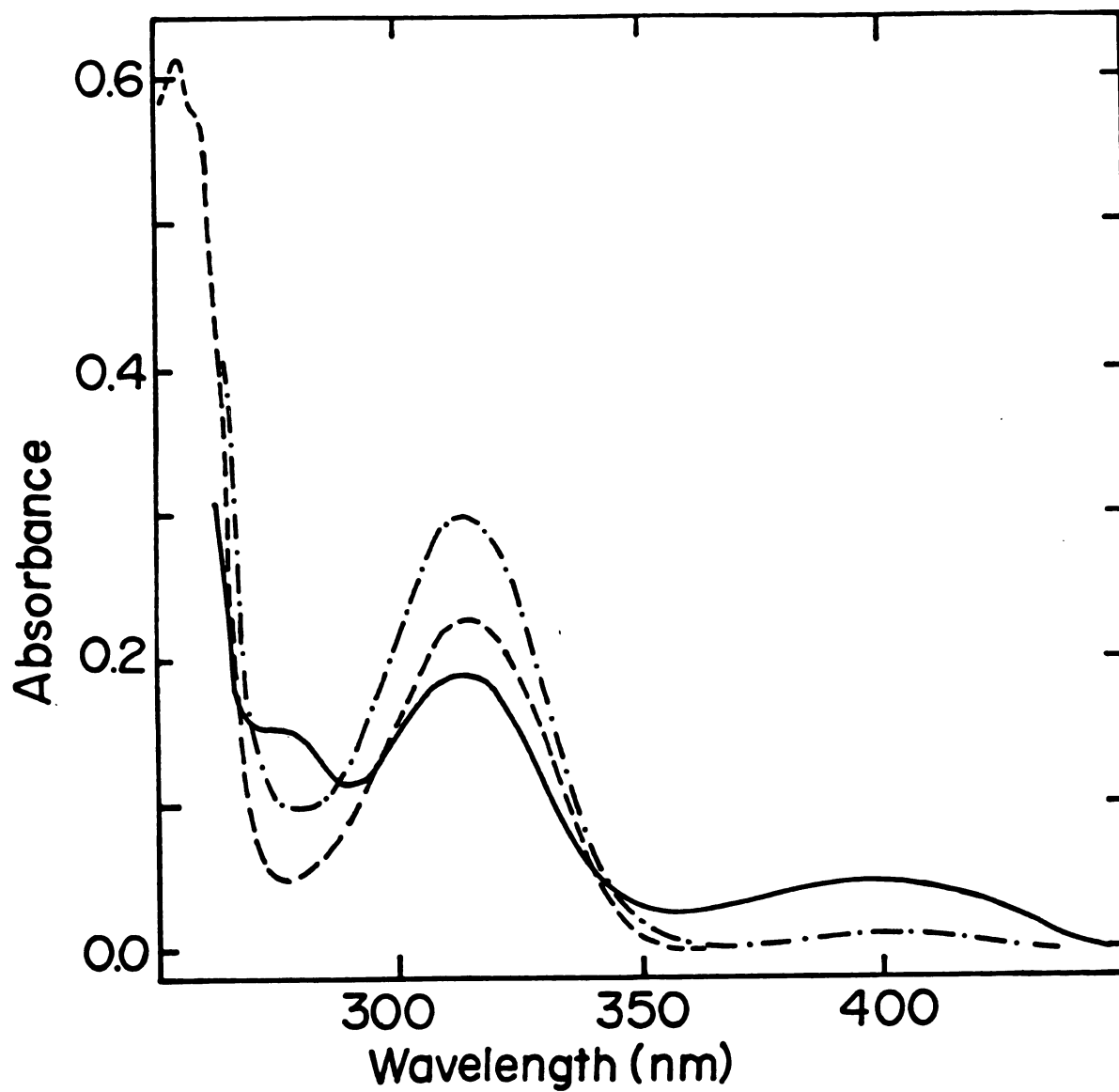


Figure 7. Room temperature absorption spectra of dilute solutions (5×10^{-5} M) of compound I-b in different solvents, ethanol (—), dioxane (---) and DMSO (-·-·-·).

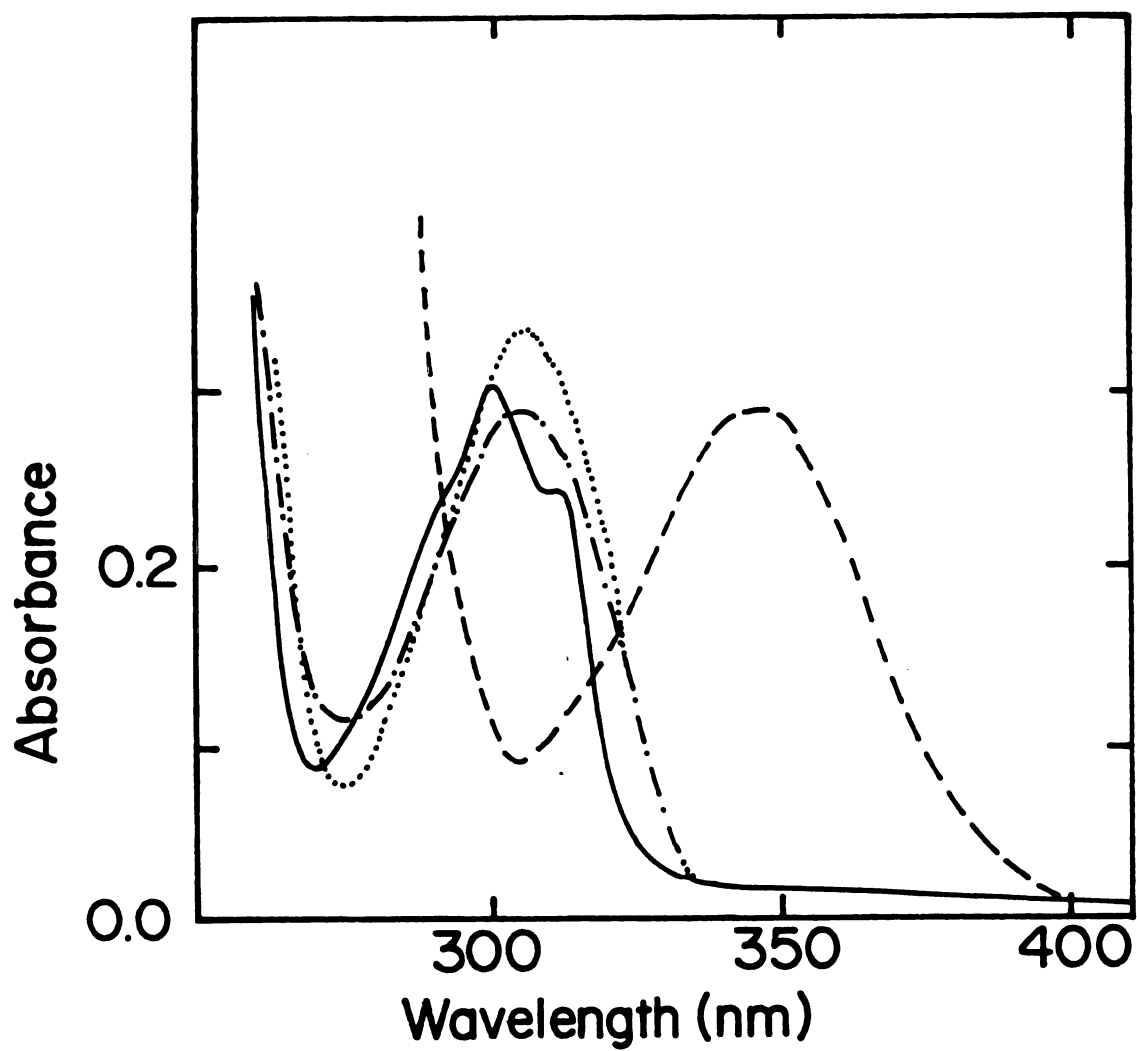


Figure 8. Room temperature absorption spectra of dilute solutions (5×10^{-5} M) of compound II-b in ethanol (-·-·-), acidic ethanol (----), dioxane (.....) and 3MP (—).

i.e., the equilibrium between the tautomers in the ground state is overwhelmingly shifted towards the enolimine tautomer. This observation reflects the high basicity of the azomethine nitrogen compared with the carbonyl oxygen. The spectra of the Schiff bases with potassium valinate in different solvents are shown in Figure (9). Table (2) summarizes these results. In the case of valinate Schiff bases the keto-enol equilibrium is shifted more towards the more stable ketoenamine tautomer.

Figures (10) and (11) show the absorption spectra of salicylaldehyde Schiff bases I-b and I-v respectively. Each figure shows the spectrum of the neutral form as well as that of the cation and anion. In acidic ethanolic solution a band at 350 nm appears, Figure (10), (11) and (12), this band corresponds to the absorption of the cation form of the Schiff base. The red shift in this band relative to the absorption in pure ethanol is due to the increase in the electron affinity of the azomethine nitrogen due to protonation. This results in the lowering of the energy of this charge-transfer absorption band. In the case of compound IV-b, the absorption band of the cationic form is weak and appears at 315 nm, Figure (13), the large blue shift compared for example with the absorption of the cationic form of II-b which appears at 350 nm is due to a large steric effect.

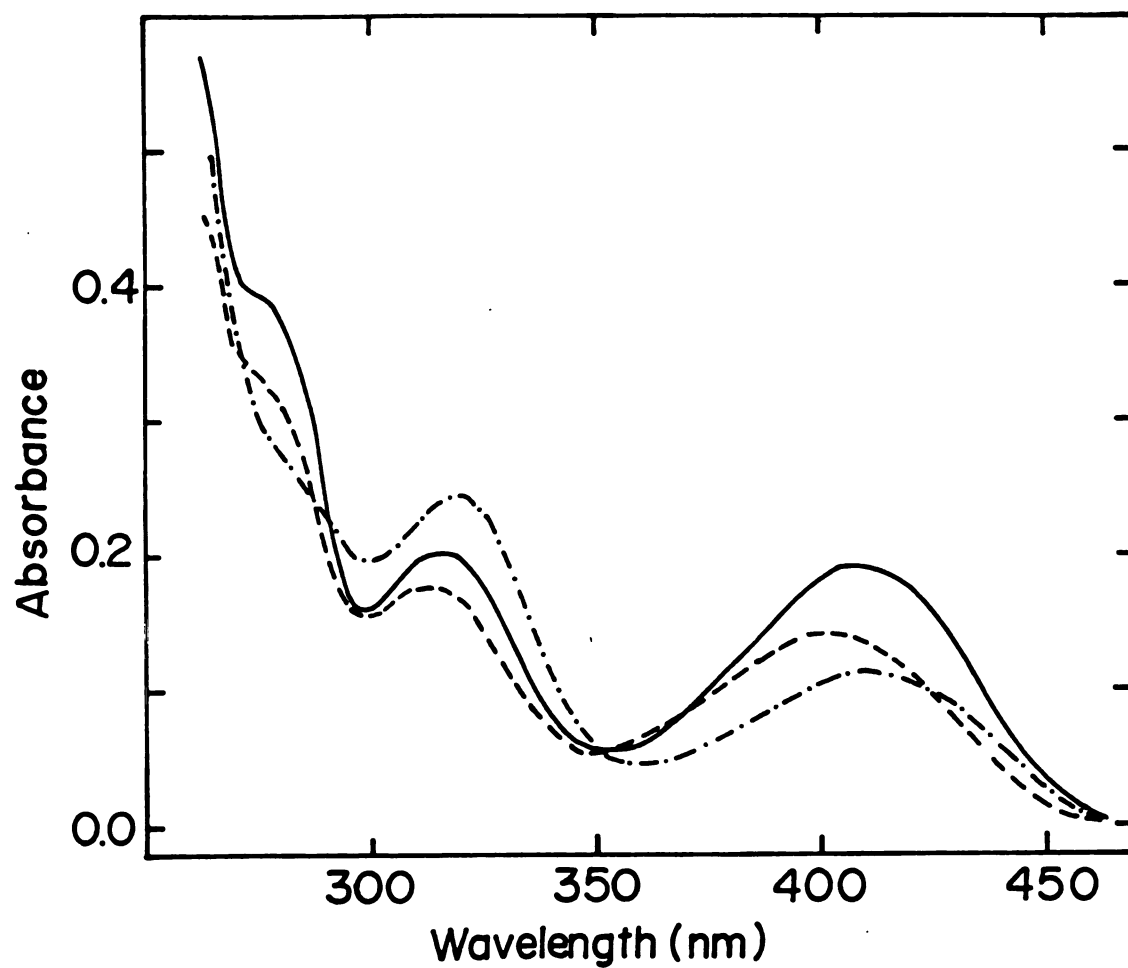


Figure 9. Room temperature absorption spectra of dilute solutions (5×10^{-5} M) of compound I-v in different solvents, ethanol (----), dioxane (—) and DMSO (-·-·-·).

Table 2. Absorption Spectra of Schiff Base Model Compounds in Different Solvents.

Solvent Compound	3MP λ_{\max} (nm)	Ethanol λ_{\max} (nm)	Dioxane λ_{\max} (nm)	Acetonitrile λ_{\max} (nm)	DMSO λ_{\max} (nm)
I-b	317	400	314	*	405
II-b	312	305	303	*	304
IV-b	318	282	317	*	314
I-v	*	402	410	408	412
II-v	*	303	314	312	315
IV-v	*	388	333	279	328

*Insoluble.

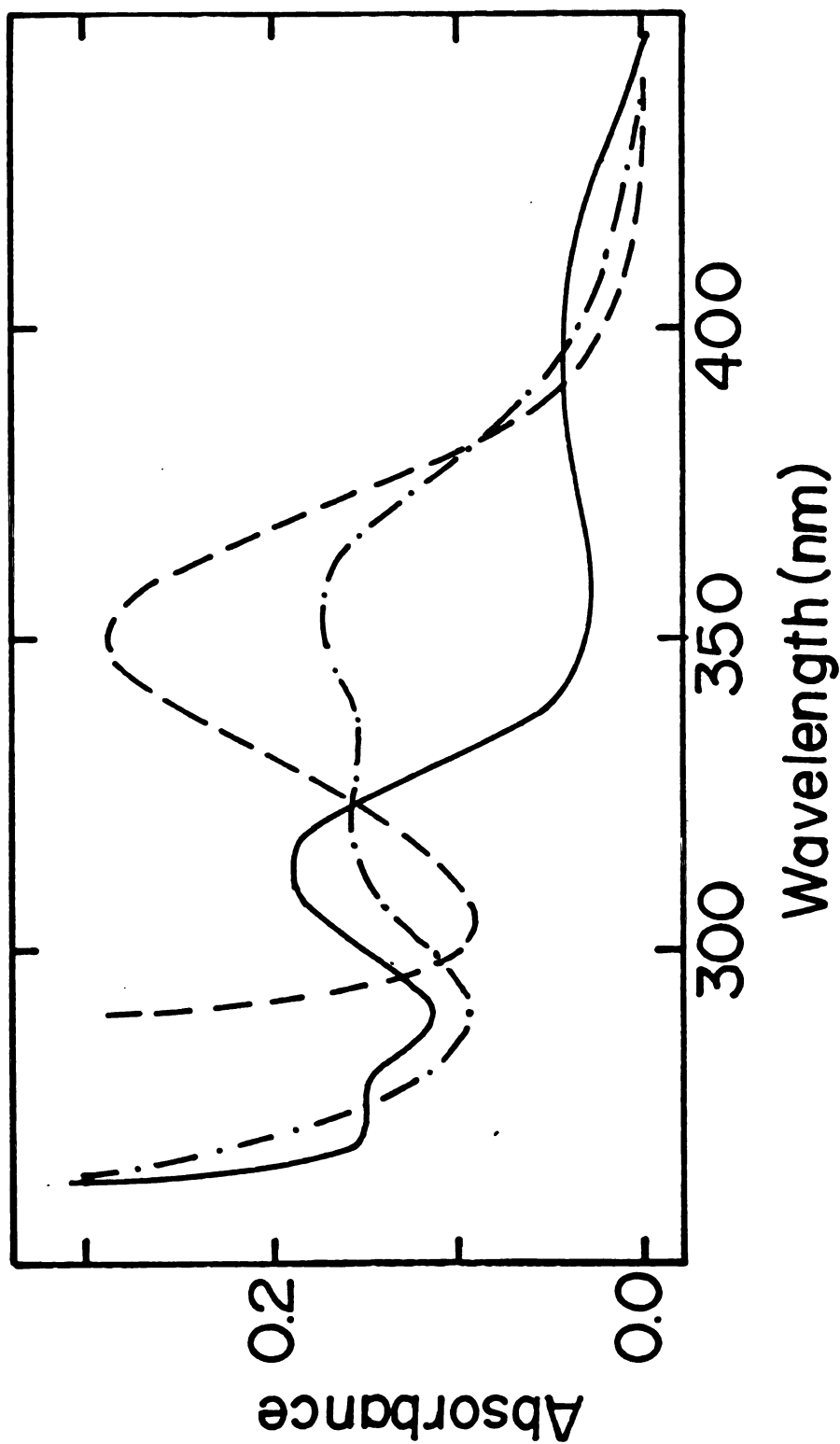


Figure 10. Room temperature absorption spectra of dilute solutions (5×10^{-5} M) of compound I-b in: ethanol (—), acidic ethanol (---) and alkaline ethanol (-·-·-·).

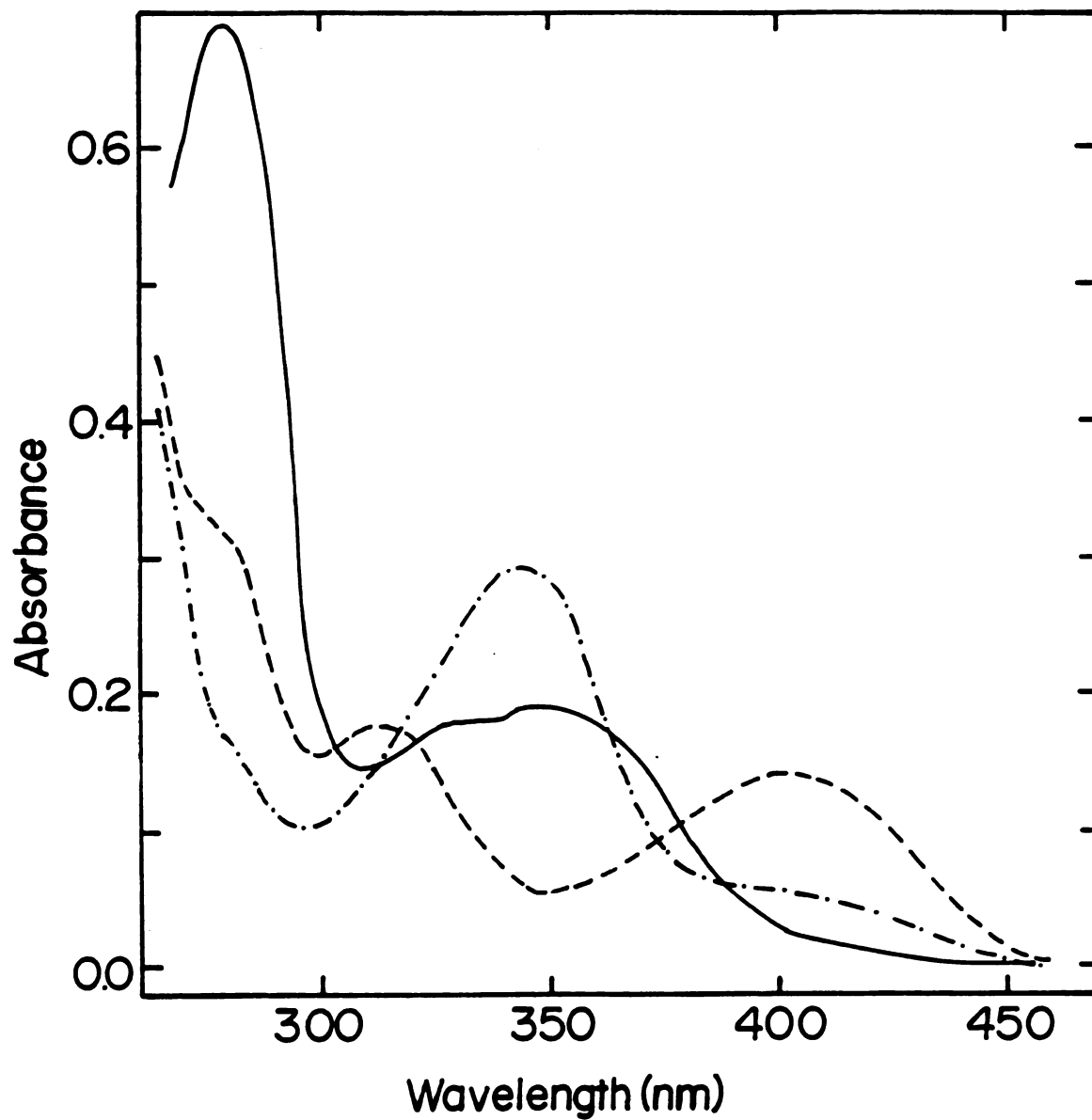


Figure 11. Room temperature absorption spectra of dilute solutions (5×10^{-5} M) of compound I-v in ethanol (----), acidic ethanol solution (—) and alkaline ethanol solution (-·-·-·).

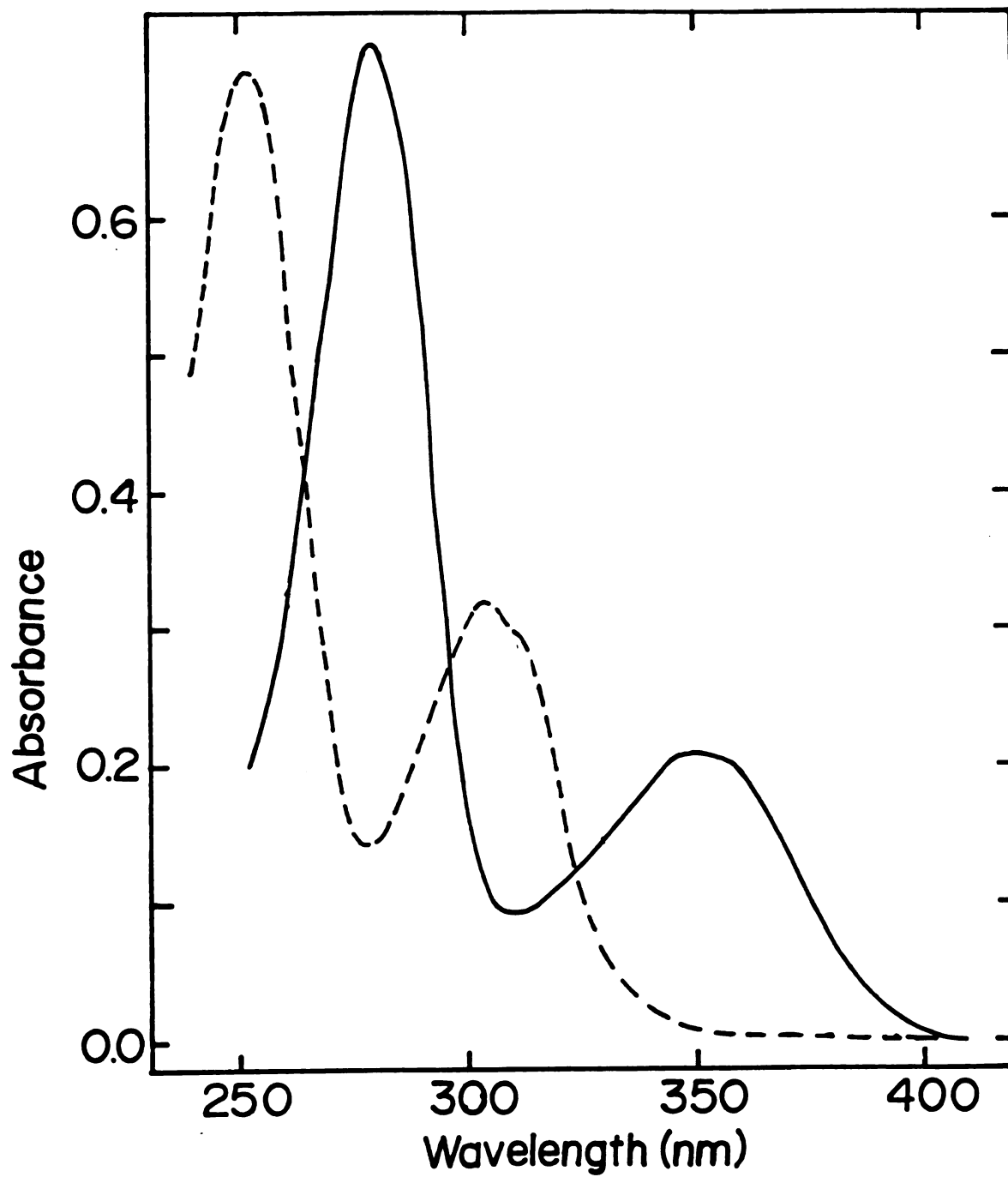


Figure 12. Room temperature absorption spectra of dilute solutions (5×10^{-5} M) of compound II-v in ethanol (----), and in acidic ethanol solution (—).

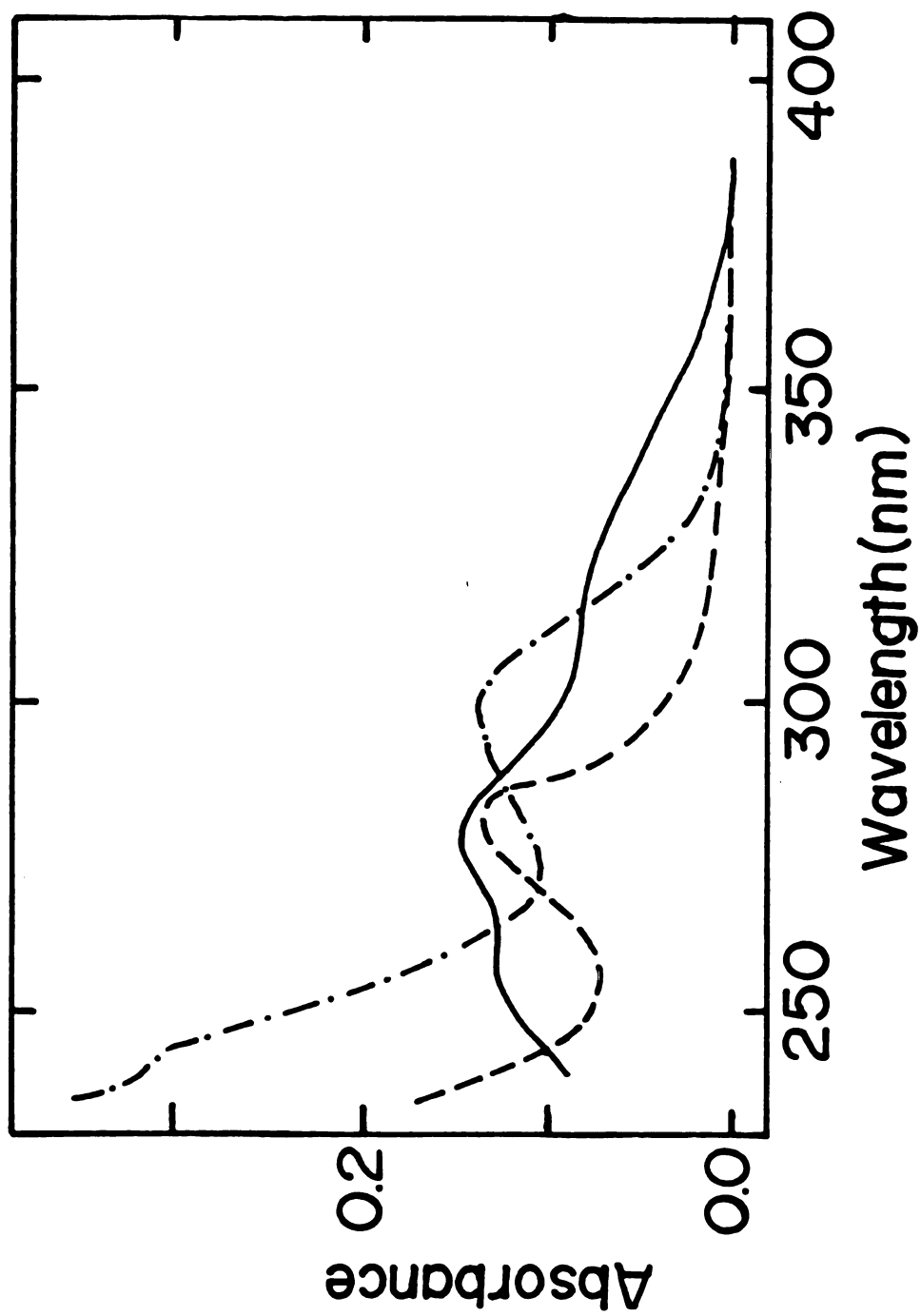


Figure 13. Room temperature absorption spectra of dilute solutions (5×10^{-5} M) of compound IV-b in: ethanol (---), acidic ethanol solution (—), and alkaline ethanol solution (-·-·-·).

III. Emission Spectra and Excited-State Proton Transfer in Salicylaldehyde Model Compounds

Salicylaldehyde (Compound I) shows a medium as well as an excitation wavelength dependent emission spectrum. In a dilute ethanol solution excitation of the neutral molecule at 330 nm gives two emission bands as shown in Figure (14). The first band at 426 nm was assigned to an emission from the neutral nonpolar form. The longer-wavelength emission at 500 nm was assigned to an emission from a bipolar form resulting from a double proton transfer involving solvent molecules. One should point out that the phenolic and carbonyl oxygens of the solute in ethanol are hydrogen bonded intermolecularly to solvent molecules. Upon excitation, charge transfer from the phenolic to the carbonyl group results in an increase in the acidity of the phenolic proton^(24,25) and an increase in the basicity of the carbonyl oxygen. Accordingly, in the excited state, the phenolic group may lose a proton and the carbonyl oxygen may pick up a proton giving rise to a bipolar species. Excitation of the neutral solution at 380 nm, where the phenolate ion absorbs, resulted in an emission at 490 nm. Similar emission, Figure (15), was observed at 490 nm when an alkaline ethanolic solution was excited at 380 nm. These results suggest that a ground-state equilibrium between the neutral and anion forms of compound I exists in ethanol solutions. In a glass solution, at 77°K, the

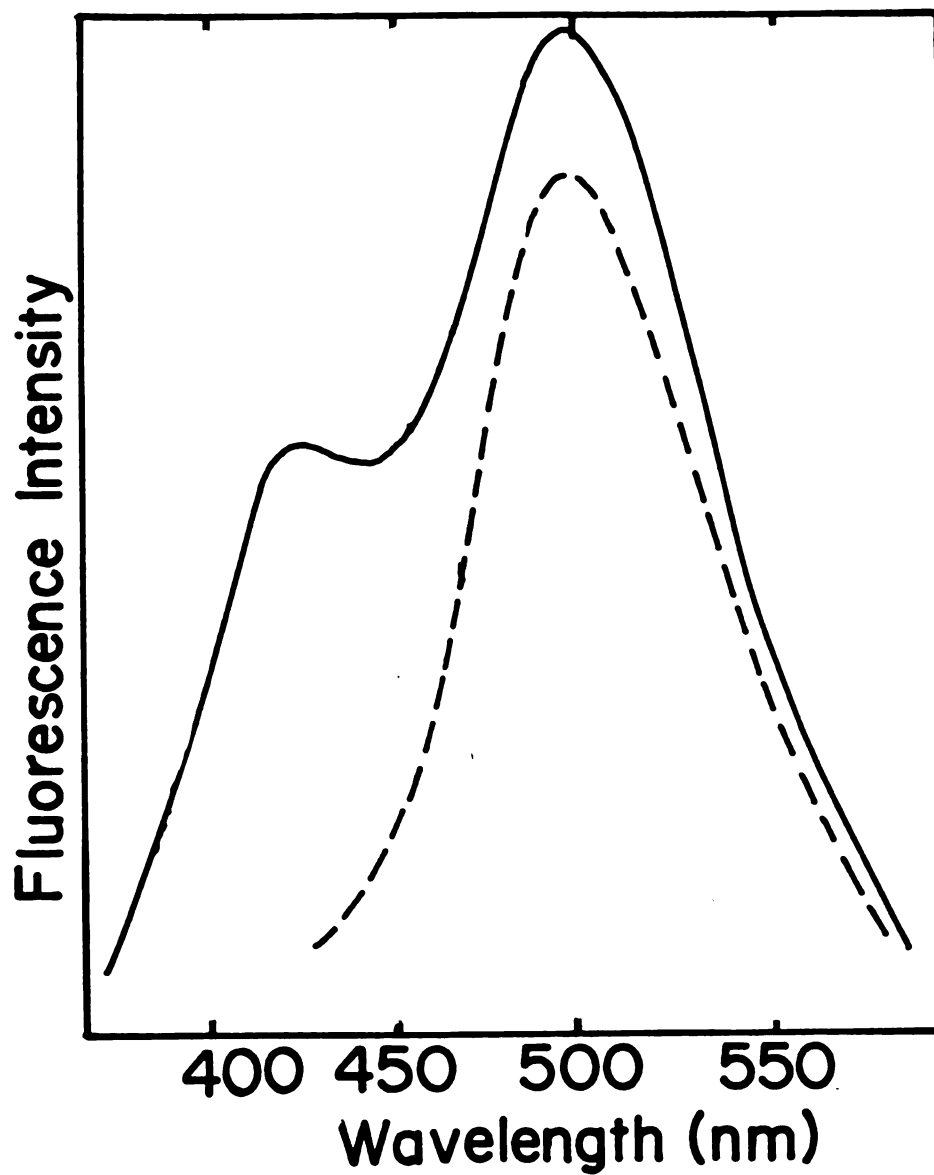


Figure 14. Room temperature emission spectra of a dilute solution (5×10^{-5} M) of compound I in ethanol at different excitation wavelengths, $\lambda_{\text{exc}} = 330$ nm (—) and $\lambda_{\text{exc}} = 380$ nm (----).

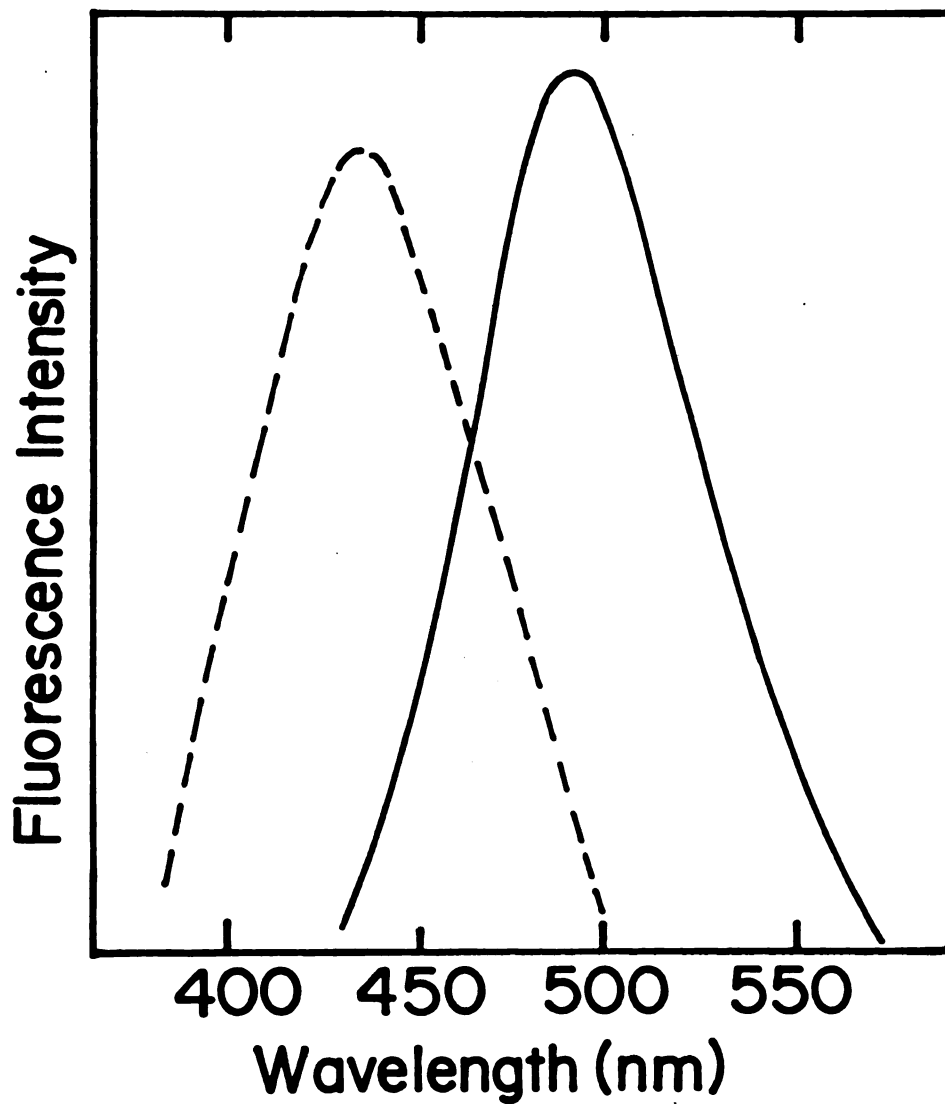
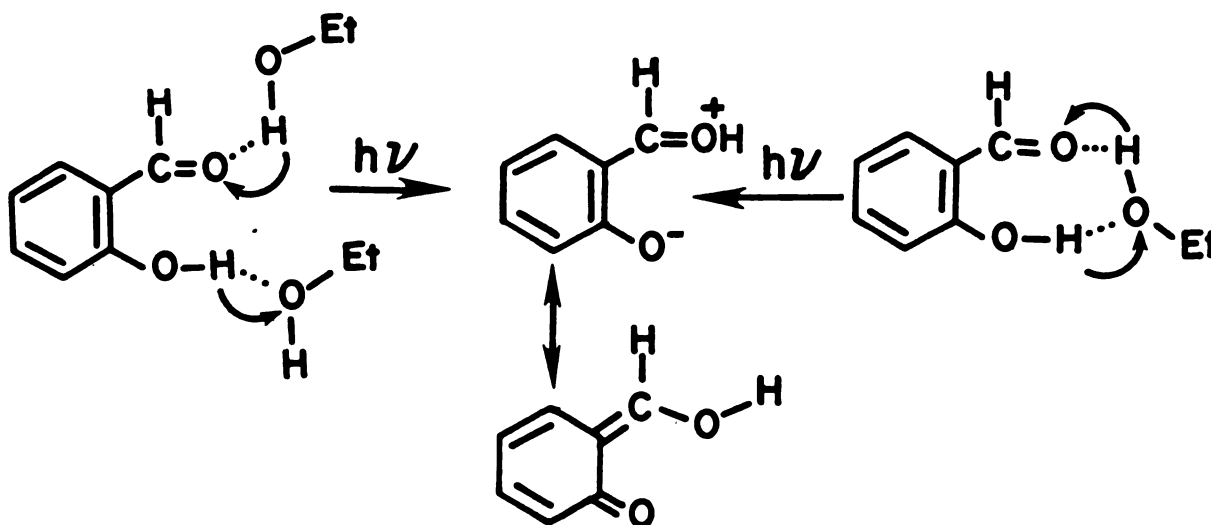


Figure 15. Emission spectra of a dilute alkaline solution (5×10^{-5} M) of compound I in ethanol, $\lambda_{\text{exc}} = 380$, at room temperature (—), and at 77°K (----).

emission of the anion is blue shifted to 434 nm. In such a rigid medium, solvent relaxation does not occur during the lifetime of the excited singlet state causing the fluorescence maximum to be blue shifted compared to the fluorescence maximum in a fluid polar medium.



In an aqueous solution, the room temperature emission spectrum shown in Figure (16) exhibits two bands upon excitation at 330 nm, a shorter-wavelength emission band at 428 due to the neutral form and a longer-wavelength emission at 505 due to the bipolar form. Excitation of an alkaline solution showed an emission at 500 nm and was assigned to the anion form.

In 3MP, the phenolic proton and the carbonyl oxygen are intramolecularly hydrogen bonded. Upon excitation,

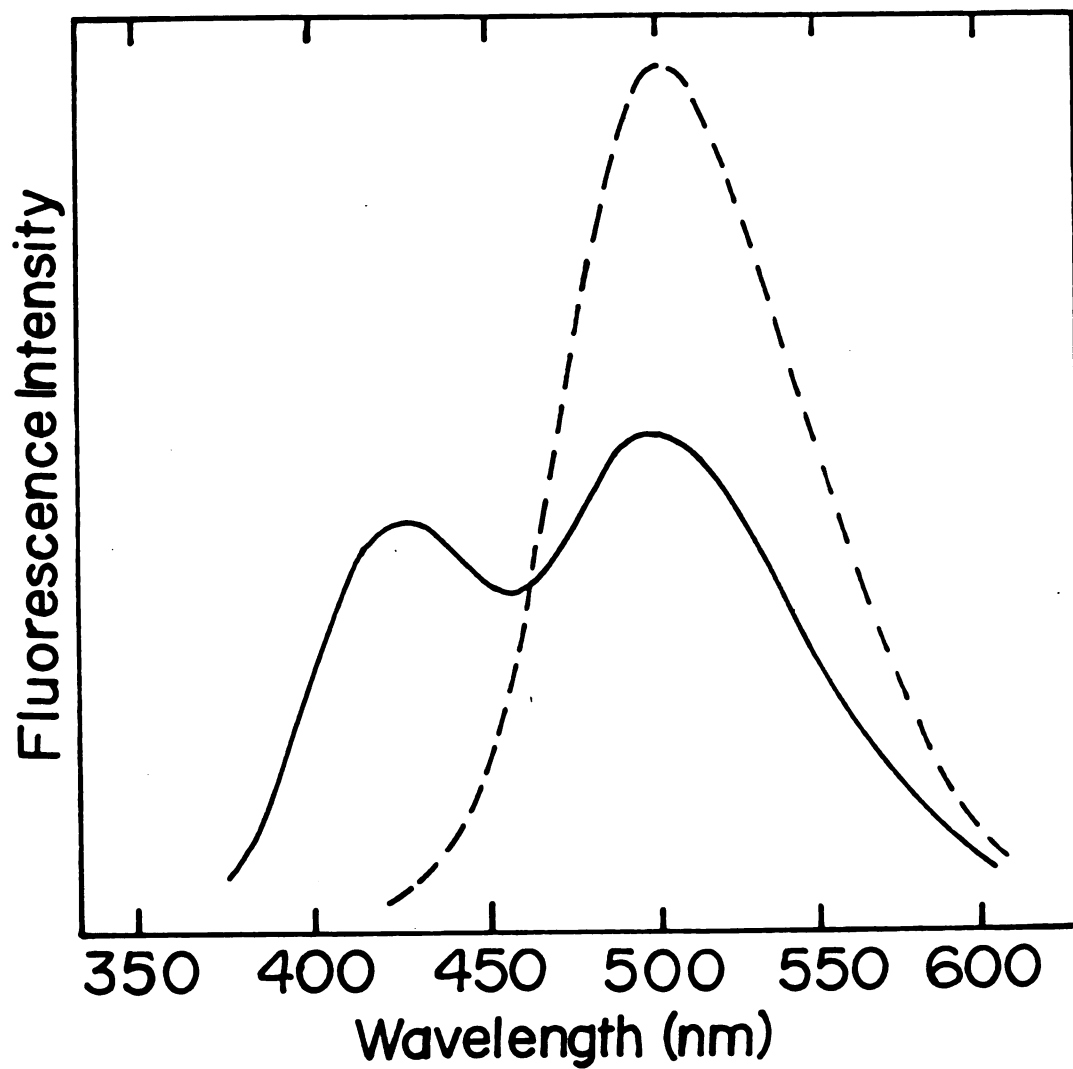


Figure 16. Room temperature emission spectra of a dilute solution (5×10^{-5} M) of compound I in water at different excitation wavelengths, $\lambda_{\text{exc}} = 320$ nm (—) and $\lambda_{\text{exc}} = 380$ nm (----).

intramolecular excited-state proton transfer will occur resulting in the formation of the bipolar form which emits at 506 nm in this solvent, Figure (17). In Table (3), emission band maxima observed in different media are summarized together with the corresponding emitting species.

In compound II, 2-methoxybenzaldehyde, the phenolic proton is replaced by a methyl group and hence it cannot undergo proton transfer. Figure (18) shows its room temperature emission spectrum in 3MP, ethanol, and water. In 3MP an emission band at 350 nm was observed, this corresponds to the neutral form. In ethanol, a single emission band appears at 376 nm. This band is blue shifted compared to the emission band of the neutral form of compound I observed at 426 nm. Such a large shift is attributed to the fact that in compound I the phenolic proton is hydrogen bonded to ethanol and such hydrogen bond becomes stronger in the excited state, in compound II this hydrogen bond is absent. In water, the larger dipole moment of water compared to that of ethanol led to further stabilization of the excited state resulting in a red shifted emission band in water at 440 nm. It is possible also that the 440 nm band in H₂O is due to a cation formed by an excited-state proton transfer to the carbonyl oxygen.

The emission spectra of ethanolic solutions of compound III, 2-hydroxyacetophenone, at room temperature and 77°K are shown in Figure (19). Intermolecular excited-state

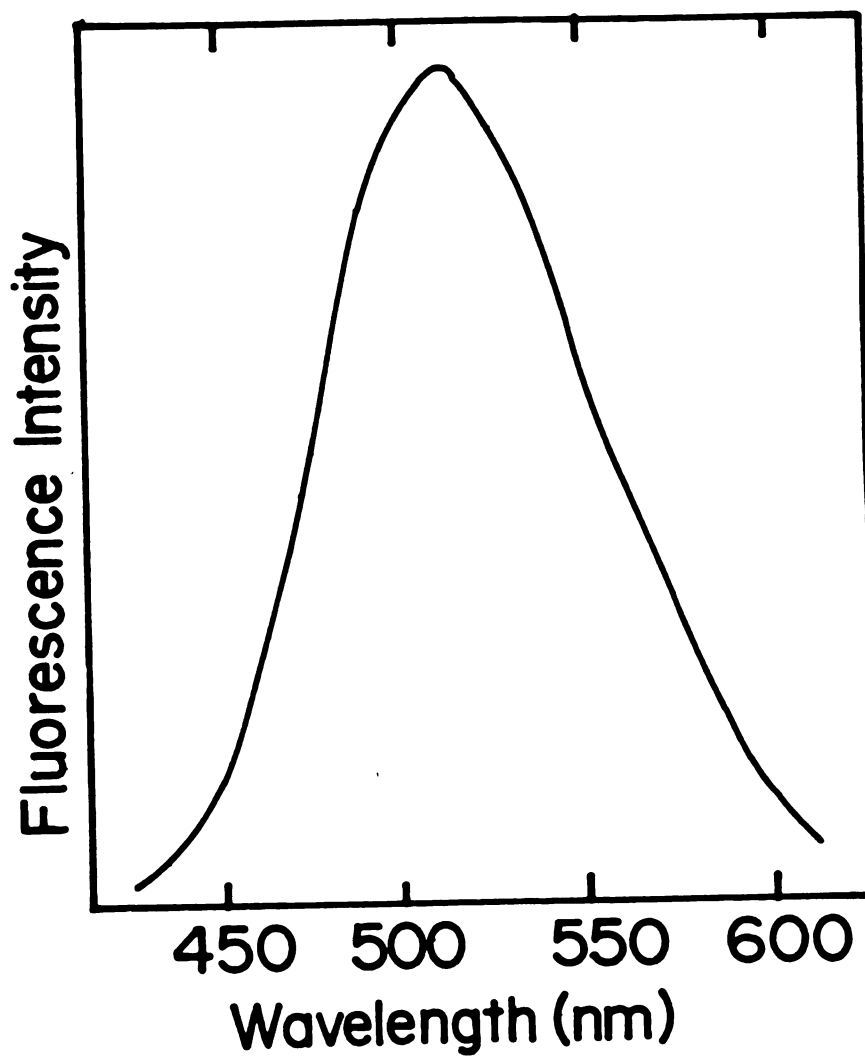
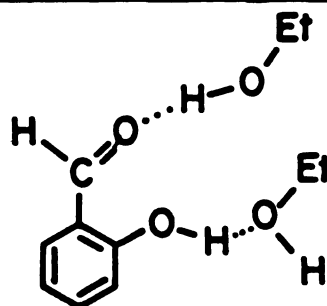
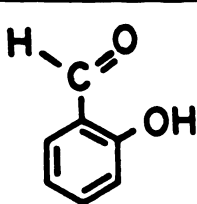
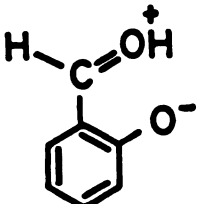
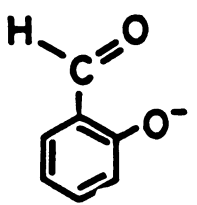
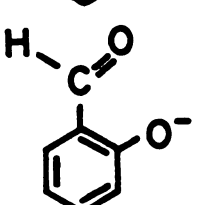
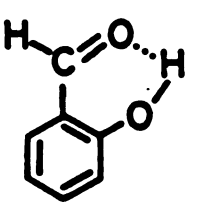
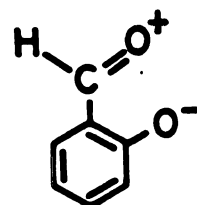
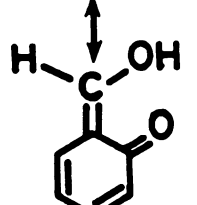
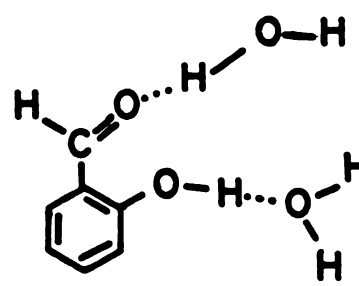
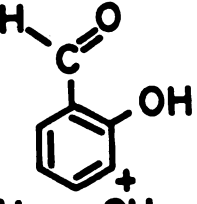
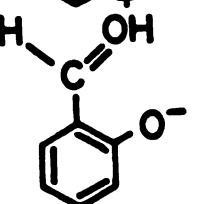


Figure 17. Room temperature emission spectra of dilute solution (5×10^{-5} M) of compound I in 3MP
 $\lambda_{\text{exc}} = 320$ nm.

Table 3. Emission Spectra of Compound I in Different Media.

Medium	Ground State Species	Excited State Species	Fluorescence max. (nm)
Ethanol			426
			500
Ethanol/ NaOH			490
3MP		 ↕ 	506
H ₂ O			428
			500

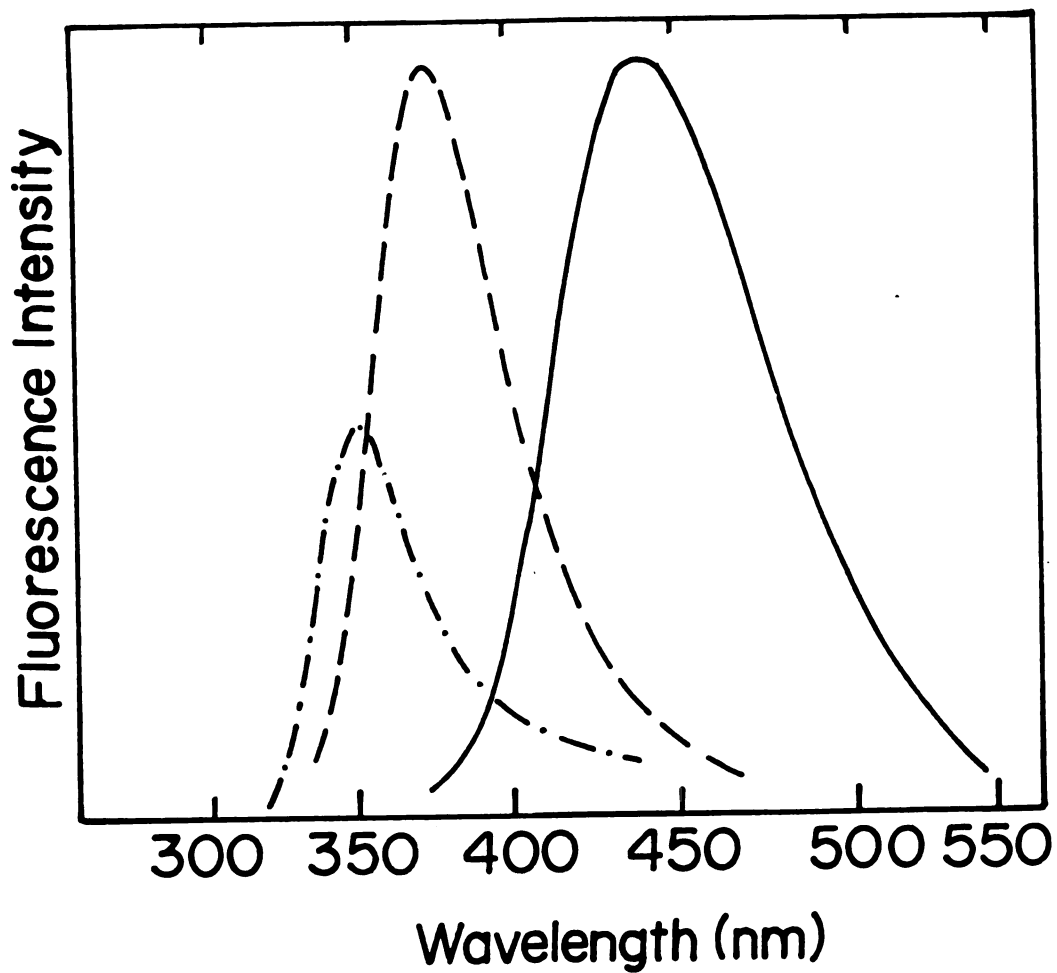


Figure 18. Room temperature emission spectra of dilute solutions (5×10^{-5} M) of compound II, $\lambda_{exc} = 320$ nm in 3MP (-·-·-·), ethanol (----) and water (—).

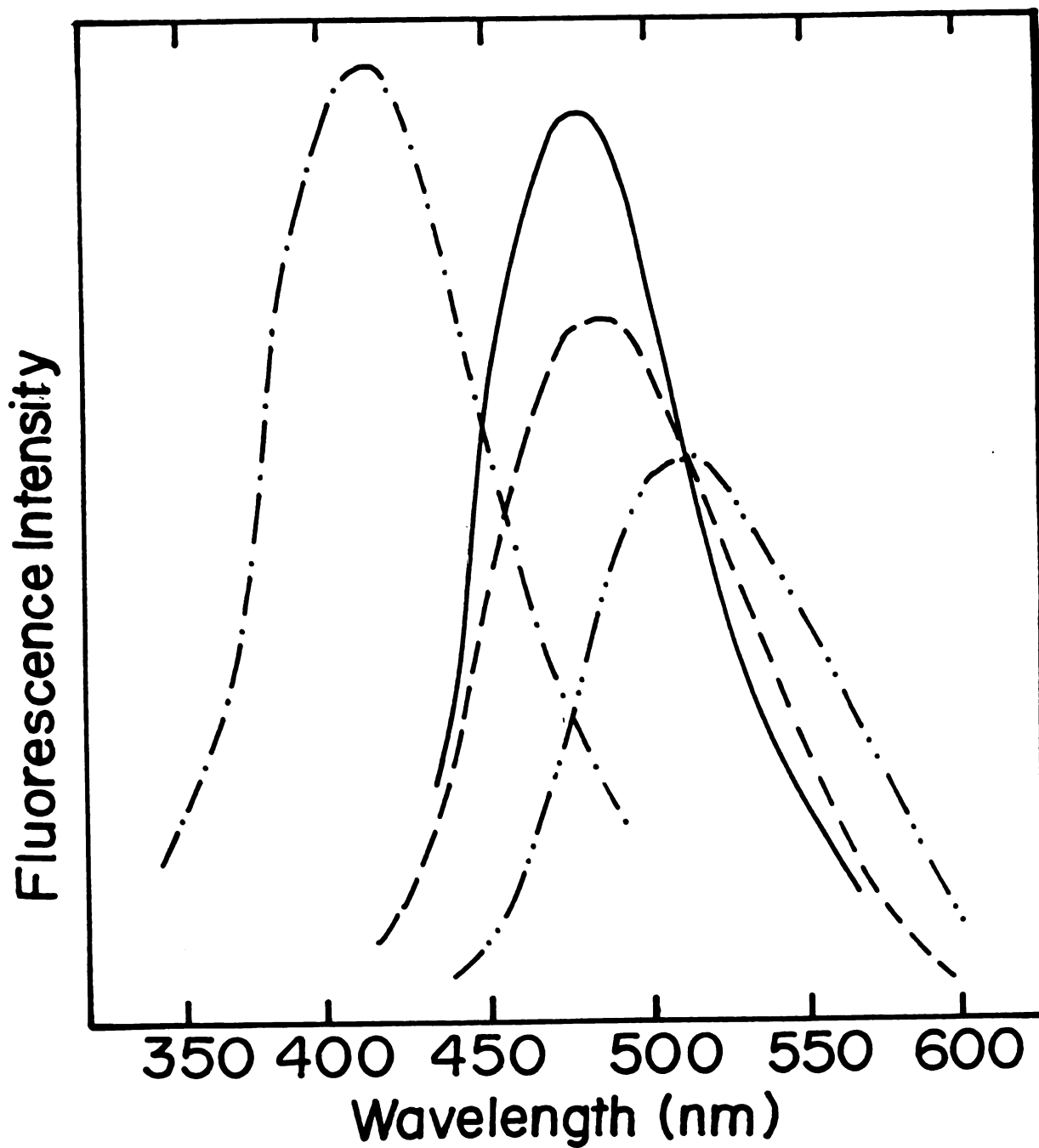


Figure 19. Emission spectra of dilute solutions (5×10^{-4} M) of compound III in ethanol; neutral solution ($\lambda_{exc} = 320$ nm) at room temperature (-·-·-·-) and 77°K (----); alkaline solution ($\lambda_{exc} = 380$ nm) at room temperature (—) and 77°K (-·-·-·).

proton transfer in the neutral solution of compound III in ethanol gives an emission band at 512 nm. The small red shift of this emission band when compared with that of compound I, which occurs at 500 nm, may be attributed to a higher basicity of the carbonyl oxygen in compound III. In an alkaline solution, the 478 nm band is assigned to the anion emission. This band is blue shifted when compared with the emission of the anion of compound I. This is probably due to the lack of planarity of the carbonyl group in the case of compound III anion. At 77°K, the emission of the bipolar form occurs at 475 nm and that of the anion at 414 nm, these blue shifts compared with the corresponding emission maxima in ethanol at room temperature is due to the freezing of solvent relaxation in rigid ethanol at 77°K. The emission of compound III in water is shown in Figure (20), the bipolar form emits at 512 nm and the anion emission occurs at 490 nm. The results in water are similar to those observed in ethanol, small red shifts in water are attributed to its larger dipole moment. In 3MP where intramolecular hydrogen bonding occurs, compound III gives rise to an emission band at 500 nm corresponding to the bipolar form resulting from an intramolecular excited-state proton-transfer.

In compound IV, 4,6-dimethyl-2-hydroxyacetophenone, the repulsion between the acetyl methyl group and the substituted methyl group in position 6- forces the acetyl

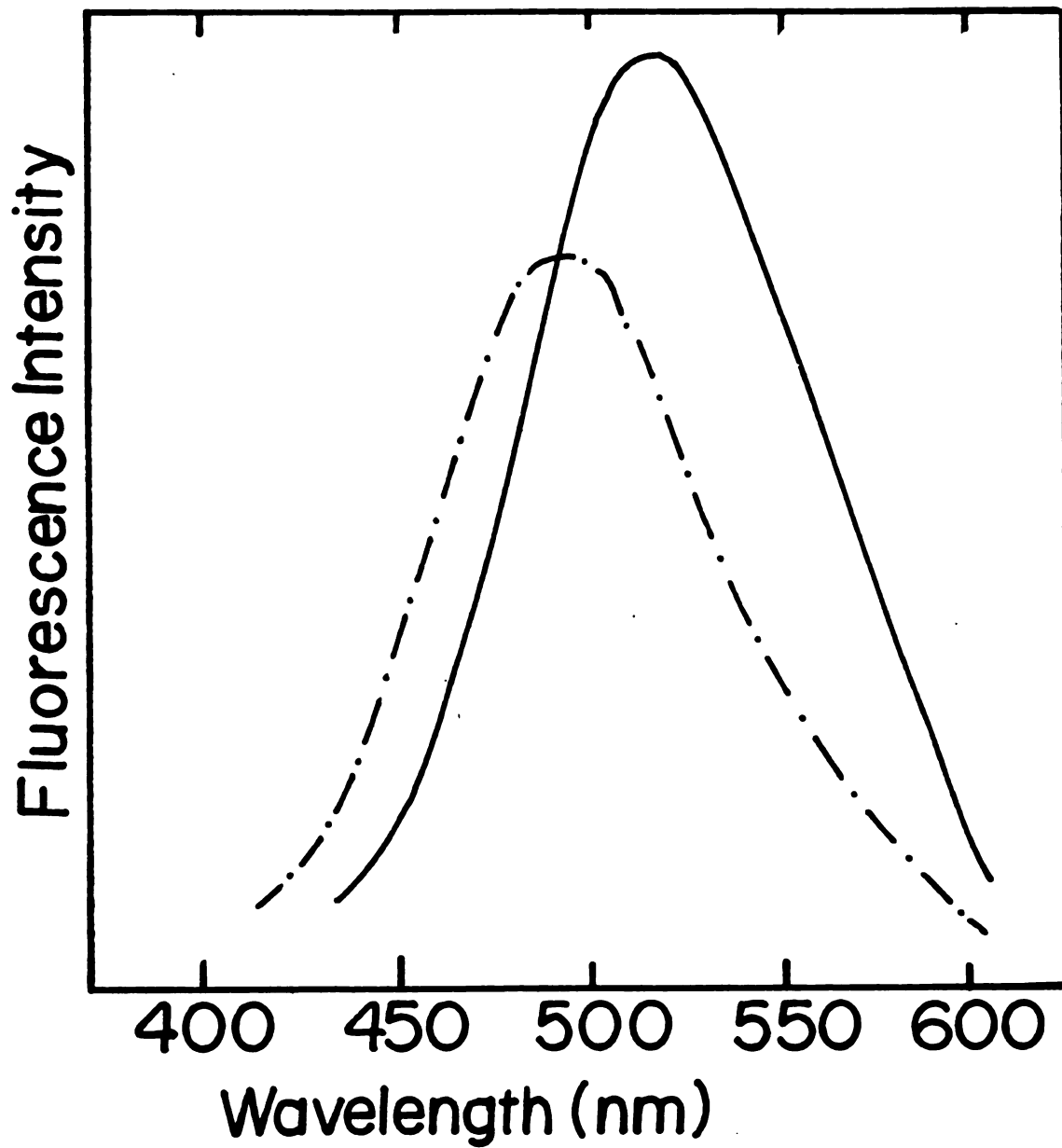


Figure 20. Room temperature emission spectra of dilute solutions (5×10^{-5} M) of compound III, in aqueous solution, $\lambda_{exc} = 320$ nm (—), and in alkaline aqueous solution, $\lambda_{exc} = 340$ nm (-·-·-·).

group to be out of plane with respect to the benzene ring. These steric effects manifest themselves in the absorption spectra as discussed before. The steric effect is expected to be more pronounced in protic solvents where intermolecular hydrogen bonds with solvent molecules are found. In nonpolar solvents like 3MP absorption spectra indicate that the molecule assumes a nearly planar structure through an intramolecular hydrogen bonding between the phenolic and carbonyl groups. In 3MP compound IV exhibits two emission bands, one at 503 nm corresponding to the bipolar form and a shoulder at 440 nm corresponding to the neutral form as shown in Figure (21). The appearance of the neutral form emission is probably due to the existence of a ground-state equilibrium between intramolecularly hydrogen bonded species and species that are not hydrogen bonded, the latter cannot undergo excited state proton transfer. Figure (22) shows the room temperature emission spectra of compound IV in ethanol, an emission band observed at 422 nm is attributed to a non planar neutral molecule; no proton transfer occurs in the excited state in neutral ethanol. Band maxima of the emission spectra of compound I-IV in ethanol, water and 3MP are summarized in Tables (4) and (5).

Pyridoxal phosphate dependent enzymes exhibit absorption bands around 415 nm and at 335 nm. The studies made with simple model compounds have shown that the 415 nm band is due to a Schiff base with structure [1], bipolar form, which is stable in polar media (hydrophilic media). The

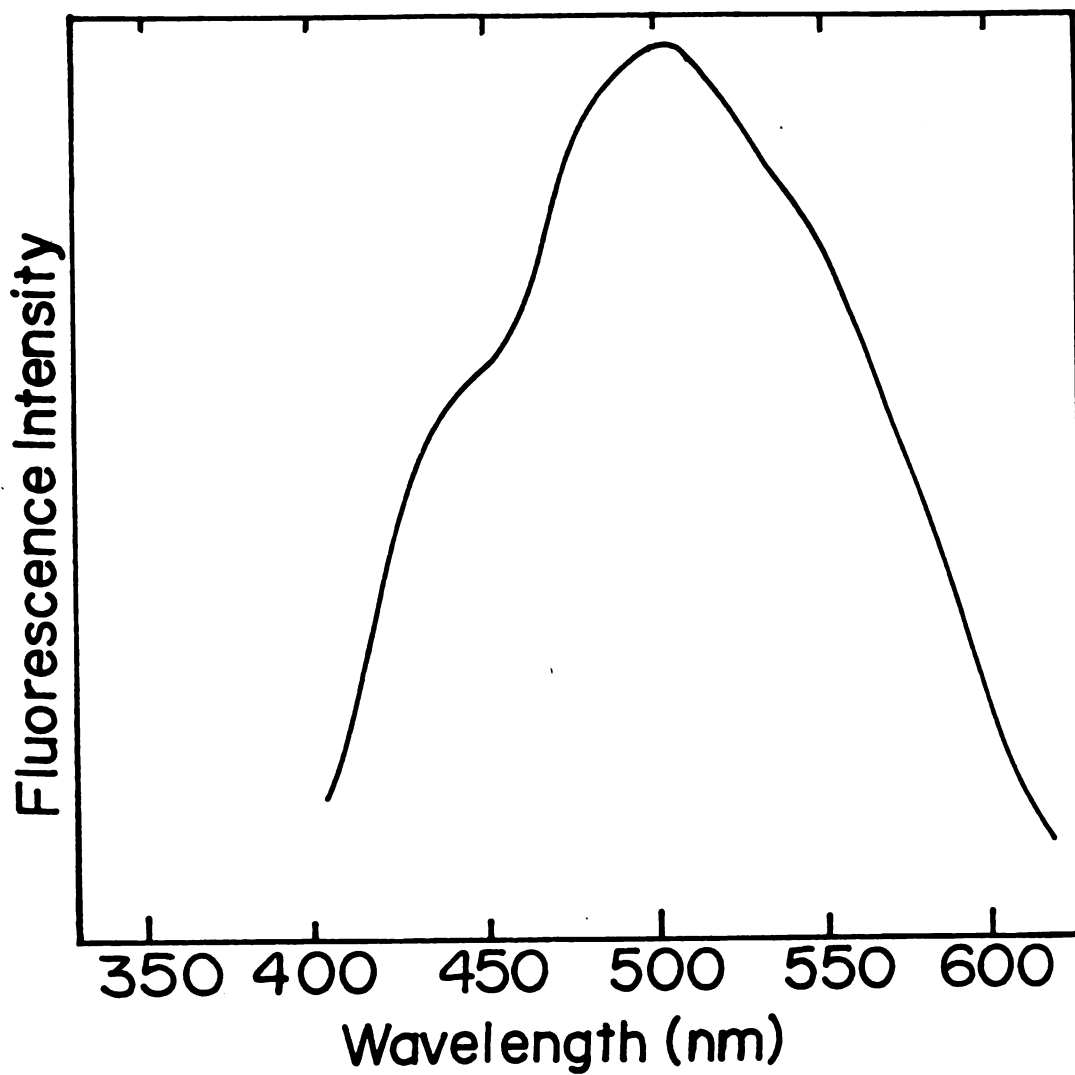


Figure 21. Room temperature emission spectra of a dilute solution of compound IV in 3MP at $\lambda_{\text{exc}} = 320$ nm.

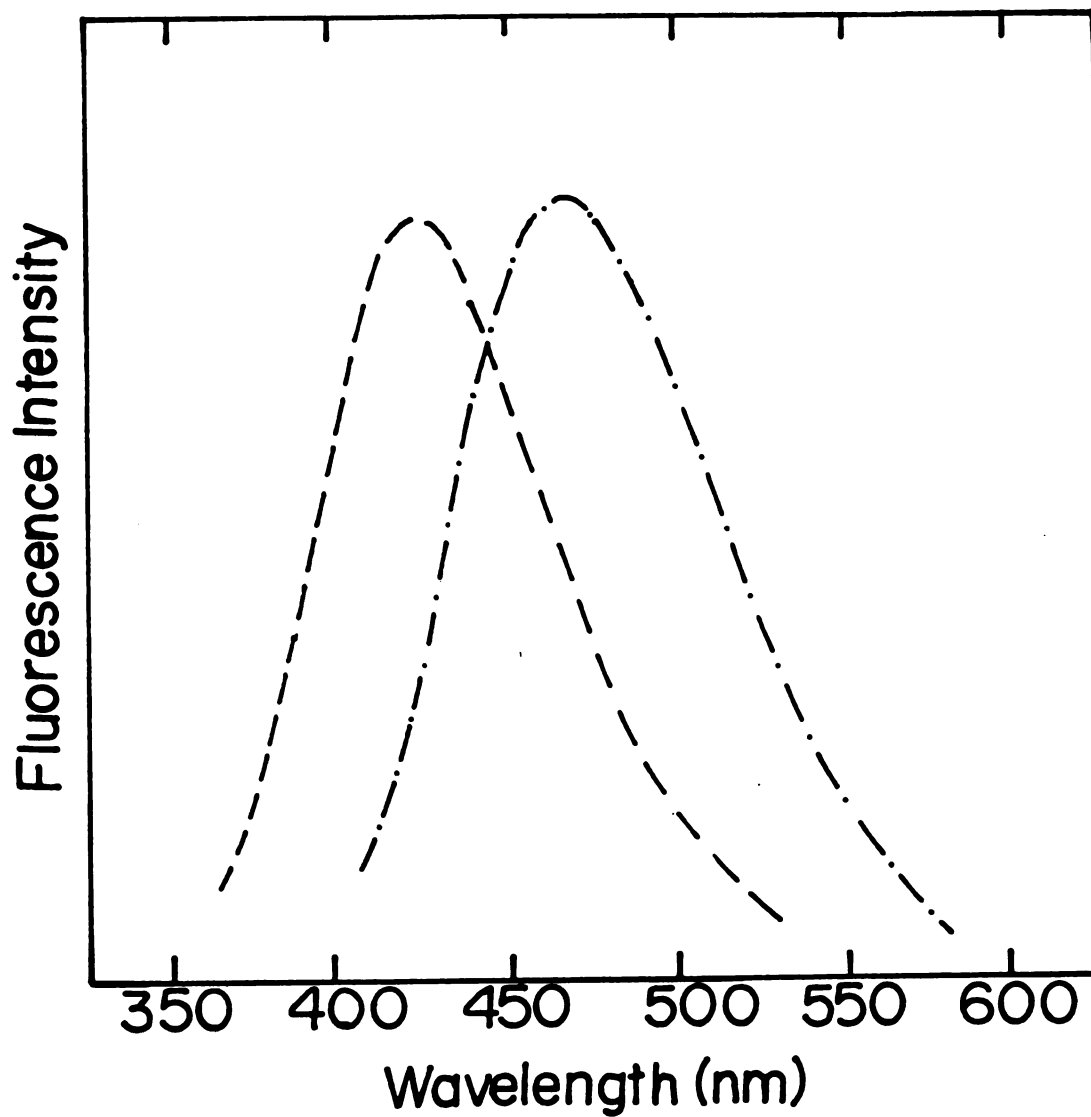


Figure 22. Room temperature emission spectra of dilute solutions (5×10^{-4} M) of compound IV, $\lambda_{\text{exc}} = 330$ nm, in ethanol (----) and in alkaline ethanol (-·-·-·-·).

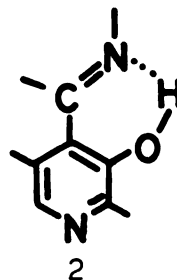
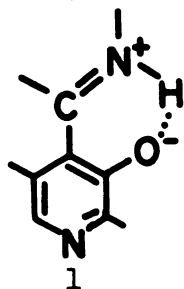
Table 4. Emission Spectra of Compounds (I-IV) in Ethanol and 3MP.

Compound	Ethanol		Ethanol/NaOH		3MP		
	RT	77°K	RT	77°K	RT	77°K	
	λ (nm)	λ (nm)	λ (nm)	λ (nm)	λ (nm)	λ (nm)	
	neutral bipolar						
I	426	500	431	490	434	506	506
I							
II	376		450			350	450
III		512	475	478	414	500	485
IV	422		430	468		505	503

Table 5. Emission Spectra of Compounds (I-IV) in Water.

Compound	H ₂ O λ (nm)	H ₂ O/NaOH λ (nm)
I	428 505	500
II	440	440
III	512	490
IV	437	422

335 nm band was assigned to structure [2], nonpolar form⁽²⁶⁾, which is stable in nonpolar media (hydrophobic media). Accordingly, the ratio between the absorbance of these two



bands can be used as a measure of the polarity experienced at the pyridoxal chromophore's site⁽²⁷⁾.

Solvent effects on the emission spectra of PLP-model compounds should also be helpful in interpreting enzyme emission data and predicting the microenvironment that the pyridoxal moiety experiences at the active site of the enzyme i.e., whether the site is a hydrophilic or hydrophobic in character. For example, glycogen phosphorylase contains one PLP molecule per protein subunit, PLP is very tightly attached to the protein through a Schiff base bond with an ϵ -amino group of a lysine residue of the protein⁽²⁸⁾. In the pH range of 5.0 to 9.5, at which the enzyme is stable, two absorption bands due to PLP are observed with peaks at 333 and 425 nm⁽²⁹⁾. These two absorption bands indicate that an equilibrium exists between the enolimine and ketoenamine forms and the active site is not hydrophilic. The enzyme shows two emission bands: one occurs at 335 nm and corresponds to the emission of

tryptophane residues in the protein; the other band at 535 nm corresponds to the emission of the ketoenamine form of PLP^(30,31). In the excited state the keto-enol equilibrium is completely shifted towards the ketoenamine form. For model systems, n-butylamine, valine, or n-hexylamine-PLP in various solvents, the observed properties of Schiff bases are very different. The Schiff base of PLP-n-butylamine in aqueous solution and the Schiff base PLP-valine in DMF exhibit two emission bands: one occurs at 510 nm from the ketoenamine form absorbing at 410 nm; the second emission at 430 nm occurs from the enolimine form which absorbs at 325 or 333 nm⁽³²⁾. In polar solvents, excitation of the enolimine form at 325 nm resulted in an emission from the ketoenamine form indicating that proton transfer occurred in the excited state. In hydrogen-accepting solvents like dioxane, the two emissions were observed from the n-butylamine Schiff base. These results can be summarized in Figure (23). In non polar solvents the ground state equilibrium is shifted towards form [1], whereas, in the excited state it is shifted towards form [2]*⁽³²⁾.

In contrast to the nitrogen hetero-atom, the phenolic group plays a major role in the spectral behavior of Schiff bases of aromatic ortho-hydroxy aldehydes. Transfer of the phenolic proton causes tautomerism in the ground state and phototautomerism in the excited state.

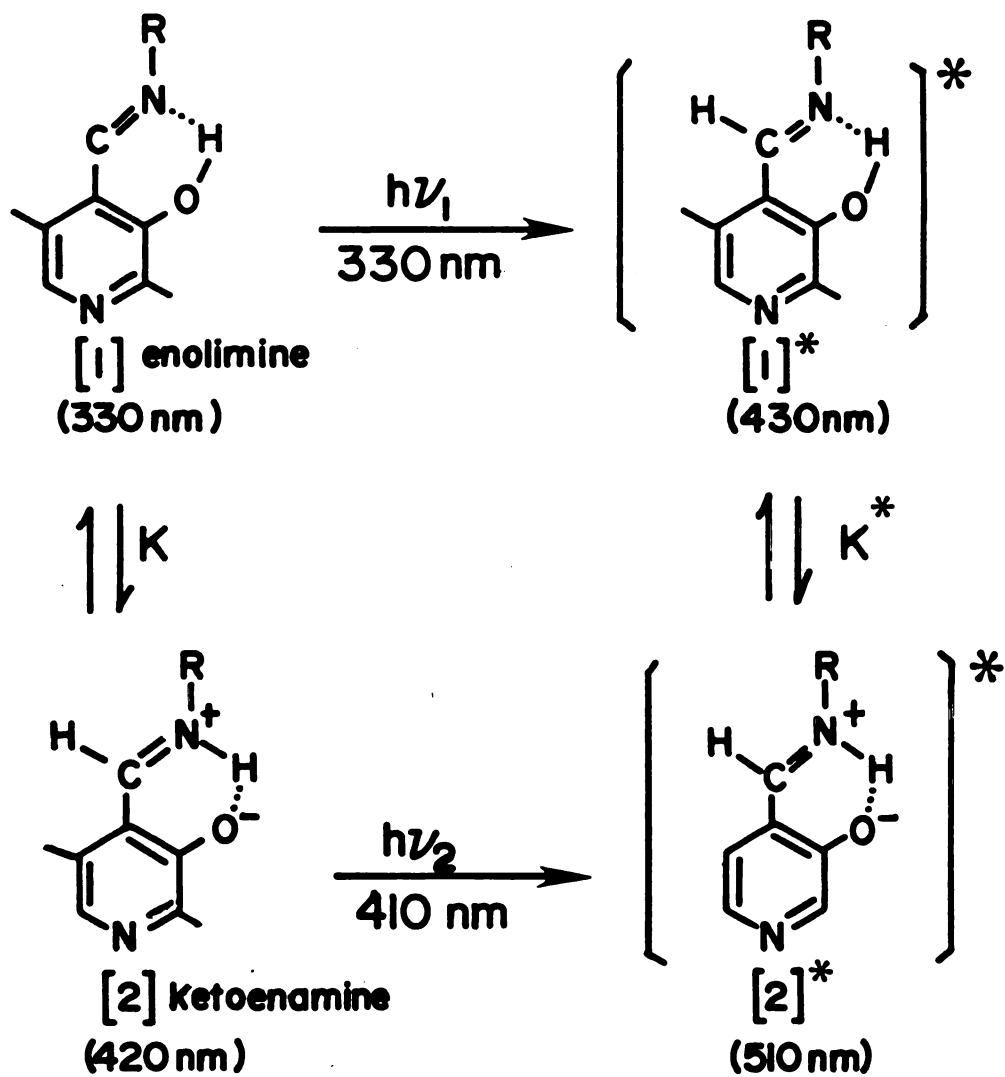


Figure 23. Absorbing and emitting species in PLP-Schiff base systems. 32

Blocking of the hydroxyl group thus dramatically modifies the absorption and emission properties characteristic of these Schiff bases⁽³³⁾. Thus Schiff bases of o-methoxybenzaldehyde is expected to show little resemblance to the optical and luminescence properties of the Schiff bases of the corresponding o-hydroxybenzaldehyde. The spectral properties of PLP-model compounds depend on whether the phenolic group forms a hydrogen bond with the azomethine nitrogen of the Schiff base or with solvent molecules. These considerations lead to our choice of the model compounds that we have studied.

Room temperature emission spectrum of compound I-b in ethanol is shown in Figure (24). Two emissions were observed when the neutral solution was excited at 320 nm where the enolimine form absorbs. The shorter-wavelength emission with a peak at 425 nm corresponds to an emission from the enolimine form and the longer-wavelength emission at 500 nm corresponds to an emission from a ketoenamine form. Excitation at 420 nm where the ketoenamine form absorbs gave only the longer-wavelength emission at 500 nm. In acidic ethanolic solution, Figure (25), an emission from the cationic form was observed at 472 nm. An alkaline solution of compound I-b in ethanol gave an emission at 510 nm when excited at 380 nm where the anion absorbs, this emission belongs to the anion form.

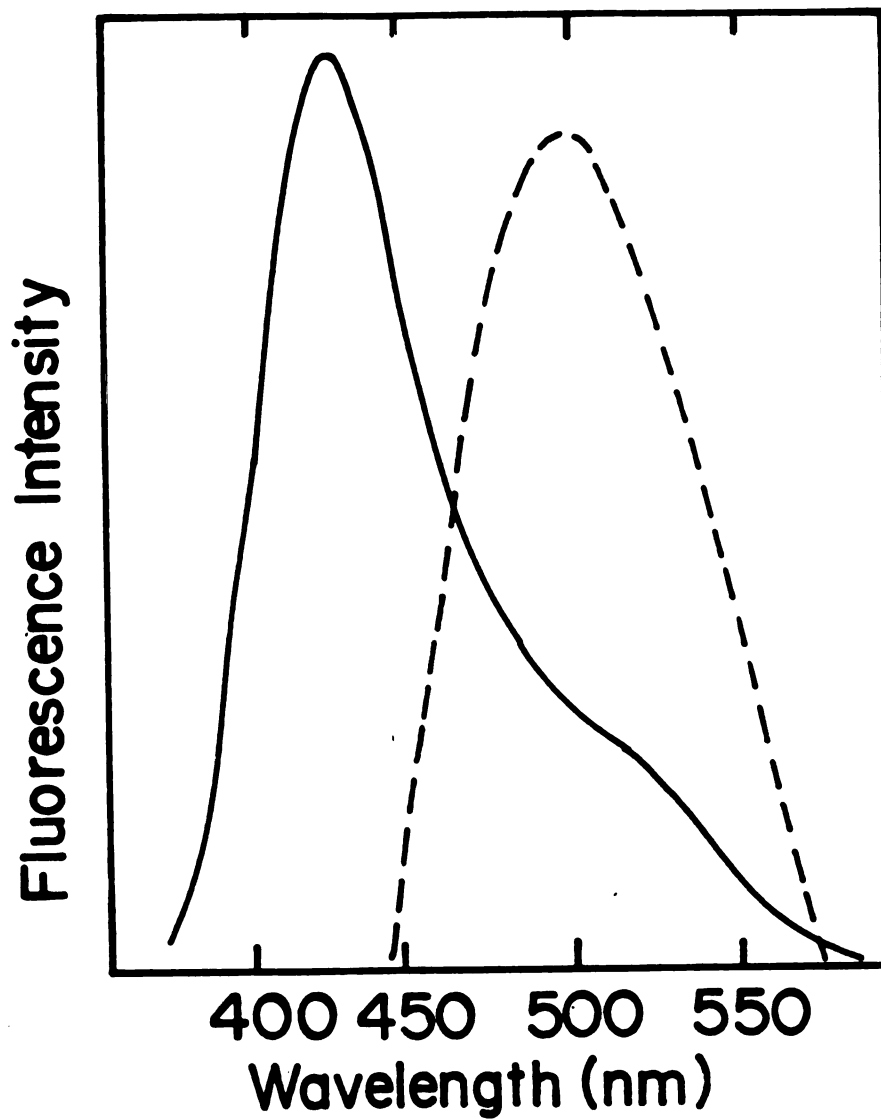


Figure 24. Room temperature emission spectra of a dilute solution (5×10^{-5} M) of compound I-b in ethanol at different excitation wavelengths: $\lambda_{\text{exc}} = 320$ nm (—), and $\lambda_{\text{exc}} = 380$ nm (----).

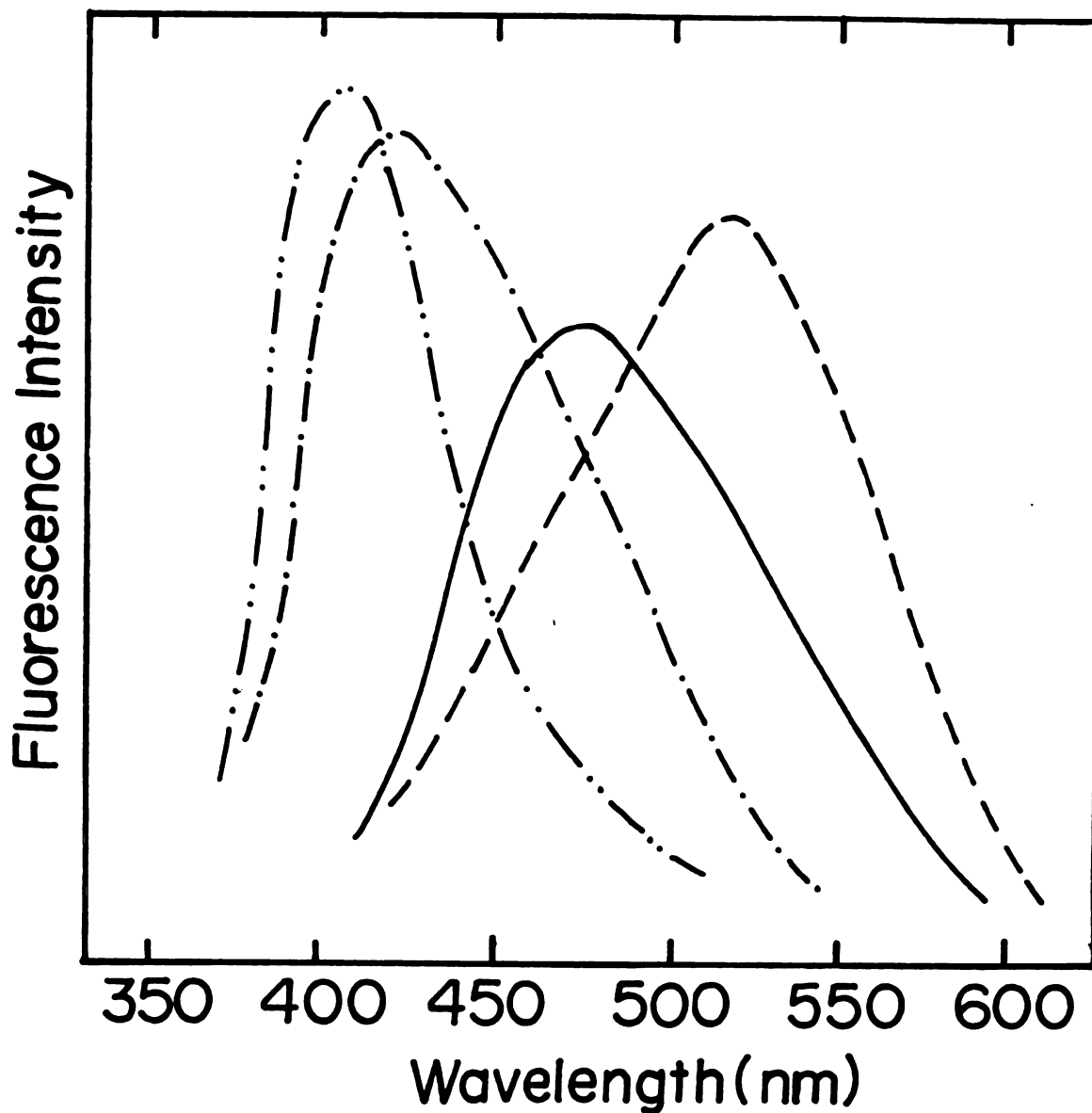


Figure 25. Emission spectra of dilute solutions (5×10^{-5} M) of compound I-b in ethanol at both room temperature and 77°K : alkaline solution $\lambda_{\text{exc}} = 380$ nm at room temperature (----) and at 77°K (-·-·-·-·-), acidic solution $\lambda_{\text{exc}} = 330\text{-}380$ nm at room temperature (—) and at 77° (-·-·-·-·-).

Emission in both acidic and alkaline solutions were blue shifted to 415 and 408 nm respectively at 77°K because of the lack of solvent relaxation. Room temperature emission spectra of compound I-v in ethanol are shown in Figure (26). Excitation at 320 nm led to an emission from the enolimine form at 450 nm, whereas, excitation of the ketoenamine form at 400 nm gave an emission at 495 nm. In acidic solution, an emission at 480 nm was observed as a result of the cation form excitation at 365 nm. In alkaline solution, excitation of the anion form gave an emission peak at 500 nm.

In compounds II-b and II-v, there is no phenolic proton. The emission spectra of compound II-b in ethanol are shown in Figure (27). Excitation of the neutral ethanolic solution at 300 nm resulted in two emission peaks. The first peak at 366 nm corresponds to the neutral form, and the second at 450 nm was assigned to an emission from a cationic form where the azomethine nitrogen accepts a proton from the solvent. This assignment was confirmed by studying the emission in acidic ethanol shown also in Figure (27). These results indicate that the basicity of the azomethine nitrogen is apparently greatly enhanced in the excited state. Figure (28) shows the emission spectra of a dilute solution of compound II-v in dioxane and ethanol. Emission from the neutral form was observed in dioxane at 352 nm. The 450 nm emission in neutral ethanol

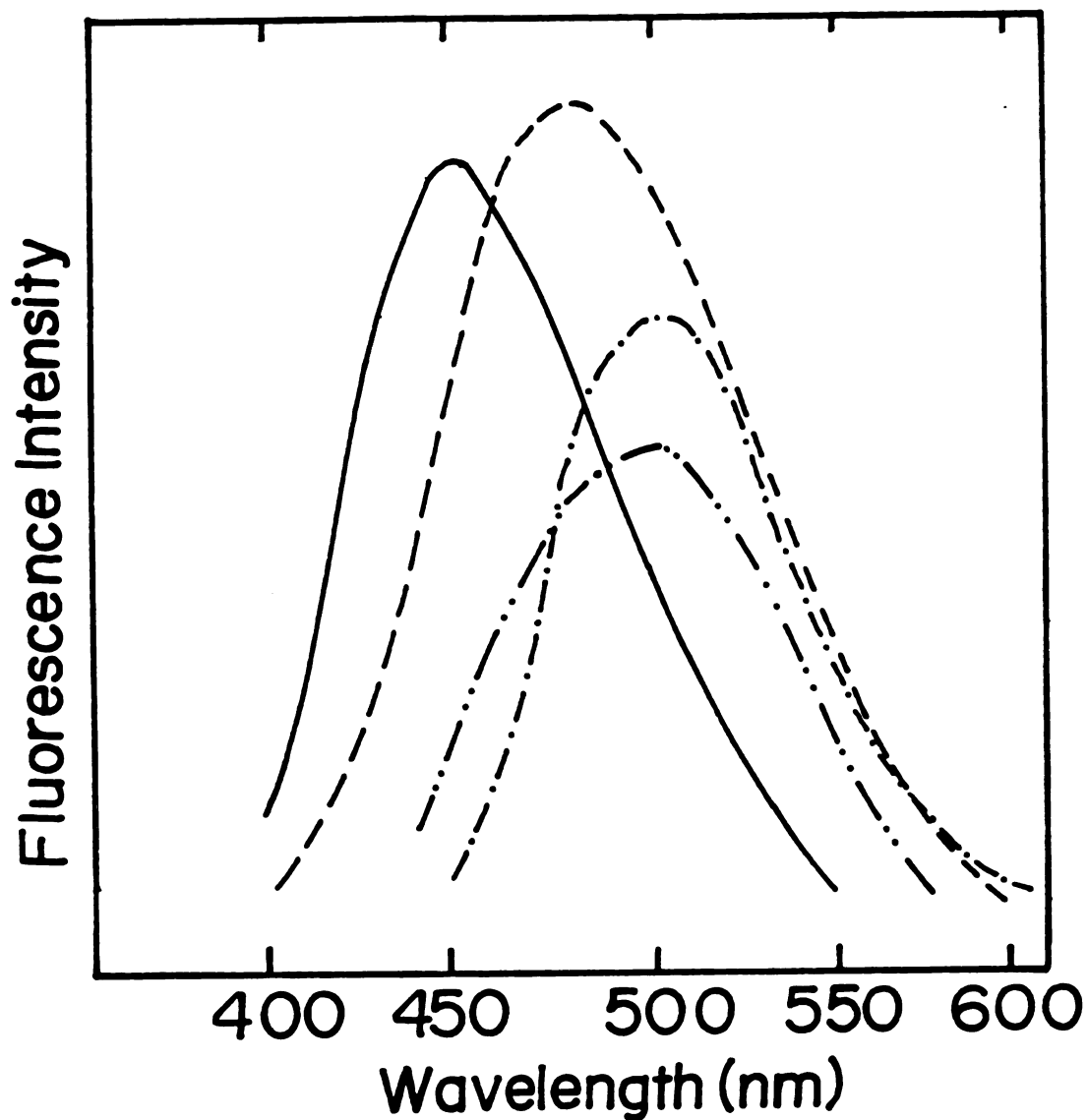


Figure 26. Room temperature emission spectra of dilute solutions (5×10^{-5} M) of compound I-v in ethanol: in neutral solution $\lambda_{\text{exc}} = 320$ nm (—) and $\lambda_{\text{exc}} = 400$ nm (-·-·-), in acidic solution $\lambda_{\text{exc}} = 365$ nm (----), and in alkaline solution $\lambda_{\text{exc}} = 360$ nm (-·-·-).

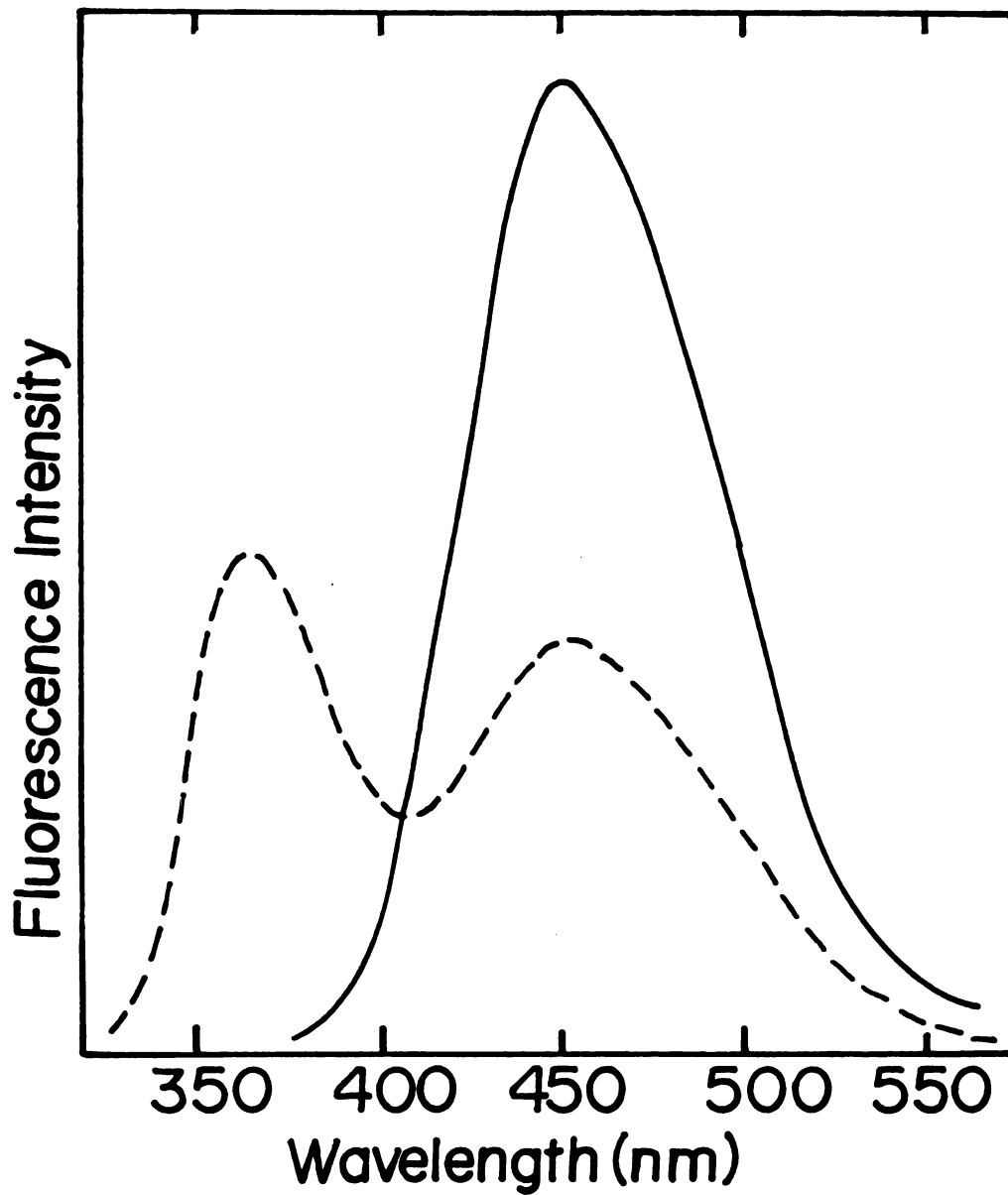


Figure 27. Room temperature emission spectra of dilute solution (5×10^{-5} M) of compound II-b in ethanol $\lambda_{\text{exc}} = 300$ nm (—) and in acidic ethanol $\lambda_{\text{exc}} = 350$ nm (----).

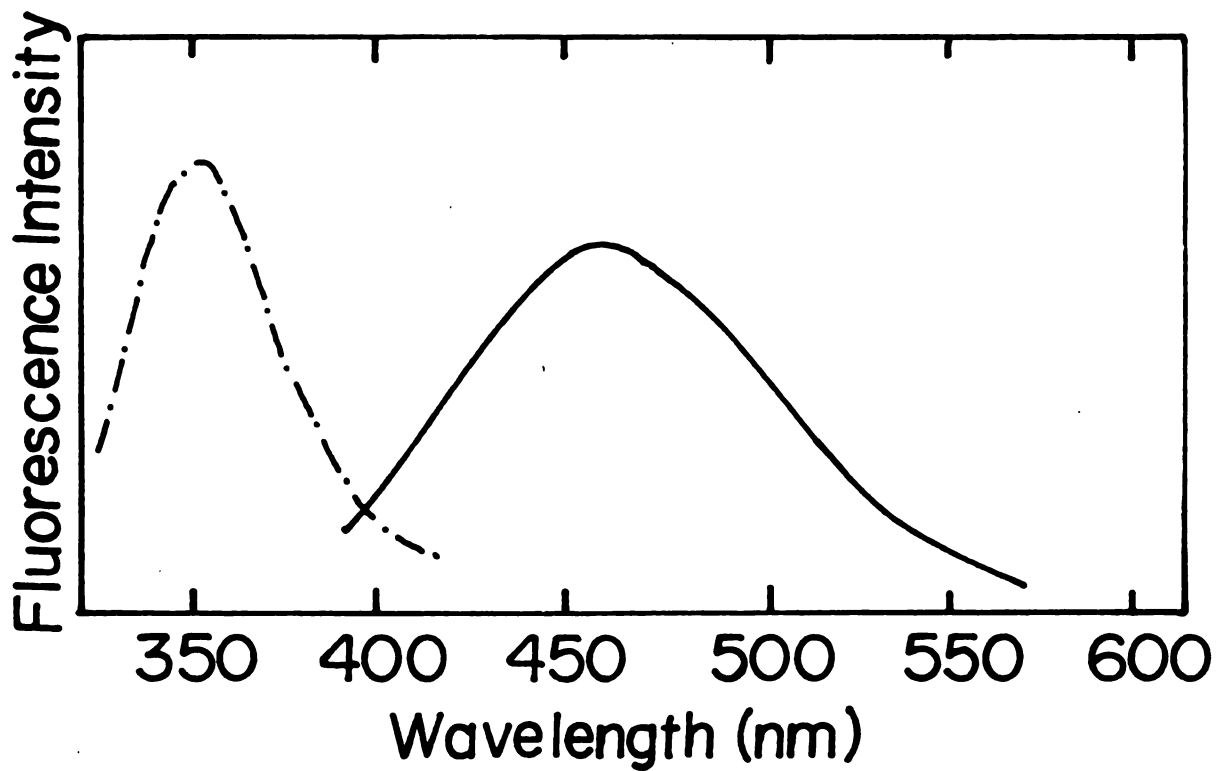


Figure 28. Room temperature emission spectra of dilute solutions (5×10^{-5} M) of compound II-v in dioxane (---) and in ethanol (—) $\lambda_{exc} = 320$ nm.

which results from excitation of the neutral form at 320 nm can be interpreted as resulting from a cation form obtained by proton transfer from solvent to the azomethine nitrogen.

Room temperature emission spectra of compound IV-b in neutral, acidic and alkaline solutions in ethanol are displayed in Figure (29). Excitation of the neutral form at 320 nm produced a broad emission with a peak at 415 nm, this band is probably a composite band consisting of emission of the neutral form at 415 nm and an emission at \sim 460 nm due to the anion emission. In acidic solution, the cation emits at 450 nm whereas, in alkaline solution the anion emits at 465 nm. In the corresponding valine Schiff base, compound IV-v, excitation of the neutral solution at 320 nm results, Figure (30), in a broad emission which can also be considered as a combination of two bands: the first around \sim 420 nm which corresponds to the neutral form emission and the second at \sim 465 nm which corresponds to the anion form. In acidic solution an emission peak was observed at 435 nm. In alkaline solution, the emission of the anion form was observed at 463 nm. The lack of excited-state proton transfer in the case of compound IV and its Schiff bases IV-b and IV-v demonstrates the lack of planarity in these molecules because of steric effects.

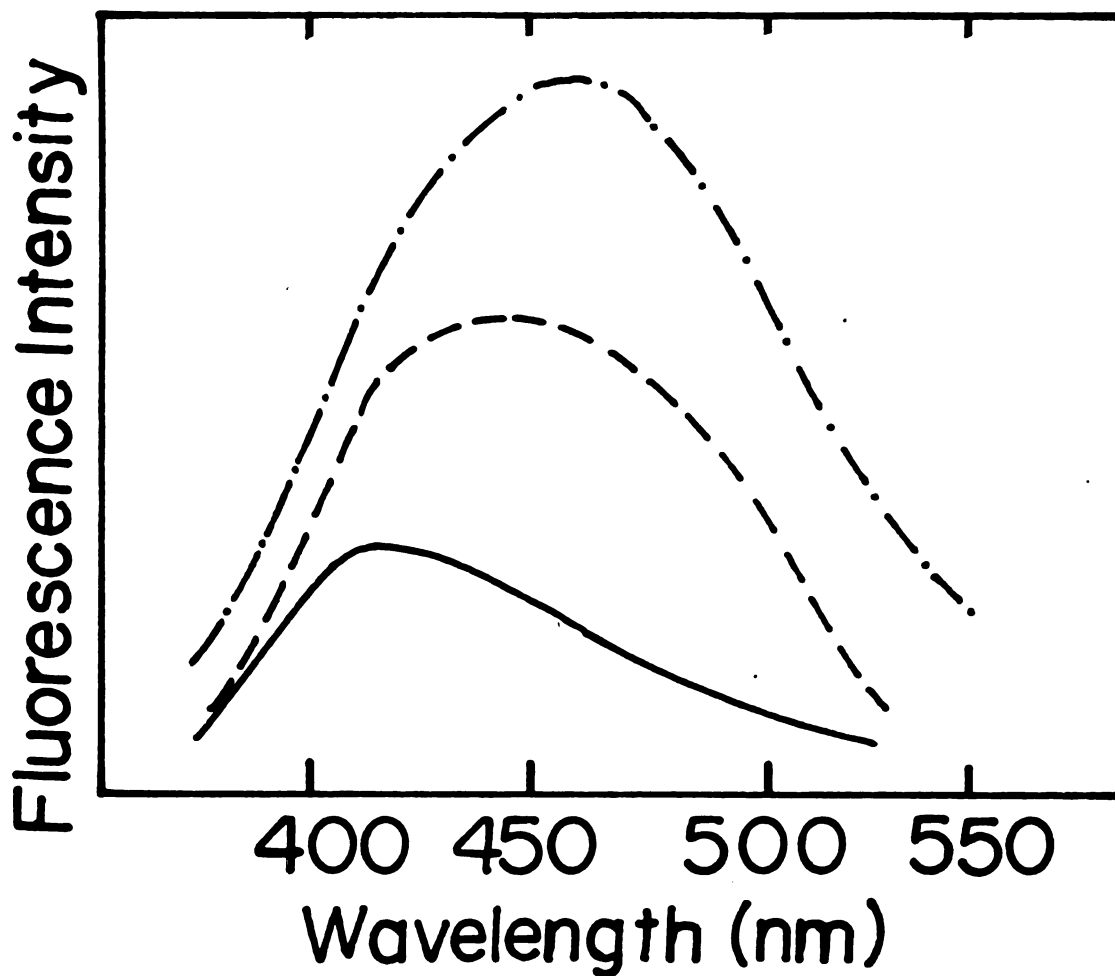


Figure 29. Room temperature emission spectra of dilute solutions (5×10^{-4} M) of compound IV-b in ethanol: neutral solution, $\lambda_{exc} = 320$ nm (—), acidic solution $\lambda_{exc} = 320$ nm (----) and alkaline solution $\lambda_{exc} = 360$ nm (-·-·-·-·).

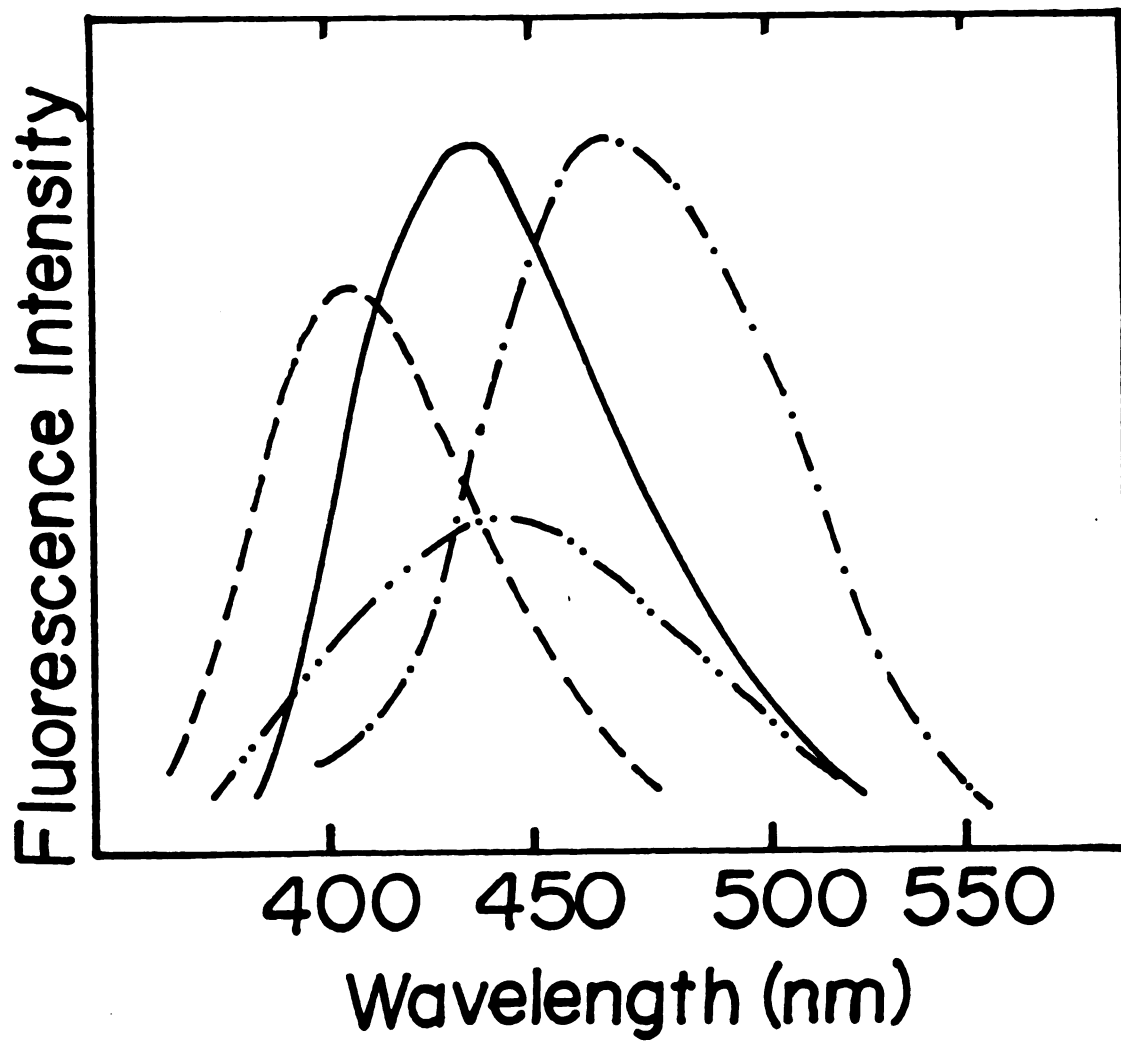


Figure 30. Room temperature emission spectra of dilute solutions (5×10^{-4} M) of compound IV-v, $\lambda_{\text{exc}} = 320$ nm in: ethanol (-·-·-·-·-), alkaline ethanol (-·-·-·-·-), acidic ethanol (—) and in dioxane (·-·-·-·-·-).

CHAPTER IV

ABSORPTION AND EMISSION STUDY OF THE ASSOCIATION OF MONOVALENT CATIONS WITH PHENOXIDE AND SALICYLALDEHYDE ANIONS

I. Introduction

The presence of a metal atom as an essential constituent of some enzymes, and the metal ion requirement of others for maximum activity, provide an obvious link between enzymatic reactions and coordination chemistry. The possible functions of metal ions in enzyme substrate systems are easily visualized⁽³⁴⁾ as follows:

(i) The metal may form a complex with donor atoms of either the enzyme or substrate and thereby enhance their tendency towards reaction;

(ii) It may serve merely as a bridge through common coordination to bring the enzyme and substrate into proximity;

(iii) While serving function (ii) it may provide as well a chemical activating influence; and

(iv) While coordinated to either the enzyme or substrate it may appropriately orient groups undergoing reaction.

The most obvious property of a metal ion is its positive charge which makes it effectively a Lewis acid, and it will have a tendency to withdraw electrons from atoms and groups to which it is attached. The catalytic efficiency will depend on the effective charge of the metal ion.

Monovalent Cation Interactions

All tryptophanases so far examined require NH_4^+ or K^+ , and the concentration required for half-maximum activity (NH_4^+ , 2-6 mM; K^+ , 8-20 mM) is similar for each enzyme⁽²⁾. Na^+ and Li^+ are essentially without activating effects in each case, but they inhibit the E.coli enzyme when added together with NH_4^+ or K^+ ⁽³⁾. At optimal concentrations, NH_4^+ permits a level of activity at least equal to and usually slightly greater than K^+ , Rb^+ also activates but less effectively than K^+ ⁽⁴⁾. Tl^+ also replaces K^+ for the E. coli enzyme and has a greater affinity (0.35 mM gives approximately half-maximum activity⁽³⁵⁾).

Equilibrium dialysis studies showed that apotryptophanase binds one mole of pyridoxal phosphate per 57,500 grams of protein⁽³⁶⁾, that is four pyridoxal phosphate molecules per molecule of native tetrameric enzyme (molecular weight 220,000). K^+ and Na^+ are equally effective in permitting the dissociation of tetrameric to dimeric apotryptophanase at low temperature⁽³⁷⁾, and it is unlikely therefore, that this effect serves as a basis for their

markedly different catalytic effects. In addition, distinct spectral differences are observed in the presence of K^+ versus Na^+ . Holotryptophanase shows characteristic pH-dependent absorption maxima at 420 and 337 nm in the presence of the catalytically essential K^+ or NH_4^+ ions. At equivalent concentrations of Na^+ or imidazole, only the 420 nm band is formed, Figure (31), at pH 8.0⁽⁵⁾. In the presence of K^+ , at the same pH, the 337 nm band is formed. In the enzymatically inactive form with λ_{max} 420 nm, intramolecular hydrogen-bond between the phenolic group and the azomethine nitrogen was proposed, whereas, in the active form with $\lambda_{max} = 337$ nm, the phenolic group lost its proton⁽⁵⁾. Recent studies^(6,7), using a rapid-scanning stopped-flow absorption technique, of the interconversion between the 420 and 337 nm absorbing species showed that the form absorbing at 337 nm is the inactive form but acts as a reservoir for the active form which absorbs at 420 nm.

The activity as well as the spectroscopic behavior in the presence of K^+ or Na^+ ions demonstrate a difference in the tertiary structure of tryptophanase and in the mode of binding of pyridoxal-p in the two environments that is consistent with a more compact structure and tighter binding of pyridoxal-p in the K^+ environment. This difference is sufficient to explain the requirement for K^+ (or NH_4^+) for catalysis, but does not elucidate the molecular basis for this behavior. In this regard, we have studied the

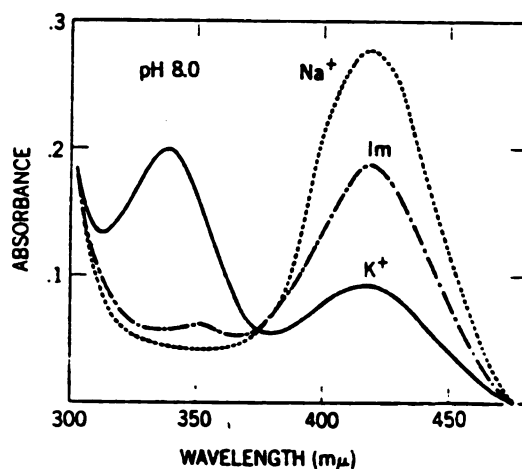


Figure 31. Comparative effects of monovalent cations on the spectrum of holotryptophanase at 21°. Samples contained 2.0 mg of enzyme per 1.0 ml of 0.02 M imidazole-HCl buffer (pH 8.0), 2 mM mercaptoethanol, and either 0.1 M NaCl, 0.1 M KCl, or 0.1 M imidazole-HCl (Im), as indicated.⁵

the monovalent cation interaction with some pyridoxal phosphate model compounds. In media favoring ion-association, e.g., tetrahydrofuran, we have studied both absorption and emission properties in order to examine the affinity of ion-pair formation both in the ground and excited states. Before discussing our results, a short review of the spectroscopic methods of studying ion association is given.

II. Spectroscopic Studies of Ion-Pair Formation

The concept of ion pairs was introduced in 1926 by Bjerrum⁽³⁸⁾. It was known in those days that ionophores-compounds built up of ions and not neutral molecules - are completely dissociated in aqueous solution, and it was expected that they should behave in the same way in other solvents. It therefore came as a surprise when Krauss⁽³⁹⁾ reported that sodium chloride, a typical ionophore, behaves like a weak electrolyte, an ionogene, when dissolved in liquid ammonia. The electric conductance of such a solution is given by the law governing the conductance of aqueous solution of acetic acid indicating that only a small fraction of the dissolved salt is dissociated into free ions. To account for these observations, Bjerrum proposed that in liquid ammonia and in other nonaqueous solvents the oppositely charged ions are associated into neutral ion pairs which do not contribute to the electric

conductance.

Solute-solute interactions result in the formation of ion pairs or of higher aggregates. The extent of ionic aggregation will depend not only on the dielectric constant of the solvent but also on its solvating ability (donicity) as well as on the nature of the ions. Ion pairing can result in contact pairs, solvent shared pairs or separated pairs⁽⁴⁰⁾. At higher concentrations and/or in solvents of low dielectric constant and low donicity ionic triplets, quadruplets, etc. may also form. It should be noted also that the introduction of a salt into a solvent may affect the solvent-solvent interaction especially in highly structured solvents such as water or dimethylsulphoxide (DMSO).

To solve this complex puzzle, we must have the means of identifying the various chemical species present in a given solution. Once all species are identified, we may then study their interactions and the equilibria that exist amongst them. Such data are the key for understanding chemical processes in solutions. For many years studies of electrolyte solutions were limited to electrochemical measurements or measurements of colligative properties of solutions. It was only since 1960 that the behavior and structure of ion pairs and ion-pair complexes in solution have been extensively investigated by using a variety of spectroscopic techniques such as electron paramagnetic and nuclear magnetic resonance, ultraviolet, visible, infrared,

and Raman spectroscopy. A brief summary of the type of results obtained using these various techniques is now given.

A. Ultraviolet-Visible

One drawback of this technique is the inability to decide whether an observed solvent effect is due to a ground state interaction, an excited state interaction or both. The large band width of absorption bands observed in solution requires large spectral shifts if ion-pair association⁽⁵⁾ are to be detected by this technique. In spite of these shortcomings, ultraviolet-visible absorption spectroscopy is an attractive technique for studying ion-pair interactions due to the simplicity of its execution and the straightforwardness of data analysis. Moreover, it is not limited to paramagnetic species like electron spin resonance methods, and does not require high concentrations of reagents which is often imperative in the nuclear magnetic resonance studies.

Warhust et al.⁽⁴¹⁾ were perhaps the first to observe shifts in optical spectra arising from ion pairing. They reported that the absorption peaks of ion pairs of alkali and alkaline earth salts of ketyls of benzophenone, fluorenone and other ketones shift towards longer wavelengths when the radius of the cation increases. Similar effects were later observed by Hogen⁽⁴²⁾ for fluorenyl salts, Waak⁽⁴³⁾

for organolithium salts and by Zaugg and Schaefer⁽¹⁴⁾, for alkali salts of phenols and enols. Warhust et al.⁽⁴¹⁾ pointed out that the perturbation of the molecular orbital levels of an organic anion due to the field of the cation associated with it depends on the electrostatic interaction energy. Therefore its magnitude is approximately proportional to the reciprocal of the interionic distance given by the sum of the cation radius r and a constant representing the corresponding contribution of the anion. The observed bathochromic shift as the radius of the cation increases was interpreted⁽⁴⁴⁾ in terms of a greater destabilization of the ion pair in the ground state. In the ground state of an ion pair the cation is located close to the atom possessing the highest electron density. As the size of the cation increases the distance between the cation and anion forming the ion pair increases leading to a destabilization of the ion pair. Since redistribution of charge occurs upon excitation, such delocalization effect is smaller in the excited state and a progressive blue shift is observed as the cation becomes smaller. Consequently, the excited state is less stabilized by the counter ion than the ground state, and the smaller the cation the larger becomes the increase in the transition frequency. Moreover, as expected from the Frank-Condon principle, the cation has no time to readjust its position during the excitation causing a further increase in the

transition frequency due to this Frank-Condon effect.

Kosower⁽⁴⁵⁾ investigated the spectra of pyridinium iodides, which are extensively sensitive to the variation in solvent polarities. The relevant optical transition is associated with the transfer of a negative charge from the iodide anion to the pyridinium cation and indeed the dissociation of these ion pairs eliminates the charge transfer band. The interaction of an ion pair with the oriented molecules of solvent, which stabilizes the ground state, is therefore lost upon excitation.

The absorption maxima of a variety of anionic species show hypsochromic shifts when they become paired with cations. The absorption bands of the fluorenyl contact ion pair shifts to lower wavelength as the radius of the cation decreases. This is shown in Figures (32) and (33)⁽⁴⁶⁾. For example, the observed blue shift due to the formation of a contact ion pair between 9-fluorenyl anion and Li^+ is $1,900 \text{ cm}^{-1}$ while with Na^+ the blue shift is $1,300 \text{ cm}^{-1}$, the radius of Li^+ and Na^+ are 0.60 and 0.96 \AA , respectively. The formation of solvent-separated ion-pairs is greatly facilitated by increasing solvent polarity. Often, small changes in the solvent structure can drastically affect the equilibrium between contact and solvent separated ion pairs. Typical examples of the effects exerted by solvents on the absorption spectrum of fluorenyl-lithium are depicted in Figure (34)⁽⁴⁷⁾. The spectral

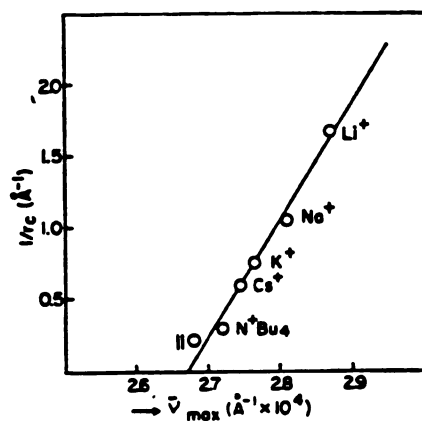


Figure 32. Correlation between wave number and the inverse of the cationic radius for contact fluorenyl ion pairs in THF at 25°C.⁴⁶

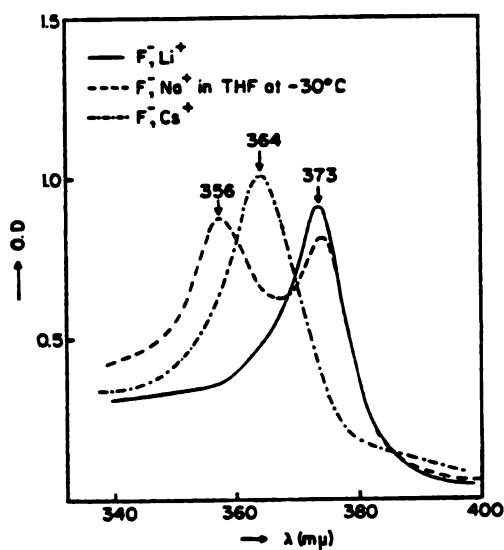


Figure 33. Absorption spectra of fluorenyl salts in THF at -30°C for various counterions.⁴⁶

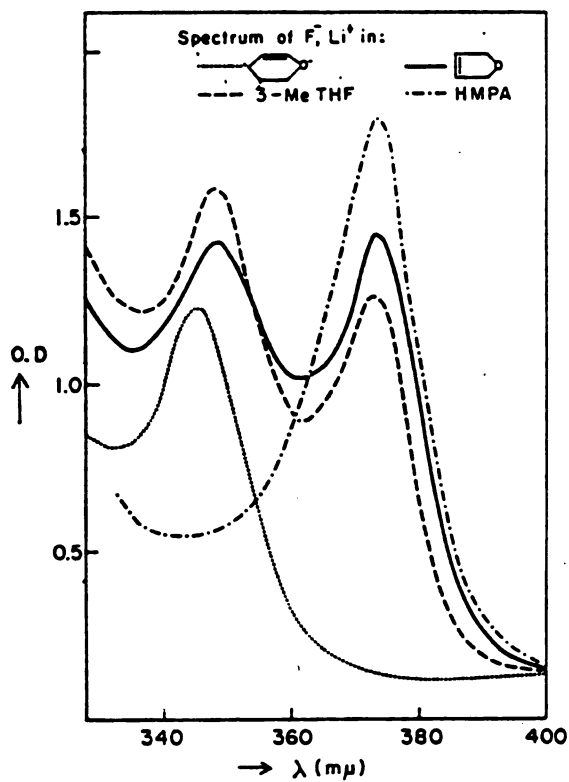


Figure 34. Optical spectrum of contact and separated ion pairs of fluorenyllithium at 25°C in 3,4 dihydropyran, ...; 3-methyltetrahydrofuran, ----; 2,5 dihydrofuran, —; and hexamethylphosphoramide, -.-.-.-.47

shifts are the result of a decreased influence of the cation on the anion, caused by specific cation-solvent interactions which led to a partial separation of ions. A pronounced effect was observed with solvents containing small amounts of reagents capable of coordinating strongly with the cation, for example, DMSO and hexamethylphosphoramide^(42,47). The lithium salt was singled out for these studies because of the strong specific interaction of the small Li^+ ion with solvent molecules permits studies of low polarity media in which the Na^+ salt exists only as a contact ion pair. Moreover, the overlap of the absorption peaks corresponding to the two types of ion pair (contact and solvent separated) is the smallest for Li^+ salt, and this facilitates the calculation of equilibrium constants between contact and solvent-separated ion-pairs. The enthalpy change, ΔH , governing the equilibrium between the two kinds of ion pairs is a significant thermodynamic quantity, knowledge of which permits the discussion of energetics of ion-pair separation. It also plays an important role in determining the temperature dependence of the reactions in which the two kinds of ion pairs simultaneously participate, each with its own rate constant^(48,49). The value of ΔH for a given equilibrium between contact and solvent-separated ion-pairs can be obtained from a plot of K_1 (the ratio between both types of ion pairs) versus $1/T$, which gives a straight line with slope = ΔH . A ΔH value

of -7.5 Kcal/mole was obtained for the formation of solvent-separated ion-pairs from contact ion pairs for fluorenyllithium in THF. The first evidence for the existence of contact and solvent-separated ion-pairs in solutions of carbanion salts came from the study of the temperature-dependent spectrum of fluorenylsodium in THF, Figure (35), and even more dramatic spectral changes are depicted in Figure (36)⁽³⁹⁾ which shows that 9(2-hexyl)fluorenyllithium in 2,5-dimethyltetrahydrofuran is transformed from a predominantly contact ion pair state at -20° to virtually 100% solvent separated ion pair at -40°.

The effect of pressure upon the equilibrium between contact and solvent separated ion pairs of fluorenyllithium and sodium in THF was investigated by Szwarc et al.⁽⁵⁰⁾ and by LeNoble and Das⁽⁵¹⁾. Spectroscopic observations, extended to pressure as high as 5000 atm., show that the equilibrium shifts to the separated ion pairs as the pressure increases, Figure (37)⁽⁵¹⁾. This observation was explained in terms of electrostriction (the observed volume contraction resulting from a light binding of solvent molecules around the cations of the separated ion pairs). The binding of one mole of THF to separated ion pairs is calculated to cause a volume contraction of about 8 ml., approximately 10% of the solvent molar volume. Such contraction of the volume of the pure solvent requires pressures of about 2000 atm. It therefore seems that the

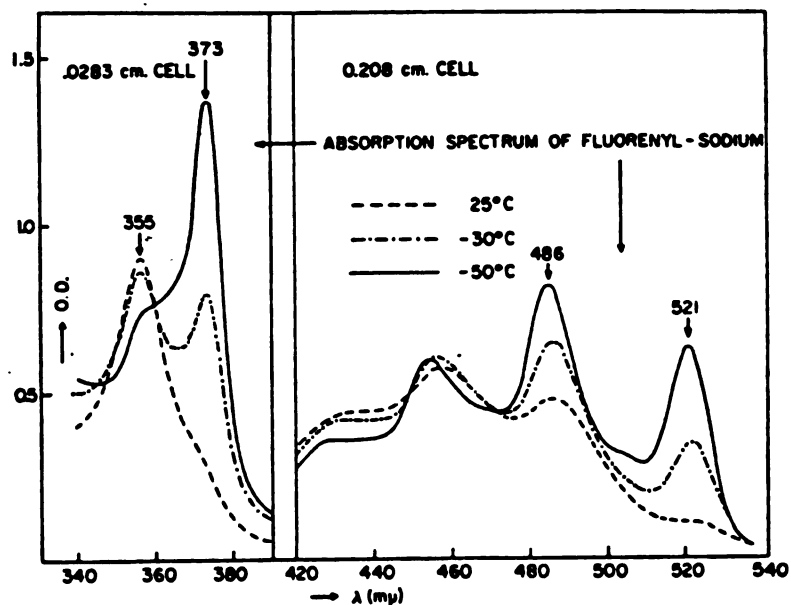


Figure 35. Optical absorption spectrum of fluorenyl-sodium in THF at 25, -30, and -50°C.³⁹

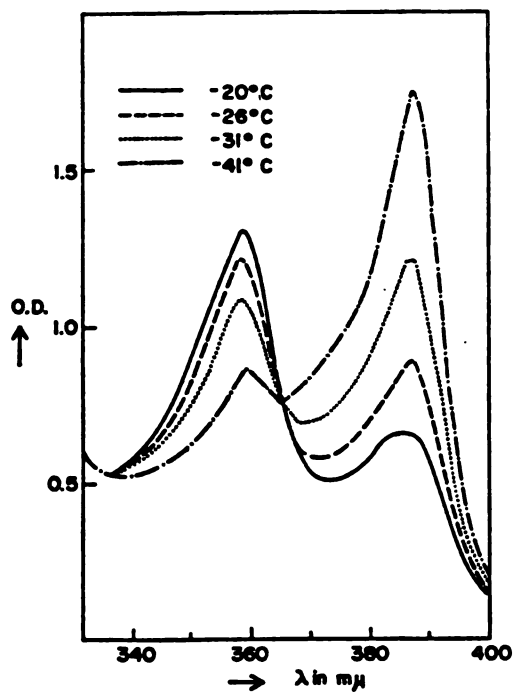


Figure 36. Temperature dependence of the contact-solvent-separated ion-pair equilibrium of 9(2-hexyl)-fluorenyllithium in 2,5-dimethyltetrahydrofuran.³⁹

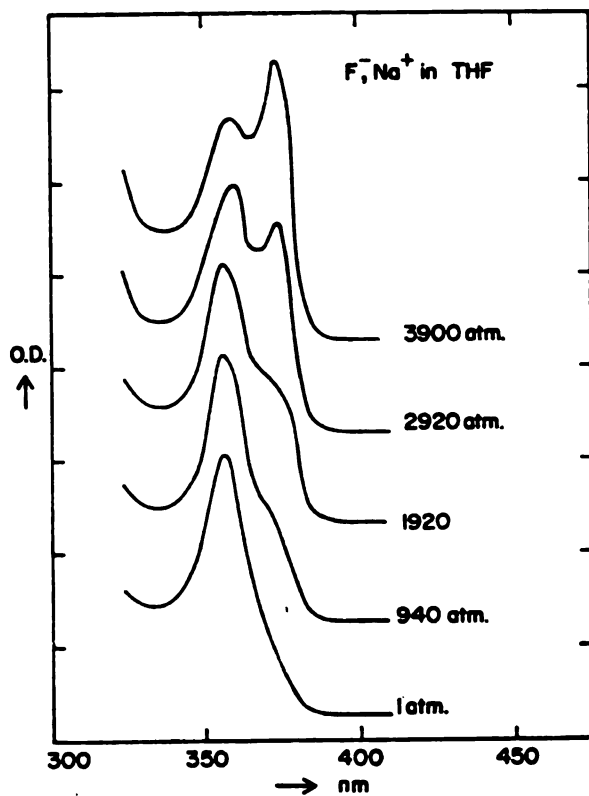


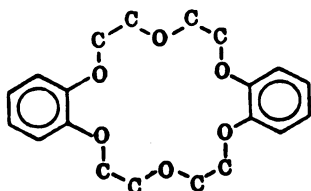
Figure 37. Pressure dependence of the contact-solvent-separated ion-pair equilibrium of fluorenyl-sodium in THF at 25°C.⁵¹

forces contracting the solvent around the ion pairs are equivalent to those produced by pressure of 2000 atm.

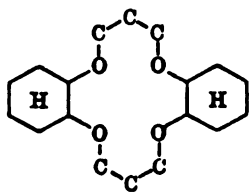
In powerful cation solvating media such as ethylenediamine, DMSO, or polyglycoldimethylethers, referred to as glymes with general formula $\text{CH}_3\text{O}[\text{CH}_2\text{-CH}_2\text{O}]_x\text{CH}_3$, most of the fluorenyl salts form only separated ion-pairs. Studies on ion-pair solvation by such reagents may be carried out in a mixture of the solvating agent with a relatively low-polarity solvent in which the fluorenyl salt predominantly exists as a contact ion-pair. For example, small quantities of DMSO added to a fluorenyllithium solution in dioxane converts the contact ion-pairs to DMSO-separated ion-pairs⁽⁴²⁾.

Shinohara et al.^(52a,b) have shown that addition of small quantities of glymes drastically increases the rate of anionic polymerization of styrene in THF. For example, at a polystyrylsodium concentration of 5×10^{-5} M, the polymerization rate increases by nearly a factor of 200 when glyme-5 is present at a concentration of 10^{-3} M. The formation of reactive glyme-separated ion-pair and an increase in the fraction of reactive free ions was responsible for this effect.

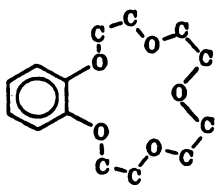
Pedersen^(53a,b) developed a class of very strong cation-binding complexing agents referred to as macrocyclic polyethers or crown ethers. Some of these compounds are displayed in Figure (38). The first number refers to the total number of atoms in the ring, the second number corresponds to the number of the ring oxygen atoms. These



(I) Dibenzo-18-crown-6.



(II) Dicyclohexyl-14-crown-4.



(III) Monobenzo-15-crown-5.

Figure 38.

crown ethers considerably increase the solubility of inorganic salts in non-polar media and form crystalline complexes with many salts.

The stability of these complexes depends on the size of the cation relative to that of the hole of the macrocyclic polyether, the charge on the ion, the number of the ring oxygen atoms, their basicity, coplanarity and symmetrical placement, steric-hindrance in the polyether ring, and the extent of ion association with the solvent^(53a). For example, the small Li^+ ion fits the hole of a 14-crown-4 polyether, but the larger Na^+ and K^+ ions do not. However, the Na^+ and K^+ ions can be accommodated by the cavity of an 18-crown-6 ether. The stability of the complex is increased as more oxygen atoms are available for coordination, provided they are favorably located in the polyether ring. In this respect, the dibenzo-18-crown-6, Figure (38), is one of the best complexing agents for Na^+ and K^+ ions.

Similar to the effect of glymes, addition of dibenzo- or dicyclohexyl-18-crown-6 to fluorenylsodium in THF yields 1:1 complex absorbing at 372 nm, the optical spectra are identical to that of the solvent-separated ion-pairs⁽⁵⁴⁾.

The size of metal ion plays an important role in determining the stability of its complex with the complexing agent (crown ether or cryptand). It is evident from Figure (39)⁽⁵⁵⁾ that maximum stability for complexes of

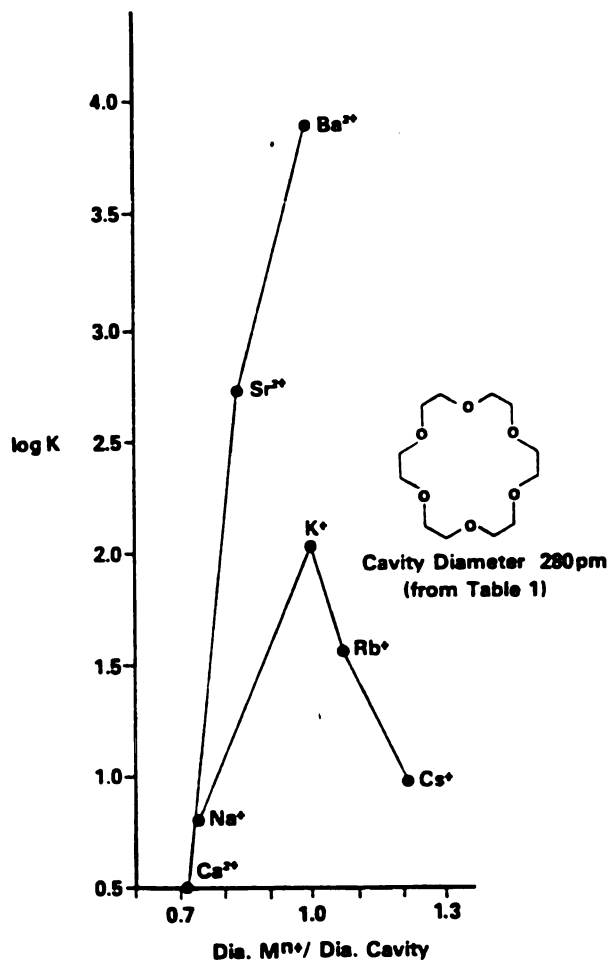


Figure 39. Selectivity of 18-crown-6: log K values for reaction of 18-crown-6 with metal cations in H₂O vs. ratio of cation diameter to 18-crown-6 cavity diameter. Value for Ca²⁺ reported <0.55

18-crown-6 with both the alkali and alkaline earth cations occur at metal ion to cavity diameter ratio of unity (K^+ and Ba^{2+}) i.e., greater stability for complexes with cations diameter more closely matching that of the ligand cavity⁽⁵⁶⁾. Table (6)⁽⁵⁶⁾ illustrates that in the case of 18-crown-6, increased stability of the complexes of K^+ and Ba^{2+} over those of other ions in the series is largely due to the enthalpy term. This undoubtedly corresponds to the greater electrostatic bond energy for those ions that better fit the ligand cavity.

Eyring and co-workers^(57a,b) concluded that the high selectivity of 18-crown-6 for K^+ over other alkali cations, Table (7), arises from the slowness of the dissociation step.

The structure and properties of ion-pairs containing divalent cations are less known than those of the alkali salts. The barium salt of the fluorenyl carbanion was prepared by Hogen Esch and Smid⁽⁵⁸⁾ and by Pascault⁽⁵⁹⁾ as orange crystals. A solution of this salt in THF showed a sharp absorption maximum at 347 nm, Figure (40)⁽⁵⁸⁾. The fraction of separated ion-pairs is low even at -70°C , whereas for the sodium salt it exceeds 0.9 under these conditions. In 1,2-dimethoxyethane (DME) at 25°C the barium salt is also essentially a contact ion-pair. The strontium salt yields higher fractions of separated ion-pair. The spectrum of this salt in THF at -25°C reveals

Table 6. Log K, ΔH , and T ΔS for the Formation of 18-Crown-6 Complexes with Metal Ions in H₂O at 25°C. (56)

Ion	Log K	ΔH (Kcal mol ⁻¹)	T ΔS (Kcal mol ⁻¹)
Na ⁺	0.8	-2.25	-1.16
K ⁺	2.03	-6.21	-3.40
Rb ⁺	1.56	-3.82	-1.7
Cs ⁺	0.99	-3.97	-2.6
Sr ²⁺	2.72	-3.61	0.1
Ba ²⁺	3.87	-7.58	-2.3

Table 7. Rate Constants for Reaction at 25°C in H₂O, $\mu = 0.3$ (57a,b):
 $M^+ + 18\text{-Crown-6} \xrightleftharpoons[k_d]{k_f} M\text{-crown}^+$

Cation	k_f (M ⁻¹ s ⁻¹)	k_d (s ⁻¹)
Na ⁺	$\sim 2.2 \times 10^8$	3.4×10^7
K ⁺	$\sim 4.3 \times 10^8$	3.7×10^6
Rb ⁺	$\sim 4.4 \times 10^8$	1.2×10^7
Cs ⁺	$\sim 4.3 \times 10^8$	4.4×10^7
Ag ⁺	$\sim 11.3 \times 10^8$	3.6×10^7
Tl ⁺	9.9×10^8	5.3×10^6
NH ₄ ⁺	$\sim 5.6 \times 10^8$	4.4×10^7

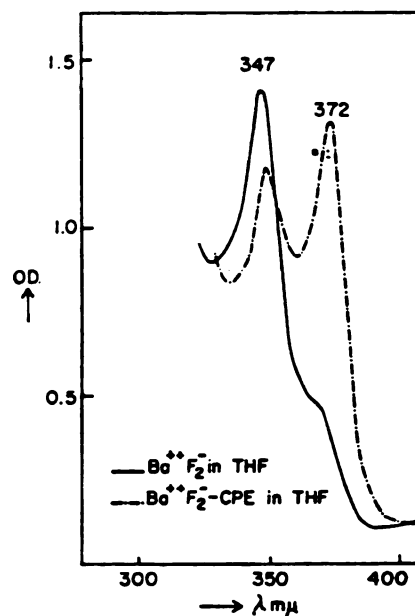


Figure 40. Optical absorption spectrum of barium fluorenyl and its 1:1 complex with dimethyldibenzo-18-crown-6 between 320 and 400 nm in THF at 25°C.⁵⁸

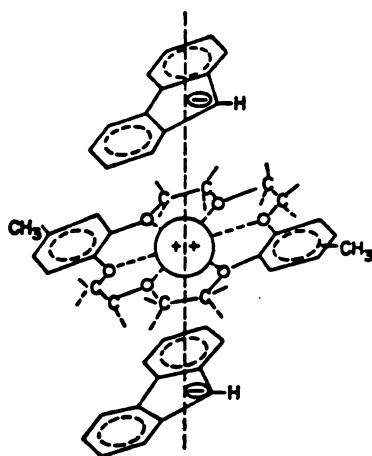


Figure 41. Possible structure of the barium fluorenyl-dimethyldibenzo-18-crown-6 complex in THF or pyridine.⁵⁸

two absorption band maxima of approximately equal intensities at 347 and 371 nm, indicating an appreciable proportion of separated ion-pairs. A mixture of equimolar quantities of dibenzo-18-crown-6 and barium difluorenyl (or the corresponding strontium salt) in THF produces a 1:1 complex, the spectrum of which reveals approximately equal fractions of tight and loose ion-pairs. Their proportion is not changed on further addition of macrocyclic ether. A similar behavior is observed with glyme-6. A possible structure of the complex is shown in Figure (41)⁽⁵⁸⁾ (page 88) in which the Ba^{2+} -crown complex is sandwiched in between the two fluorenyl moieties.

B. Infrared and Raman

The discovery^(60a,b) that alkali ions vibrate in solution offers a new fundamental way of obtaining information about electrolytic solutions. The infrared bands at long wavelength associated with this phenomenon arise from the excitation of quantum states of the solution connected with motion of solution elements adjacent to the alkali ion. Infrared spectroscopy can be used to obtain information about the forces acting on the ions and the structure of solvent molecules surrounding the ion.

In a study of far-infrared spectra of tetraalkylammonium salts in benzene, Evans and Lo⁽⁶¹⁾ found a band which could not be assigned either to the solvent or to

the salt. The authors assumed that it was due to a certain cation-anion vibration. Calculations based on a simple diatomic model supported their assumption.

Far-infrared bands arising from the motion of alkali cation in THF solutions of lithium, sodium and potassium tetracarbonyl cobaltate, $M[Co(CO)_4]$, and pentacarbonyl manganate were observed by Edgell and co-workers⁽⁶¹⁾. The large dependence of the frequency of the band on the nature of the cation, Table (8), and to some extent on the anions, suggests that the vibrating species are ion pairs or higher aggregates. Far-infrared spectra were also obtained for large numbers of alkali salts in a polar and highly solvating solvent, DMSO^(62a,b). The observed bands were strongly dependent on the nature of the cation but completely independent of the anion. The bands were very broad and their integrated intensities are directly proportional to the concentration of the salt. The relative intensity, however, decreases with the increasing mass of the cations. These bands were assigned to the vibration of the cations in a solvent cage. This was confirmed by studying the isotopic substitution^(62a) effect by using $^7Li^+$ and ND_4^+ instead of $^6Li^+$ and NH_4^+ in d_6 -DMSO which showed that both the cation and the solvent participate in the observed vibration. In solvents of low donicity and/or low dielectric constant e.g., 1-methyl-2-pyrrolidone, solutions of salts with polyatomic anions show a constant frequency for the absorption band, while with some halide anions a

Table 8. Absorption Bands of Alkali Metal Salts in Dimethylsulphoxide. (62a,b)

Salt	$\nu(\text{cm}^{-1})$	Salt	$\nu(\text{cm}^{-1})$
LiCl	429	KBr	153
LiBr	429	KI	153
LiI	429	KNO ₃	154
LiNO ₃	428	KSCN	153
LiClO ₄	429		
		RbBr	125
NH ₄ Cl	214	RbI	123
NH ₄ Br	214	RbNO ₃	125
NH ₄ I	214		
NH ₄ NO ₃	214		
NH ₄ ClO ₄	214	CsI	110
NH ₄ SCN	214	CsClO ₄	109
NaCl	199		
NaBr	199		
NaI	198		
NaNO ₄	206		
NaClO ₄	200		
NaSCN	200		
NaBPh ₄	198		

10-15 cm^{-1} shift to lower frequency was observed. It seems reasonable to assume that the change in the frequency of the solvation band is due to a change in the nature of the solvent cage around the cation. A simple explanation of this change would be that a small counter-ion, such as a halide ion, replaces a solvent molecule in the inner solvation shell forming a solvated contact ion pair. The cation in such cases vibrates in a cage composed of solvent molecules and a counter-ion.

Tsatsas and Risen^(63a) studied the far-infrared spectrum of sodium tetrabutylaluminate (NaAlBu_4). In cyclohexane solutions two solvation bands at 195 and 160 cm^{-1} were observed. In THF solution, however, only one band at 195 cm^{-1} was observed. Addition of THF to a sodium solution of tetrabutylaluminate in cyclohexane resulted in the disappearance of the 160 cm^{-1} band as the THF/ NaAlBu_4 molar ratio exceeded 1:1. It should be noted that Edgell et al.^(62a,b) showed that, in general, the far-infrared solvation bands are Raman-inactive, which is indicative of the largely electrostatic nature of the cation-solvent or cation-anion interaction. Tsatsas and Risen, however, found a 202 cm^{-1} Raman band in cyclohexane solutions of NaAlBu_4 . This band, however, was not observed in THF solution, which indicates that in cyclohexane the ion-solvent interaction responsible for the 200 cm^{-1} band has a significant degree of covalent character.

The addition of a complexing agent, dibenzo-18-crown-6 to sodium and potassium salt solutions in THF and in pyridine produced a marked change in the spectra^(63b). The absorption bands were shifted to higher frequency and became independent of the solvent as well as of the anion. It is clear that in this case the cation is accommodated in the ligand and vibrates within the ring formed by the ether oxygens.

C. Electron Spin Resonance (ESR)

Application of ESR spectroscopy to study ion-pair systems has been recently reviewed by Simon⁽⁶⁴⁾. Although it is limited to the study of dilute paramagnetic solutes, the technique of ESR spectroscopy has taken its place amongst other forms of spectroscopy as a useful method for obtaining structural and dynamic information about solvation. In the field of ion-pair formation, ESR stands out as the most powerful technique for learning about their presence, structure and energies^(65a-c). Weismann and his co-workers⁽⁶⁶⁾ discovered that the ESR spectra of certain radical-anions in low polarity solvents contained hyperfine features characteristic of the alkali-metal ions. The reason alkali metal nuclei frequently give rise to detectable hyperfine coupling is that a slight electron-transfer from the paramagnetic anions which are, of course, powerful electron donors takes place into the outer s-orbital of

the cation; and hence even a small transfer gives an easily detectable coupling.

In the ESR spectra of the benzophenone ketyl anion and the naphthalene radical anion, each line splits into four lines by coupling to ^{23}Na as a result of close association of the anion with the sodium cation^(67,68). The effect of ion-pairing on the g-value has been studied by Williams et al.⁽⁶⁹⁾. Evidence that different types of ion pairs are sometimes formed in a solution are strong. Hirota⁽⁷⁰⁾ found that lithium anthracenide in diethylether gave spectral features for the normal ion pair showing cation hyperfine coupling together with a species showing no cation coupling, but having proton splittings that were different from the normal solvated ion values. A more definitive study is that of Hofelmann et al.⁽⁷¹⁾ for sodium naphthalenide in THF. Contact ion-pairs [$A(^{23}\text{Na}) = 1.23 \text{ G}$] together with another type of ion pair, solvent separated, [$A(^{23}\text{Na}) = 0.38 \text{ G}$] were detected when tetraglyme was added to the solution. Excess glyme gave only the latter species. Triplet-ions formation has also been detected by ESR. The addition of sodium tetraphenylborate to sodium-2,5-di-t-butyl-p-benzoquinone in THF resulted in a spectrum characteristic of the triplet ion⁽⁷²⁾.

D. Nuclear Magnetic Resonance (NMR)

In recent years the use of NMR in the study of electrolyte solutions has become quite popular. Proton and ^{13}C NMR have been widely used for the studies of ionic interactions in solutions. At low temperatures, exchange between bulk water molecules and those in the inner solvation shell of a cation is slower than the NMR time scale and, therefore, two separate resonances are observed for the free and bound water. Hydration numbers for a number of transition metal cations were obtained⁽⁷³⁾ by using acetone-water solvent mixture, acetone was assumed to act only as a completely inert diluent.

Alkali metal NMR as well as halogen NMR has been particularly fruitful in the elucidation of the structure of alkali salt solutions in nonaqueous solvents. A comprehensive study of sodium iodide solution in nonaqueous solvents has been reported by Bloor and Kidd⁽⁷⁴⁾. Twelve solvents were used and chemical shifts varied from +9.9 ppm (upfield) shift for acetic anhydride to -13.1 ppm (downfield) for ethylenediamine, the chemical shifts were related to the aqueous pK_a of these solvents. More detailed studies by Popov *et al.*^(75,76) of different salts indicated that the counter-ions also play an important role in determining the behavior of the ^{23}Na chemical shifts.

The concentration dependence of ^{23}Na chemical shift in the sodium halides and thiocyanate solutions in different

solvents can be ascribed to the formation of contact ion-pairs in these solutions⁽⁷⁷⁾.

The ${}^7\text{Li}$ nucleus has a spin of $3/2$ and thus is amenable to NMR studies. Although the nucleus has a quadrupole moment, the ${}^7\text{Li}$ resonance lines for Li^+ ion are exceptionally narrow and the chemical shifts can be measured with considerable accuracy.

Studies by Maciel et al.⁽⁷⁸⁾ and by Akitt and Downs⁽⁷⁹⁾ in several nonaqueous solvents showed that the frequency of the ${}^7\text{Li}$ resonance is very sensitive to the environment.

While a large number of ${}^7\text{Li}$, ${}^{23}\text{Na}$ and ${}^{133}\text{Cs}$ NMR studies have appeared, ${}^{39}\text{K}$ and especially ${}^{89}\text{Rb}$ NMR investigations are scarce due to the low sensitivity in ${}^{39}\text{K}$ and the broad resonance lines obtained with ${}^{89}\text{Rb}$.

In dilute solutions of lithium perchlorate in nitromethane and THF the width at half-height of the ${}^{35}\text{Cl}$ resonance was 10-20 Hz. Considerable broadening was obtained with increasing the salt concentration in both solvents whereas, very little dependence was observed in acetone, methanol and acetonitrile solutions. This broadening was due to the change in the electric field gradient at the chlorine nucleus as the perchlorate ion interacts with Li^+ to form a contact ion pair⁽⁸⁰⁾.

E. Luminescence

In comparison with the other spectroscopic methods, luminescence spectroscopy was little used in studying ion-pairs. Much information can be obtained using luminescence techniques. Due to charge redistribution in the excited state, ion-pair characteristics will be different in the excited state compared to the situation in the ground state. Excitation may cause a shift in the equilibrium between free ions and ion pairs i.e., a change in the dissociation constants.

McGlynn⁽⁸¹⁾ used the phosphorescence lifetimes of phenyl-carboxylic acids and their salts to show that the lowest triplet state of benzoic acid is not an excitation localized on the benzene ring but involves considerable delocalization onto the carboxyl group. The large spin-orbit coupling effect caused by the heavy lead ion in the lead salt of benzoic acid was completely lost in the lead salt of 4-phenyl-butyric acid, in the latter case the benzene ring is separated from the carboxylic group by three methylene groups. These observations also show that the observed effect of lead on the lifetime of the benzoic acid salt is not an external heavy-atom effect on the benzene ring. Recently, Carter and Gillispie⁽⁸²⁾ studied the luminescence of ion pairs of alkali-metal cations with dichromate anion. The influence of other alkali-metal cations on the emission of sodium dichromate was probed by adding their chloride

salts to the sodium dichromate solution. The wavelengths of the emission maximum in aqueous solution at 77°K decreased continuously in going from Na^+ to Cs^+ . The emission was assigned as phosphorescence. The greatly enhanced phosphorescence intensity when K^+ , Rb^+ or Cs^+ cations are present reflects the heavy-atom effect on the spin-forbidden process (triplet \rightarrow singlet). The magnitude of any heavy-atom effect is presumably sensitive to whether the ion pairs are loose or tight⁽⁴⁶⁾. If the ion pairs are loose the heavy-atom effect may be an external one whereas, in the tight ion pairs case it is better described in terms of an internal heavy-atom effect, i.e. because of orbital overlap between the already bended emitting species and heavy atom not through collision mechanism with the heavy atom. Accordingly, the emission at 77°K was assigned to ion-pair formation between the alkali metal cation and the dichromate anion.

III. Results and Discussion

The room temperature absorption spectrum of a dilute solution of sodium salt of salicylaldehyde in DMSO exhibits two absorption bands, Figure (42). The band absorbing at 417 nm corresponds to the absorption of the free anion. A solution of the same concentration of tetrabutylammonium salt of salicylaldehyde in DMSO absorbs at 417 nm, the bulkiness of the tetrabutylammonium cation prevents

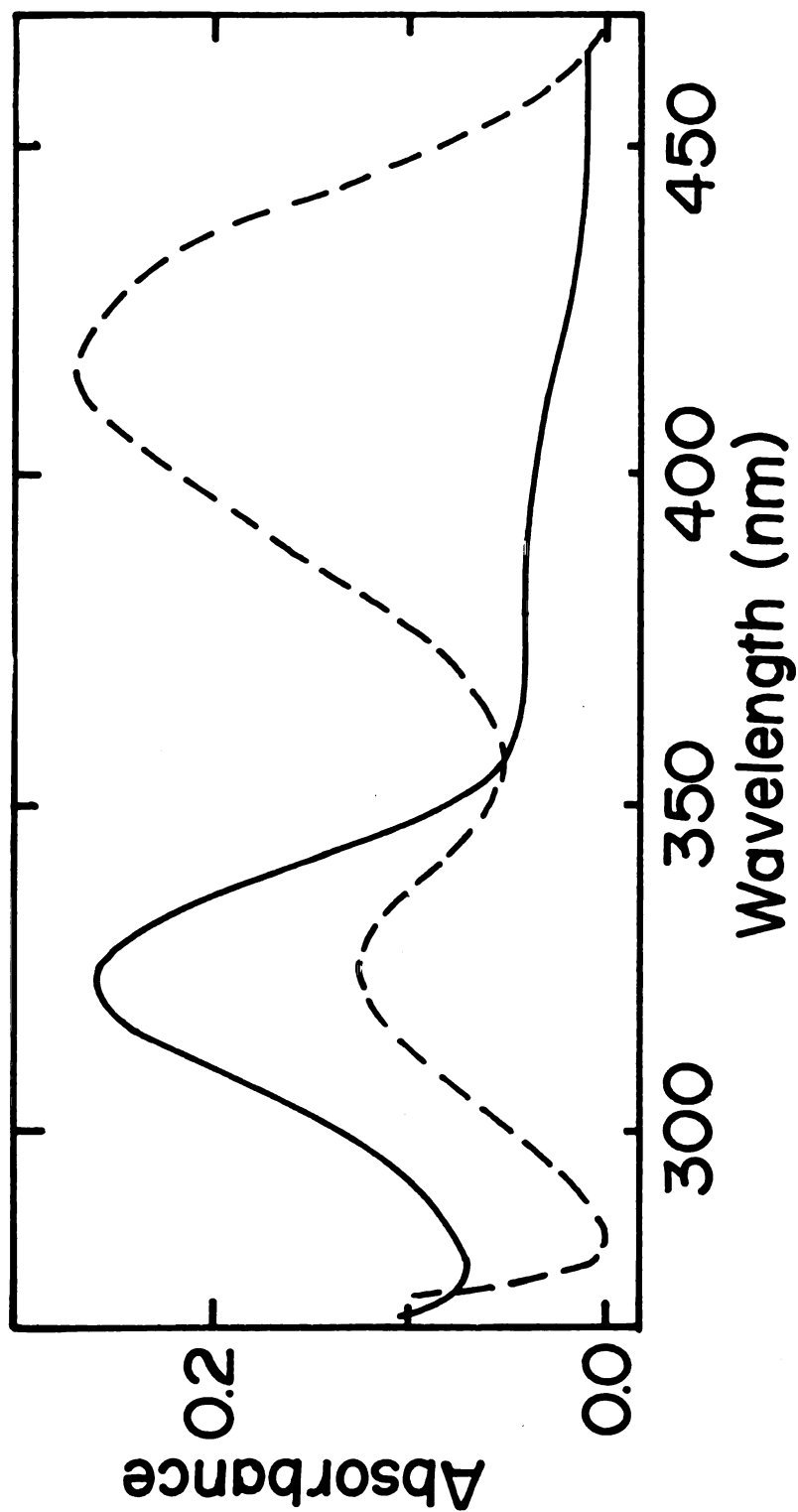


Figure 42. Room temperature absorption spectra of dilute solutions (5×10^{-5} M) of Na^+ salt of salicylaldehyde in DMSO (-----) and in DMSO in presence of 2×10^{-2} M NaBF_4 (———).

ion-pair formation. The other absorption at 323 nm is interpreted as corresponding to the absorption of the associated metal cation with the organic anion. This interpretation is consistent with the increase in absorptivity of the 323 nm band upon addition of Na^+ ions while that of the 417 nm decreases as shown in Figure (42). Similar behavior was observed for the thallous, Tl^+ , salt of salicylaldehyde, Figure (43). In the presence of excess Tl^+ ions, the maximum of the 417 nm absorption band was blue shifted, this probably reflects a change in the solvent structure while the absorptivity of the 323 nm absorption band is enhanced, Figure (43). In water the 323 nm absorption band is weak and appears only as a shoulder. Figure (44) shows the potential energy of an ion pair as a function of the interionic distance R . The absorption of the free anion is represented by ΔE . For the formation of an ion pair, the positively charged cation gets closer to the anion, the smaller the ionic radius of the cation, the closer the distance between anion and cation, resulting in a greater stabilization of the ground state of the ion pair. Because of the covalency in O-H bond, maximum stabilization corresponds to the formation of the phenolic derivative. In the excited state, the negative charge on the oxygen will have partially migrated to the ring, and will decrease the negative charge on the phenolic oxygen. Accordingly, less interaction between the cation and anion

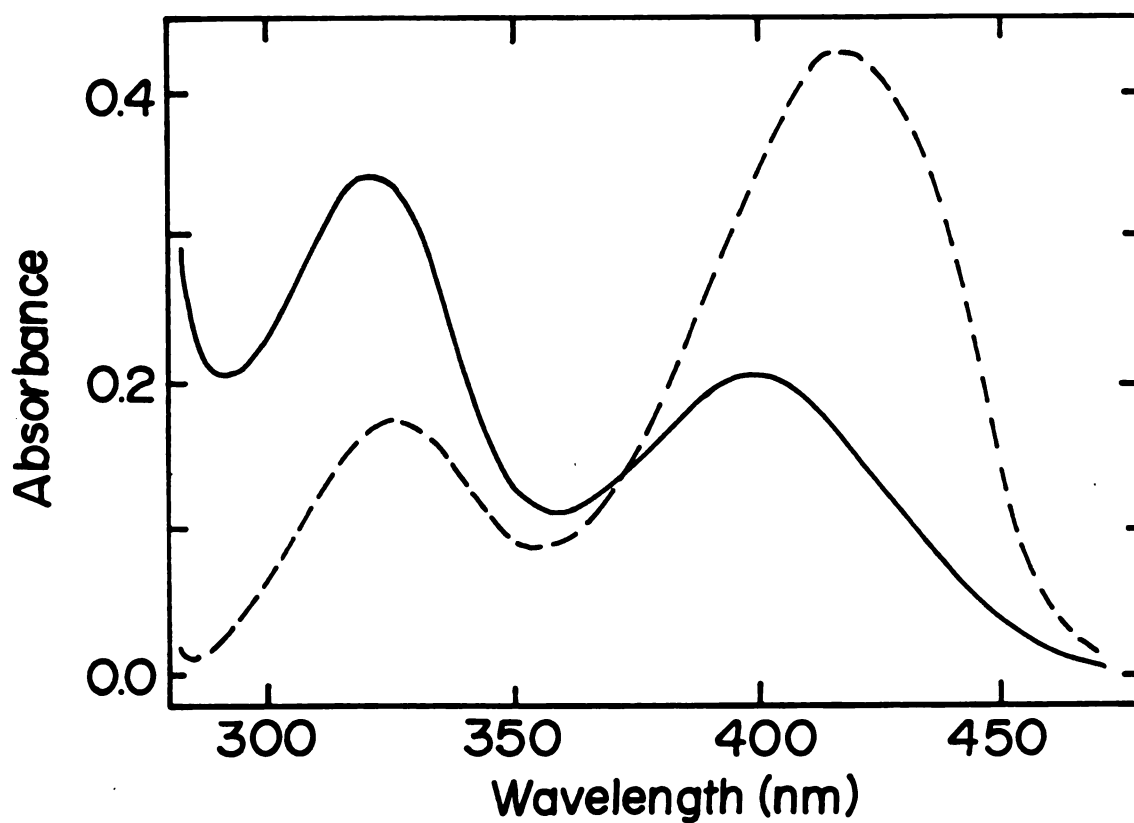
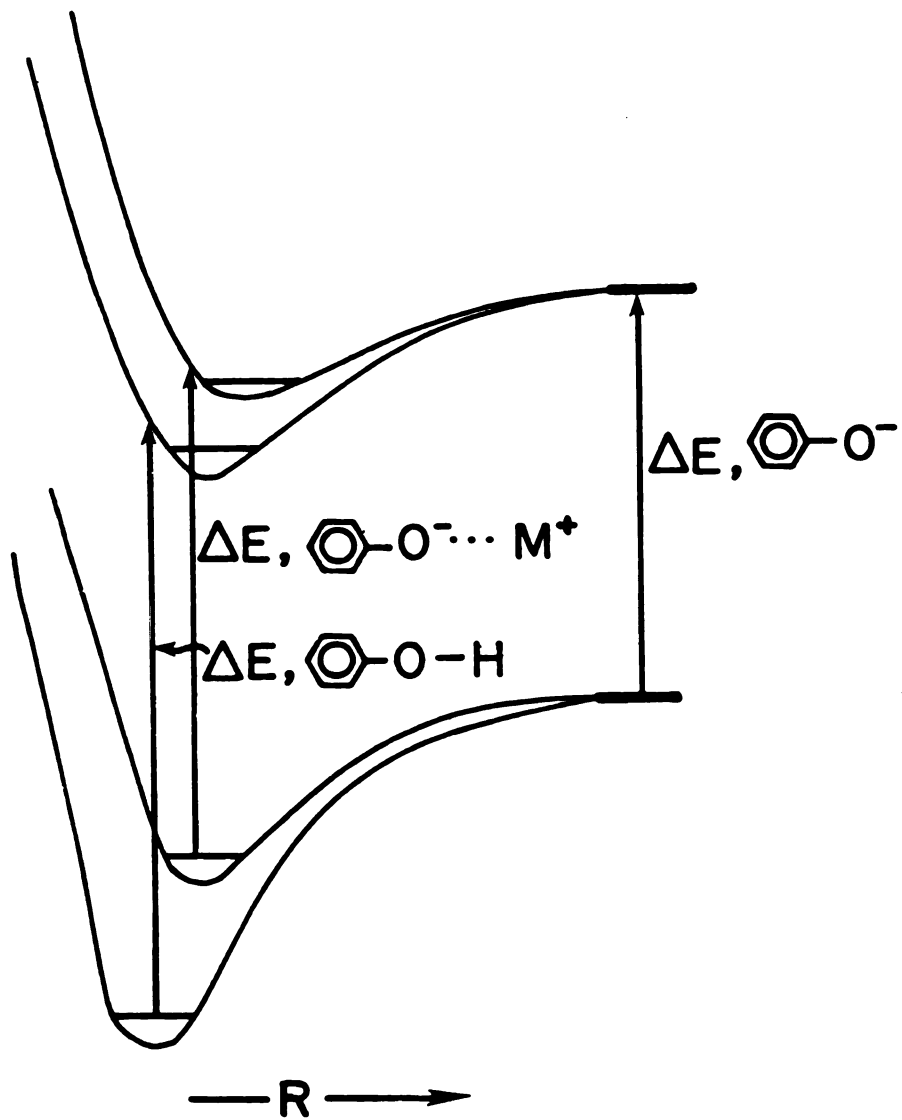


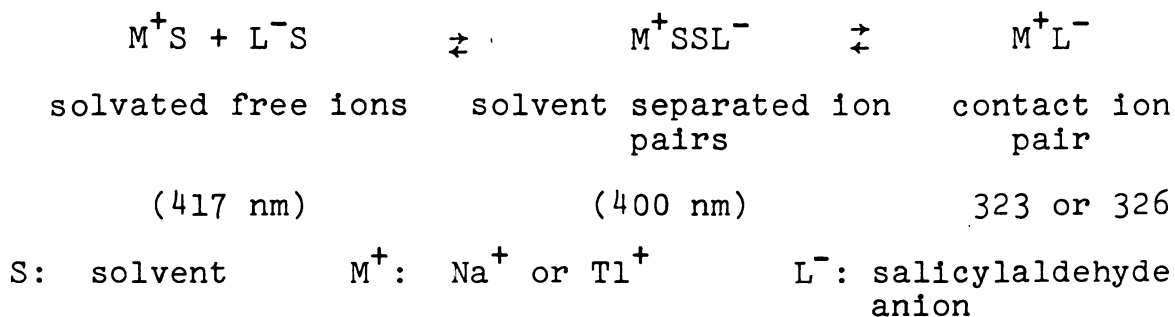
Figure 43. Room temperature absorption spectra of dilute solutions (5×10^{-5} M) of Tl(I) salt of salicylaldehyde in DMSO (----) and in DMSO in presence of 5×10^{-3} M $TlNO_3$ (—).



R : cation-anion interionic distance

Figure 44. Potential energy of ion-pair formation as a function of the interionic distance.

will occur, resulting in an increase of R and less stabilization of the ion pair in the ground state. During the absorption, the interionic distance does not change and therefore a Franck-Condon energy contributes to the transition energy. The result is a blue shift in the absorption spectra of the ion pair, with respect to that of the free ion. This blue shift increases with the decreasing cationic radius. The blue shift of the 417 nm band, Figure (43), to 400 nm in presence of excess (5×10^{-3} M) Tl^+ indicates that the solvated cation interacts with the solvated anion, i.e., solvent separated ion pairs absorbing at 400 nm are formed. Thus the following equilibria occur in solution



In ethanol, both sodium and thallium salts of salicylaldehyde show an equilibrium between the free ions which absorb at 380 nm and contact ion-pairs which absorb at 325 nm. Thus adding an excess of Tl^+ shifts the equilibrium to the right; the relative concentration of the contact ion-pairs increased. In addition, excess Tl^+ induces

structural changes in the liquid structure of the solvent. The enhanced order in the solvent structure favors the formation of solvent-separated ion-pairs at the expense of solvated free ions. In THF solution of the sodium salt of salicylaldehyde, the longer-wavelength absorption band dominates the spectrum as shown in Figure (45).

This indicates that in THF there is an equilibrium between the free ions and contact ion-pairs with the equilibrium shifted towards the free ion formation. This can be explained in view of the high solvation of Na^+ . For a thallium salt in THF, Figure (46), both absorptions of the ion pair and free ions are of comparable absorptivity. This reflects the lower solvation of the Tl^+ ion with THF compared with Na^+ because of the larger radius of Tl^+ .

Figure (47), shows a comparison between the absorption spectra of Na^+ and Tl^+ salts in THF.

When the anion of salicylaldehyde is excited, charge transfer occurs from the phenolate oxygen to the carbonyl oxygen. As a result, the negative charge density on the phenolate oxygen will be smaller in the excited state than in the ground state. This weakens the interaction between the positive and negative ions in the excited state i.e., the ion pair becomes less stable, and may lead to dissociation of the ion pair in the excited state. Figure (44) shows the energetics of both excited and ground states of ion pairs. Figure (48) displays the room temperature

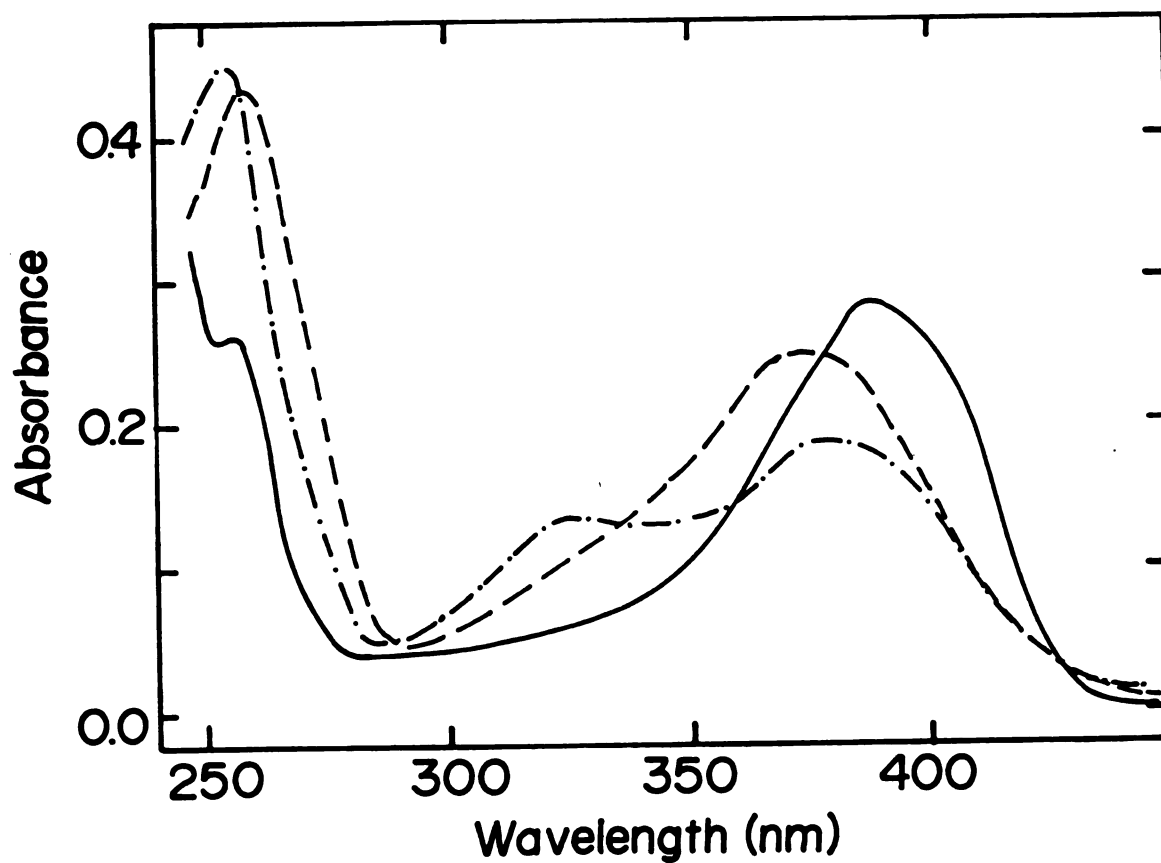


Figure 45. Room temperature absorption spectra of dilute solution of Na⁺ salt of salicylaldehyde: (4.8×10^{-5} M) in water (----), (4.5×10^{-5} M) in ethanol (-·-·-) and (4.5×10^{-5} M) in THF (—).

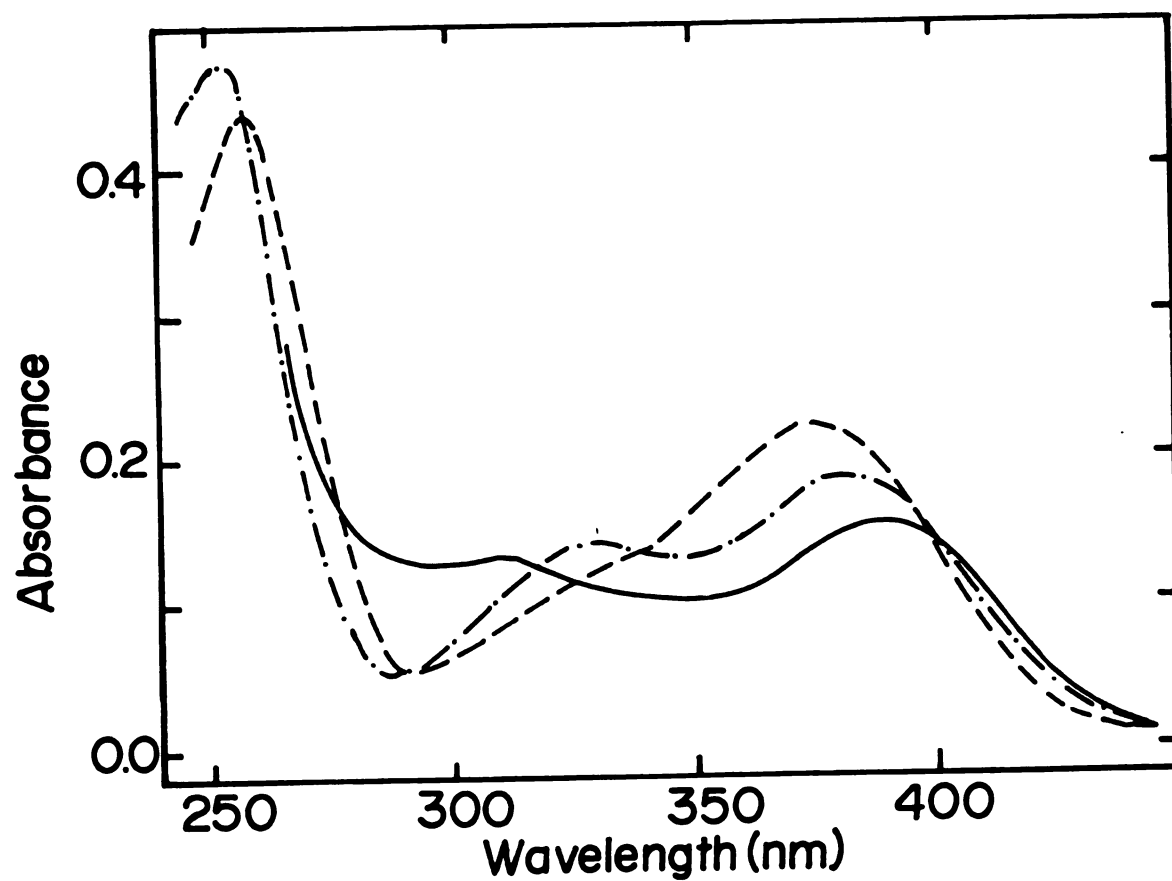


Figure 46. Room temperature absorption spectra of dilute solutions of Tl(I) salt of salicylaldehyde: (4.5×10^{-5} M) in water (----), (5.2×10^{-5} M) in ethanol (-·-·-) and (4.5×10^{-5} M) in THF (—).

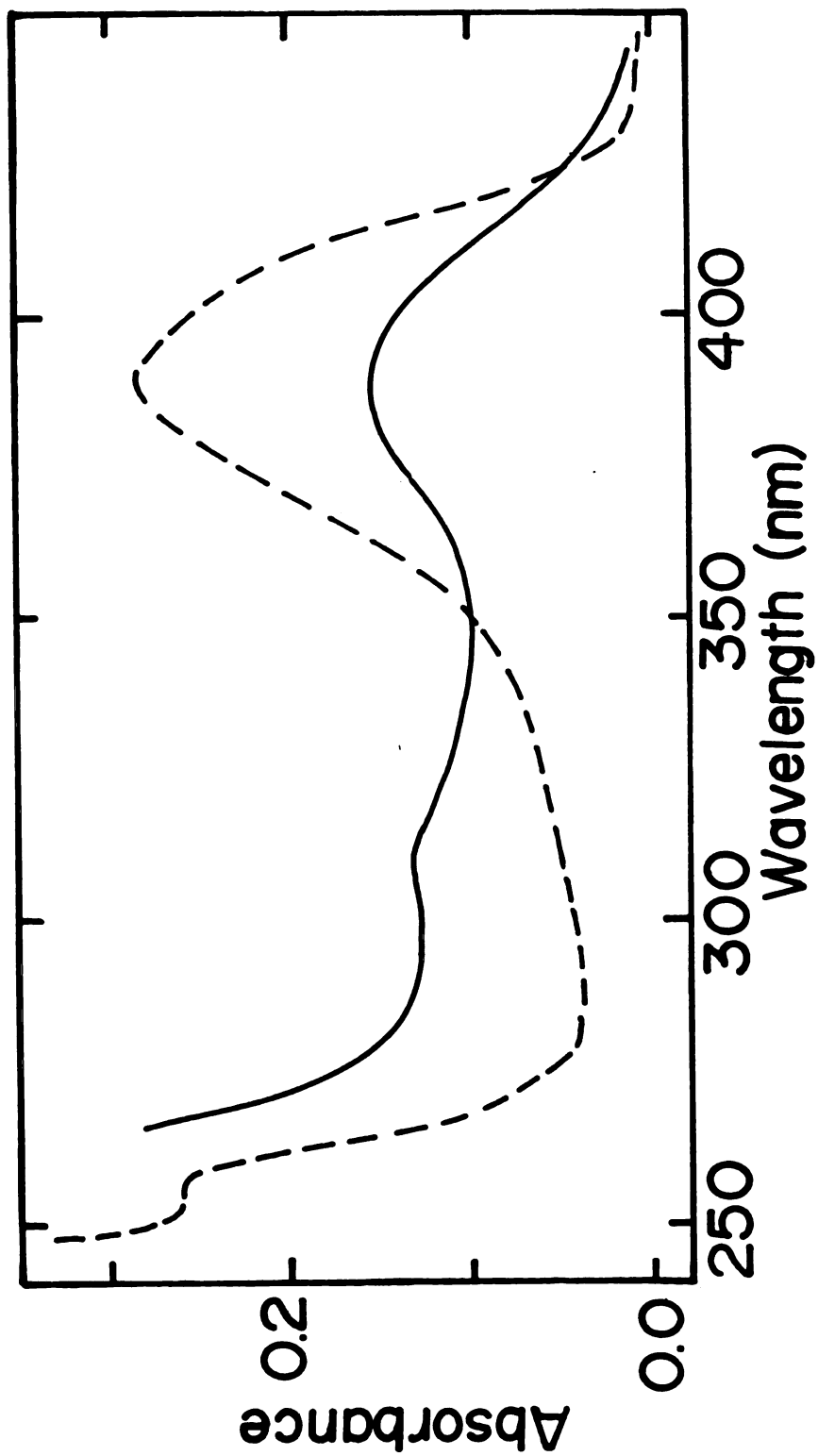


Figure 47. Room temperature absorption spectra of dilute solutions (4.5×10^{-5} M) in THF of Na⁺ (----) and Tl⁺ (—) salts of salicylaldehyde.

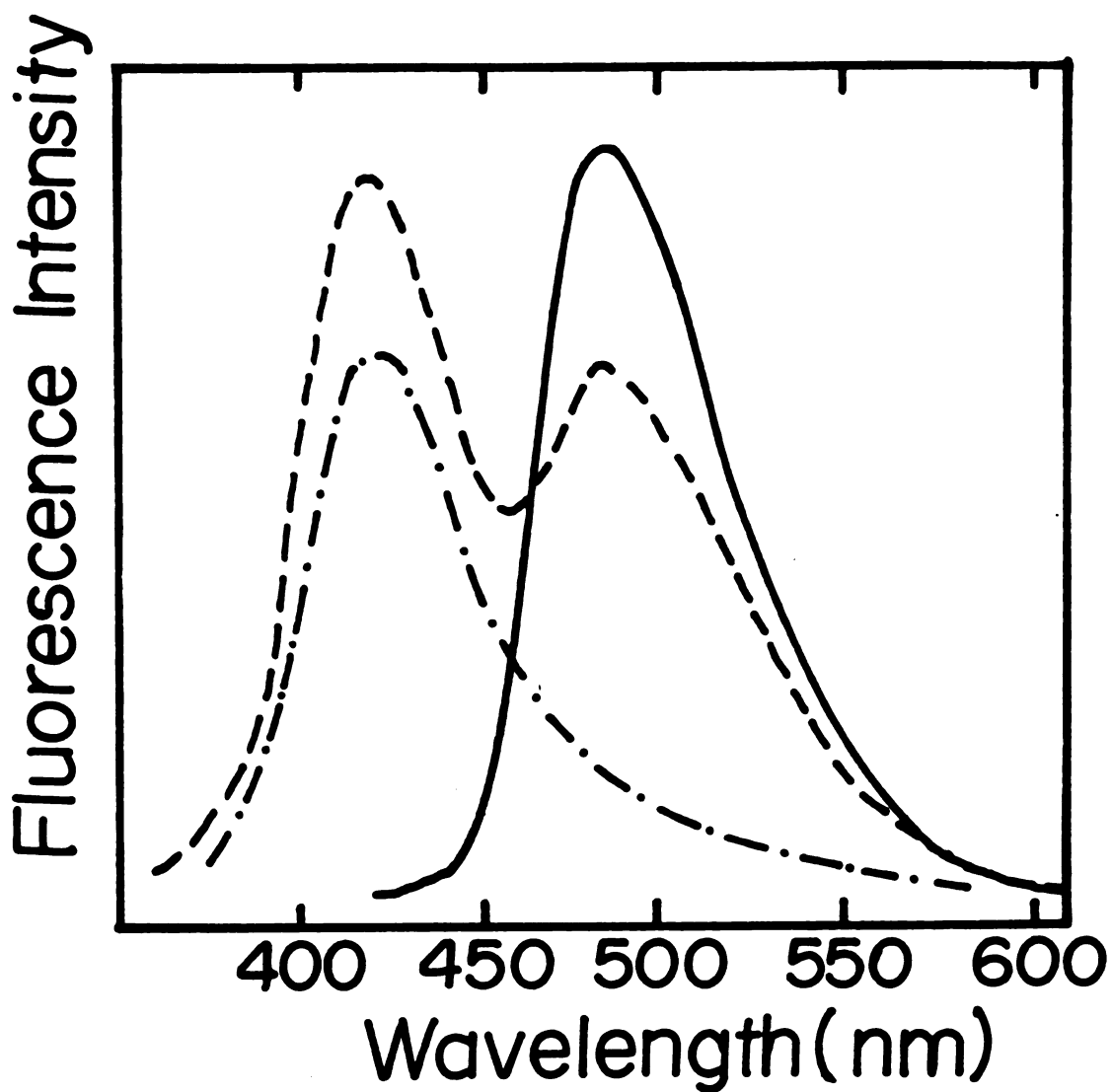


Figure 48. Room temperature emission spectra of dilute solutions of Na^+ salt of salicylaldehyde (5×10^{-5} M) in DMSO: $\lambda_{exc} = 320$ nm (----), $\lambda_{exc} = 380$ nm (—) and in DMSO in the presence of NaBF_4 (2×10^{-2} M), $\lambda_{exc} = 320$ (---·---·).

emission spectra of the sodium salt of salicylaldehyde in DMSO. Exciting at the absorption maximum of the free anion produced an emission from the free anion at 480 nm. Excitation at 323 nm, the absorption maximum of the contact ion-pair gave two emissions. The shorter-wavelength emission at 405 nm belongs to the associated pair and the longer-wavelength emission at 480 nm to the free anion. In the presence of (2×10^{-2} M) Na^+ ions, excitation at 323 nm gave only the 405 nm emission whereas, excitation of the same solution at 380 nm produced only the free anion emission. Thus, the production of two emissions when exciting at the absorption band of the contact ion pair indicates that the contact ion pair dissociates as a result of excitation i.e., the equilibrium shifts towards free ion formation in the excited state. Similar results were obtained in the corresponding thallium (I) salt. In a dilute solution of the thallium salt (5×10^{-5} M) in DMSO in the presence of (10^{-3} M) TlNO_3 , Figure (49), the anion emission was observed upon excitation at the longer-wavelength whereas, fluorescence quenching occurred when at the absorption band of the contact ion-pair was excited, this may reflect the high degree of covalency in the metal cation-salicylaldehyde anion ion-pairs. Since in the same solution the observation of the intense anion emission eliminates the quenching through collisional mechanisms by the excess Tl^+ ion present in solution, i.e., the

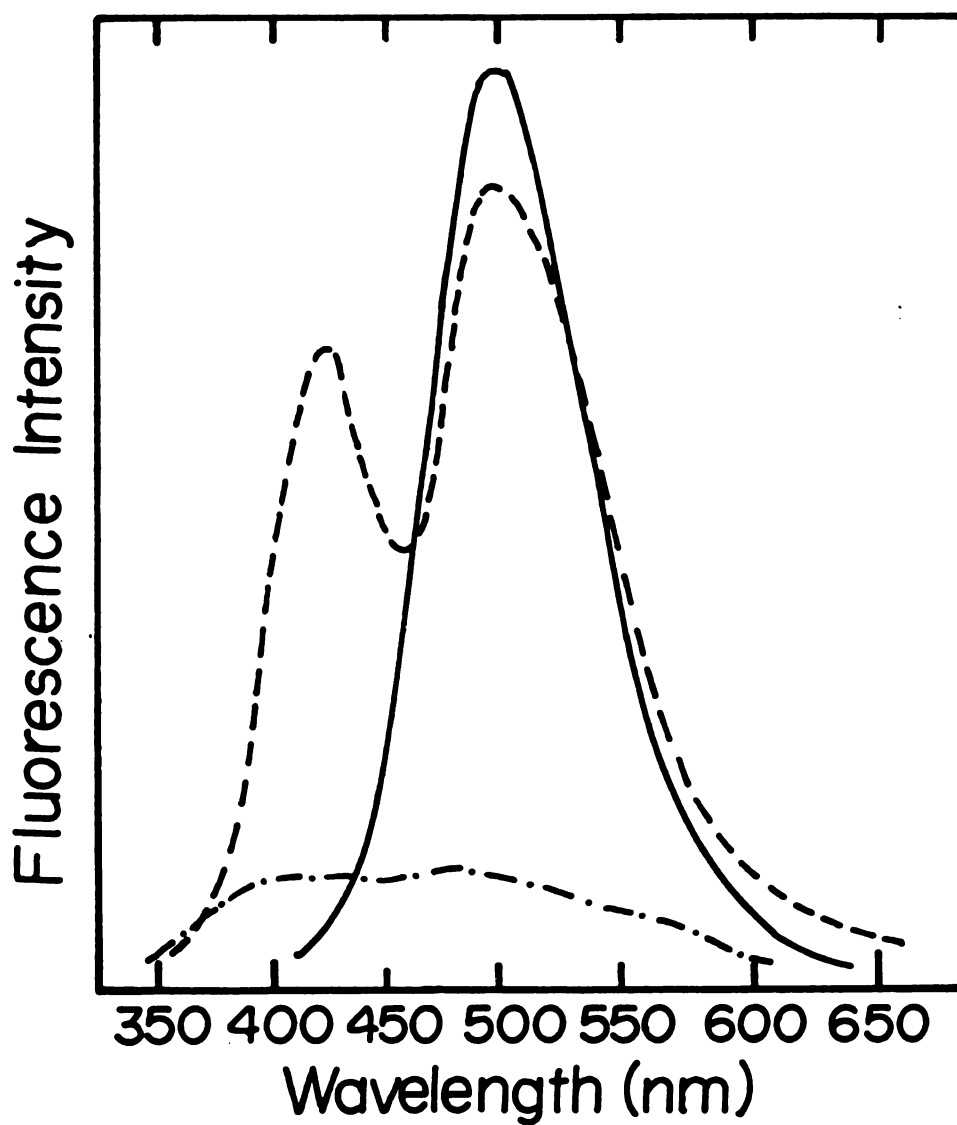


Figure 49. Room temperature emission spectra of dilute solutions (5×10^{-5} M) in DMSO of: Tl(I) salt of salicylaldehyde, $\lambda_{\text{exc}} = 320$ nm (----) and 420 nm (—); Tl(I) salt of salicylaldehyde in presence of $\sim 5 \times 10^{-3}$ M TlNO₃, $\lambda_{\text{exc}} = 320$ nm (-·-·-).

quenching is via internal heavy atom effect⁽⁴⁶⁾. In solutions of Na^+ and Tl^+ salts of salicylaldehyde in THF, Figure (50), both gave the free anion emission at 500 nm when excited at 320 nm where the ion pair absorbs, or at 380 nm where the free anion absorbs. The red shift of the emission of the anion in THF compared with that in DMSO at 480 nm can be interpreted as a result of more stabilization of the ground state in DMSO than in THF. Excitation of the anion leaves a smaller negative charge on the phenolate oxygen in the excited state compared with the ground state charge distribution. In the presence of excess metal ions the emission spectra started to show ion pair emission peaks at ~ 420 nm as well as the anion emission. The intensity of this emission was higher for the Na^+ salt than for the K^+ salt i.e., the shift in the equilibrium between the ion pairs and free ions is more shifted towards ion pair formation in the case of Tl^+ than Na salts. In aqueous solutions, complete dissociation, at least in the excited state, gave only the anion emission.

In this section, the results of our study of the interaction of monovalent alkali metal ions with three phenols, namely: p-hydroxybenzaldehyde, p-methoxybenzaldehyde, and p-methylphenol are summarized. Para-substituted phenols were chosen to contrast possible interaction unique to ortho-substituted derivatives. It should be pointed out that Zaugg and Schafer⁽¹⁴⁾ studied the

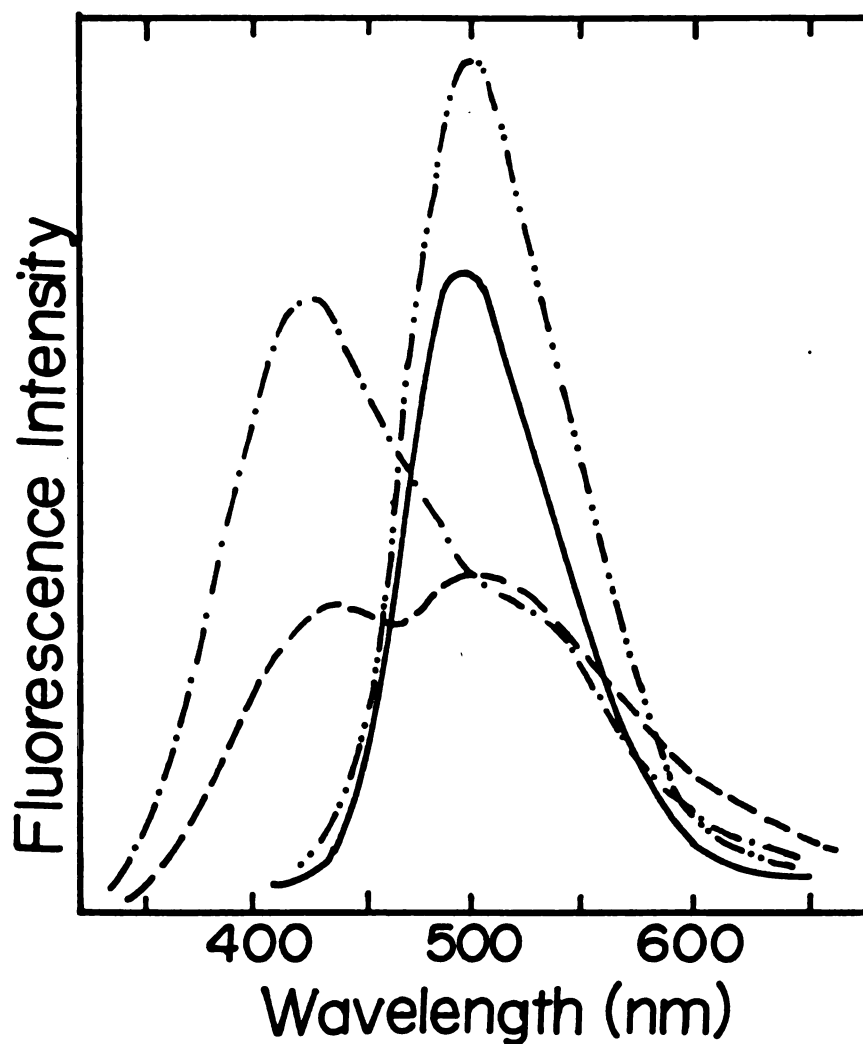


Figure 50. Room temperature emission spectra of dilute solutions (5×10^{-5} M) of Na^+ and Tl^+ salts of salicylaldehyde in THF. Na^+ salt, $\lambda_{\text{exc}} = 320$ and 390 nm (—); Na salt in presence of $\sim 2 \times 10^{-2}$ M NaBF_4 , $\lambda_{\text{exc}} = 320$ nm (----); $\text{Tl}(\text{I})$ salt, $\lambda_{\text{exc}} = 320$ and 390 nm (-·-·-·-·-); and $\text{Tl}(\text{I})$ salt in presence of $\approx 5 \times 10^{-3}$ M TlNO_3 , $\lambda_{\text{exc}} = 320$ nm (-·-·-·-·-).

cation and solvent effects on the ultraviolet absorption spectra of alkali metal salts of some phenols and enols. They reported a red shift in the absorption spectrum of alkali salts of a phenol in dimethoxyethane as the radius of the cation is increased. These results were interpreted in terms of an increased interionic distance, and hence smaller interaction between the anion and cation forming the contact ion pairs.

The absorption spectra of dilute solutions (5×10^{-5} M) of p-hydroxybenzaldehyde and its Li^+ , Na^+ and K^+ salts in THF are shown in Figure (51). The phenol absorbs at 272 nm. When LiH was added to the phenolic solution, the obtained absorption spectrum showed two bands: one identical to that of the phenol and another band with maximum at 328 nm. The shorter-wavelength absorption band is due to unreacted phenol; while the absorption band at 328 nm is due to ion-pair formation. Addition of NaH or KH to the phenolic solution produced the sodium or potassium salt respectively, and the reactions were complete. The absorption maxima occurred at 334 nm for the Na^+ salt and at 347 nm for the K^+ salt. The increase in the radius of the cation leads to progressive red shift of the absorption of the ion pair from 328 nm for Li^+ salt to 347 nm for the K^+ salt. The free anion of p-hydroxybenzaldehyde absorbs at 360 nm in THF as obtained from the absorption spectrum in the presence of tetrabutylammonium hydroxide. When 18-crown-6

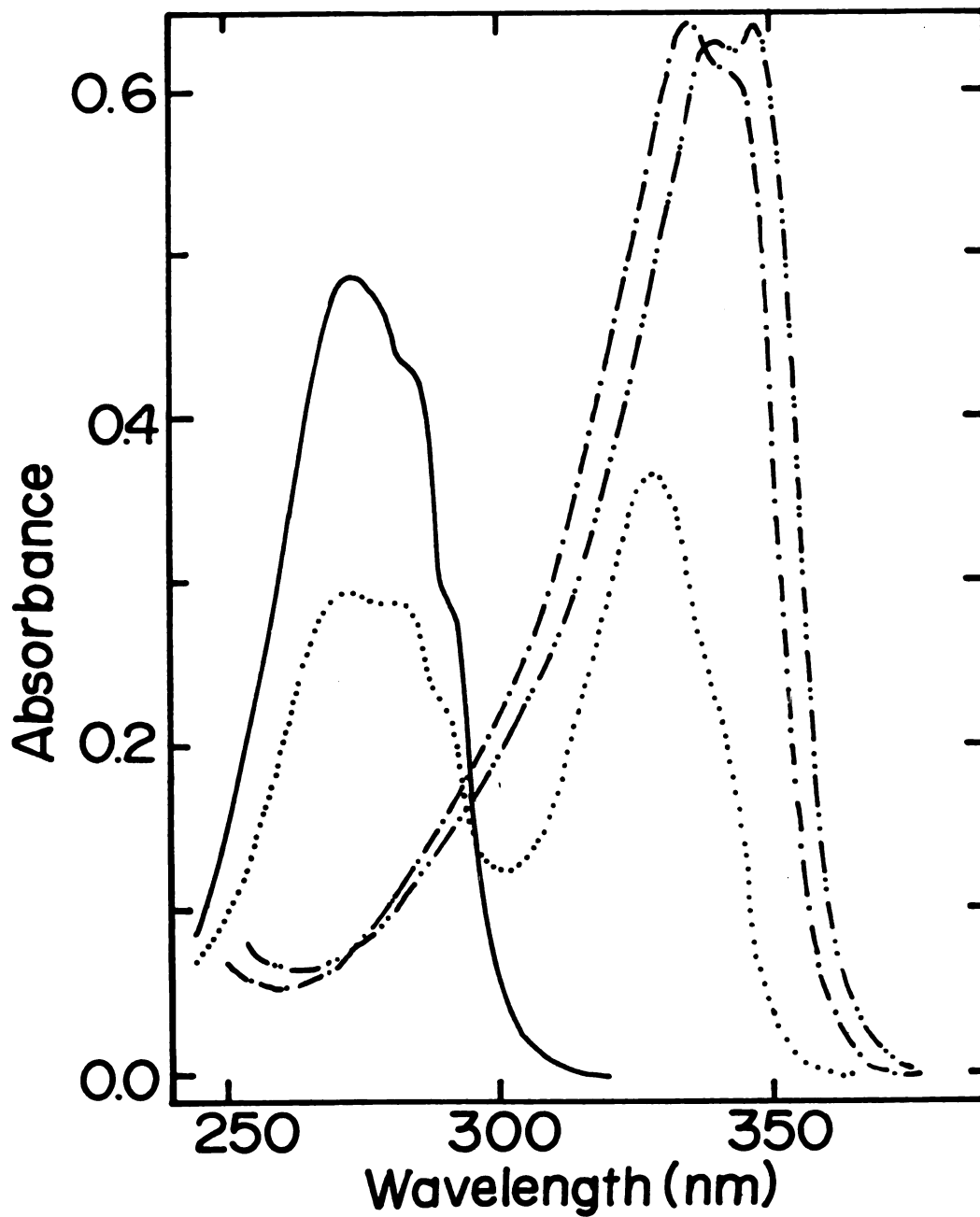


Figure 51. Room temperature absorption spectra of dilute solutions (5×10^{-5} M) of alkali-metal salts of p-hydroxybenzaldehyde in THF. P-hydroxybenzaldehyde (—); Li⁺ salt (.....); Na⁺ salt (-·-·-·-) and K⁺ salt (- - - - -).

was added to metal salt solution, no effect was observed for the Li^+ salt. Li^+ does not form stable complexes with 18-crown-6. However, in the case of the Na^+ and K^+ salts, red shifts of 500 cm^{-1} and 900 cm^{-1} respectively, were observed. The stability constant of the K^+ complex with 18-crown-6 is larger than that of Na^+ . These red shifts are interpreted in terms of the crown ether forming a complex with metal cation in the ion pair. Such interaction will decrease the interionic separation, decreasing the perturbation influence of the positive charge of the cation, causing a red shift, i.e., the spectrum approaches that of the free anion. The room temperature emission spectra of p-hydroxybenzaldehyde salts in THF are shown in Figure (52). The emission maxima of the Li^+ , Na^+ and K^+ salts occur at 357, 361, and 365 nm respectively. It is clear that the emission maximum undergoes a red shift with the increasing radius of the metal ion. In the presence of 18-crown-6 both Na^+ and K^+ salts produced the same emission maximum at 372 nm which is the same emission of the free anion in THF. These results indicate that the ion-pair, weakened by cation interaction with 18-crown-6, dissociates upon electronic excitation giving rise to the excited free anion.

Comparing the absorption and emission spectra of the salts of ortho and para hydroxybenzaldehyde leads to the conclusion that a tighter ion pair is formed with salicylaldehyde and that a metal chelate is formed with the former

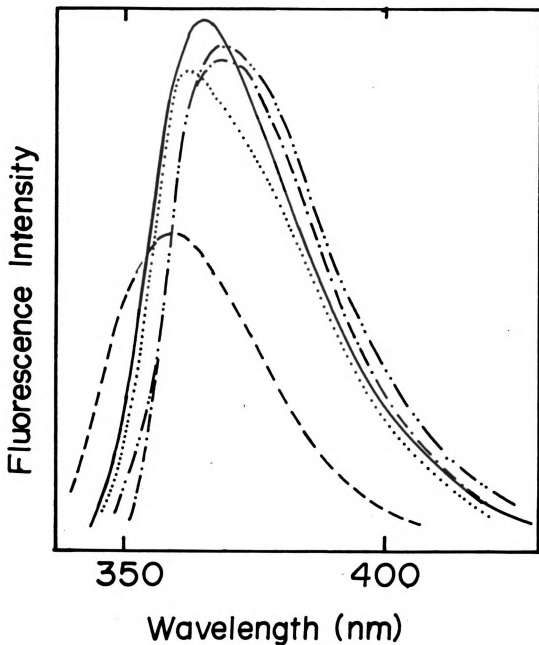


Figure 52. Room temperature emission spectra of dilute solutions (5×10^{-5} M) of alkali-metal salts of p-hydroxybenzaldehyde in THF. Li^+ salt, $\lambda_{\text{exc}} = 335$ nm (----), K^+ salt, $\lambda_{\text{exc}} = 345$ nm (—) and K^+ salt in presence of 10^{-3} M 18C6, $\lambda_{\text{exc}} = 345$ nm (-·-·-·), Na^+ salt $\lambda_{\text{exc}} = 340$ nm (....), Na^+ salt in presence of 10^{-3} M 18C6, $\lambda_{\text{exc}} = 340$ nm (-·-·-·).

where the ortho-substituted anion acts as a bidentate ligand with both phenolate and carbonyl oxygen atoms.

Similar results were obtained for p-methoxyphenol, the absorption spectra of its metal salts are shown in Figure (53). Addition of LiH did not change the absorption spectrum of the phenol, it appears that no salt formation occurred. The absorption maxima of the Na⁺ and K⁺ salts indicate that ion pairs are formed in THF solutions. The corresponding emission spectra of the two salts are displayed in Figure (54). The emission spectra of both Na⁺ and K⁺ salts are blue shifted compared to that of the parent phenol. When 18-crown-6 was added to the Na⁺ salt in THF, a new emission was observed at 440 nm, but the original emission at 364 nm of the salt while diminished in intensity still occurred. In the case of the K⁺ salt, addition of 18-crown-6 led to the disappearance of the 367 nm emission of the ion pair and only one emission band was observed at 440 nm. The latter emission corresponds to the free anion emission obtained in THF in the presence of tetrabutylammonium hydroxide. These results are interpreted in terms of the change in the stability of the ion pair upon electronic excitation. In the excited state, as mentioned before, the charge density at the phenoxide oxygen is diminished due to the charge migration to the benzene ring. This weakens the interaction with the metal ion. However, this effect does not manifest

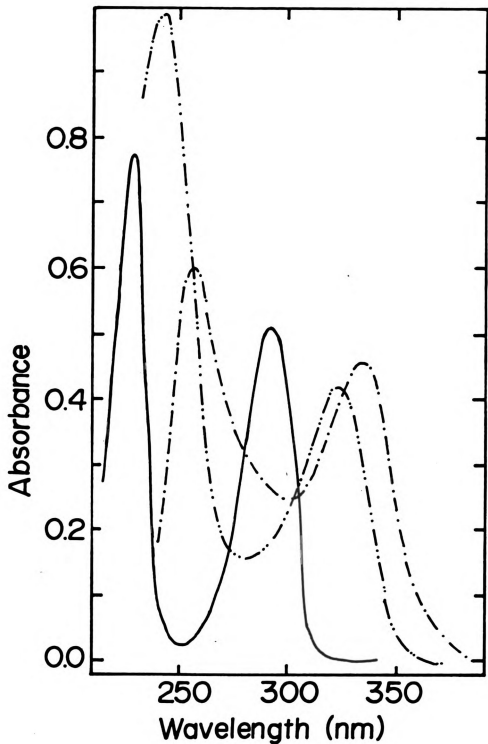


Figure 53. Room temperature absorption spectra of dilute solutions (1.8×10^{-4} M) of alkali-metal salts of p-methoxyphenol in THF. P-methoxyphenol (—), Na⁺ salt (-·-·-·) and K⁺ salt (·-·-·).

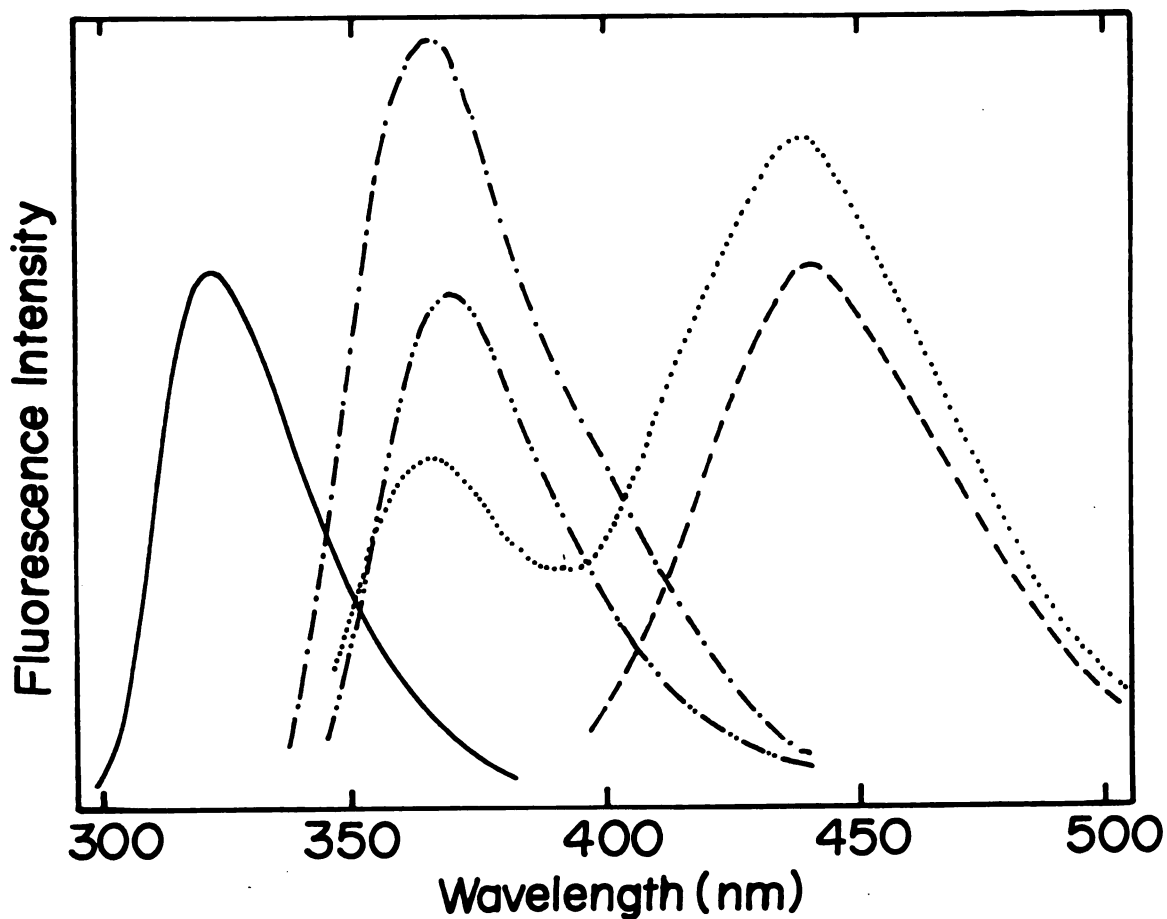


Figure 54. Room temperature emission spectra of dilute solutions (1.8×10^{-4} M) of alkali-metal salts of p-methoxyphenol in THF. P-methoxyphenol, $\lambda_{\text{exc}} = 290$ nm (—); Na^+ salt, $\lambda_{\text{exc}} = 320$ nm (-·-·-); Na^+ salt in presence of 10^{-3} M 18C6, $\lambda_{\text{exc}} = 320$ nm (....); K^+ salt, $\lambda_{\text{exc}} = 335$ nm (-·-·-·-) and K^+ salt in presence of 10^{-3} M 18C6, $\lambda_{\text{exc}} = 335$ nm (----).

itself except in the presence of the crown ether. Thus, in the excited state, the crown ether competes effectively with the phenoxide anion for the metal cation and is particularly true in the case of K^+ which has a larger radius and forms a weaker bond with the anion and also because it forms a more stable complex with the crown ether compared with Na^+ . Thus, the two emission bands observed in the case of the Na^+ salt in the presence of 18-crown-6 are due to partial dissociation of the ion pair in the excited state. In the case of the K^+ salt in the presence of 18-crown-6, complete dissociation of the ion pair occurs.

The absorption and emission spectra of alkali metal salts with p-methylphenol in THF are shown in Figure (55) and (56), respectively. Ion-pair formation occurs in THF and their absorption maxima occur at 310 nm for Na^+ and 317 nm for K^+ . In the presence of 18-crown-6 a further red shift occurs for K^+ giving an absorption at 326 nm. The emission spectra gives rise to a maximum at 344 nm and 355 nm for Na^+ and K^+ , respectively. This should be compared with 360 nm for the free anion emission in THF. Table (9) summarizes the absorption and emission spectral results of the three phenols in THF.

From the previous discussion, it is clear that monovalent cations form tight ion pairs in THF. The interionic separation increases with the size of the cation giving

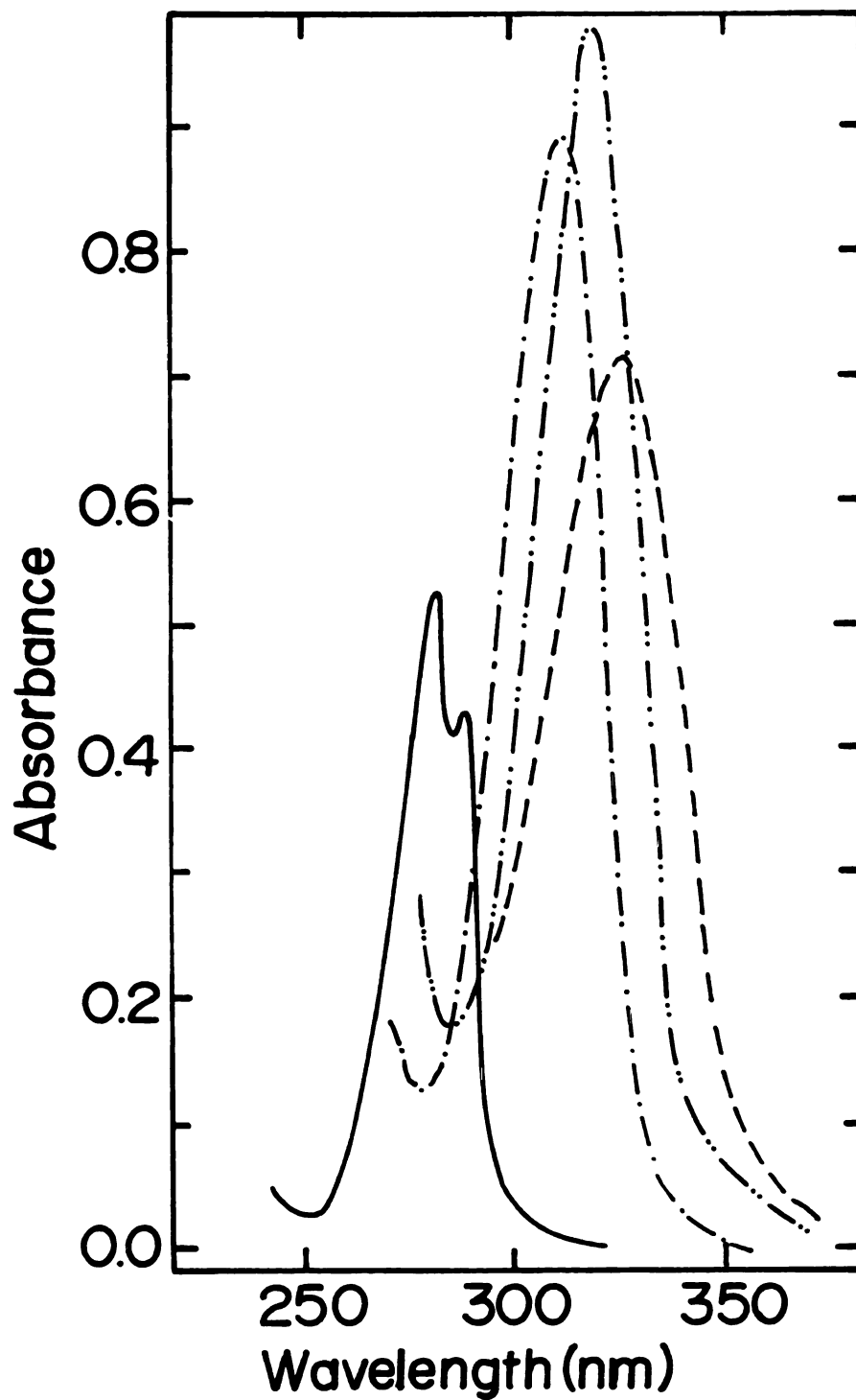
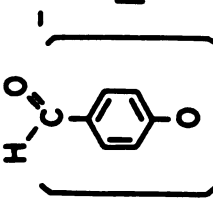
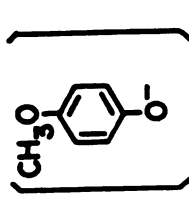
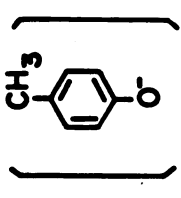


Figure 55. Room temperature absorption spectra of dilute solutions (2.5×10^{-4} M) of alkali-metal salts of p-methylphenol in THF. P-methylphenol (—), Na^+ salt (-·-·-), K^+ salt (-·-·-·) and K^+ salt in presence of 10^{-3} M 18C6 (----).

Table 9. Room Temperature Absorption and Emission Maxima of Para-Substituted Phenols and Their Salts in THF.

Compound	M ⁺	Absorption			Emission	
		λ_{\max} (nm)	$\epsilon_{\max} \times 10^{-4}$	λ_{\max} (nm) 18C6	λ_{\max} (nm)	λ_{\max} (nm) 18C6
	H ⁺	272	0.97			
	Li ⁺	328	0.73		357	
	Na ⁺	334	1.28	340	361	372
	K ⁺	347	1.28	357	365	372
	H ⁺	292	0.29		320	
	Na ⁺	323	0.24	323	364	364 440
	K ⁺	334	0.26	334	367	440
	H ⁺	282	0.21		305	
	Na ⁺	310	0.36		344	
	K ⁺	317	0.40	326	355	

18C6 = 18-Crown-6.

rise to a red shift in going from Na^+ to K^+ . In the presence of 18-crown-6 it interacts with the cation resulting in a looser ion-pair formation. In the excited state the ion pair becomes weaker due to a decrease in the negative charge on the phenoxide oxygen and in the case of bigger cation (K^+) in the presence of 18-crown-6 complete dissociation of the ion pair may occur.

CHAPTER V

EUROPIUM (III) CHELATE WITH SALICYLIDENE-VALINATE SCHIFF BASE

I. Lanthanide Ions as Luminescence Probes of the Structure of Biological Macromolecules

Calcium and magnesium occur as essential inorganic ions in living systems. A Ca^{2+} concentration gradient is maintained across many cell membranes with the concentration within the cell lower than that outside. Ca^{2+} is involved in muscle contraction, blood clotting, K^+ transport, neurotransmitter release, cellular adhesion, intercellular communication, microtubule formation, and hormonal responses. Many of these Ca^{2+} related activities occur by means of interaction with proteins, which Ca^{2+} may stabilize, activate, and modulate. In this way Ca^{2+} plays a significant regulatory role in many biological processes. Because of the lack of suitable physical techniques for studying Ca^{2+} , it has not received the attention it deserves. The electronic transitions of Ca^{2+} cannot be studied by conventional optical absorption and emission spectroscopy, and the absence of unpaired electrons precludes the use of magnetic resonance

techniques in probing the chemical and structural nature of Ca^{2+} binding sites.

Fortunately, about 12 lanthanide ions (Ln^{3+}) possess properties which make them excellent probes for Ca^{2+} ⁽⁸³⁾. In forming complexes, both Ca^{2+} and Ln^{3+} prefer charged or uncharged oxygen donor groups to nitrogen donor atoms. In aqueous solution, except for some multidentate ligands, hydroxo complex formation almost always occurs before amine nitrogen coordination takes place⁽⁸⁴⁾. Both Ca^{2+} and Ln^{3+} display a variable coordination number and a lack of strong directionality in binding donor groups. Trivalent lanthanide ions Ln^{3+} exhibit effective ionic radii that show a gradual contraction from one end of the series to the other, for example, from 1.16 Å for La^{3+} (atomic number 57) to 0.98 Å for Lu^{3+} (atomic number 71) in 8-fold coordination⁽⁸⁵⁾. For a given coordination number, the decrease in the ionic radii in going from one end of the lanthanide series to the other (0.17 - 0.19 Å) is about equal to the increase in ionic radii on going from 6- to 9-fold coordination. Thus, there are opportunities for fine adjustment upon substitution of heavier Ln^{3+} for Ca^{2+} ions either by small decreases in ionic radii or by an increase in coordination number. As an example, the ionic radius of 7-coordinate Ca^{2+} is nearly equal to the ionic radius of 8-coordinate Eu^{3+} ion. The replacement of Ca^{2+} by Ln^{3+} has been demonstrated by x-ray diffraction to occur in two proteins, carp parvalbumin^(86a) and thermolysin^(86b).

In the latter case, the results have been reported with sufficient precision to allow some comparisons of bond distances and coordination numbers between Ca^{2+} and Ln^{3+} containing proteins. Accordingly, most Ln^{3+} should be able to substitute Ca^{2+} in proteins without causing serious structural modifications in the active sites. The unit charge difference between Ca^{2+} and Ln^{3+} is apt to be of secondary importance for substitution of Ln^{3+} for Ca^{2+} . In biological systems Na^+ and Ca^{2+} of comparable ionic radii have been found to be competitive for sites as have K^+ and Ba^{2+} (87,88). Charge differences may assume more importance in rate phenomena which may be sensitive to net charge at a binding site.

Except for La^{3+} and Lu^{3+} , all 12 other available Ln^{3+} ions contain unpaired f-electrons, and both nuclear magnetic resonance (NMR) and electron spin resonance (ESR) methods may be used to investigate their environment (89a,b). Several Ln^{3+} may be used as chemical shift probes in NMR. Gd^{3+} with half-filled 4f subshell is used as a broadening probe in NMR and also is employed in ESR studies. These 12 Ln^{3+} ions also exhibit absorption spectra due to inter-configurational f-f transitions which are easily accessible to study by conventional optical absorption techniques. However, the molar absorptivity associated with these transitions are generally so low (of the order of unity) that the study of Ln^{3+} -protein systems in which Ln^{3+}

concentrations are smaller than 10^{-2} M, optical absorption spectroscopy can be performed only near the limits of instrumental sensitivity. On the other hand, luminescence due to interconfigurational f-f transitions in Ln^{3+} ions bound to protein systems remains well above detection limits even when Eu^{3+} and Tb^{3+} are present at concentrations as low as 10^{-6} M. Thus a factor of at least 10^4 in sensitivity favors luminescence over absorption spectroscopy.

In order for luminescence to occur, appropriate excited states of the emitting (luminescent) species must be populated. The use of Ln^{3+} ion emission spectra as a probe of Ln^{3+} complexes requires, then, excitation of the Ln^{3+} f-f emitting states. Excitation may be accomplished either by direct excitation of the metal ion chromophore (the exciting light being absorbed directly by the Ln^{3+} ion) or by an indirect mechanism involving optical excitation of ligand chromophores followed by sensitization of Ln^{3+} emission via radiationless energy transfer (ligand to metal ion). Because of the weak absorptivities of Ln^{3+} transitions in the visible and near-ultraviolet spectral region, direct excitation of Ln^{3+} emission requires either a powerful excitation source (such as a laser) or relatively high concentration of the metal ion ($>10^{-2}$ M). On the other hand, indirect excitation of Ln^{3+} emission may be accomplished using somewhat less intense exciting light and at lower metal ion concentrations if the ligand environment includes a highly absorbing

chromophore capable of acting as an efficient energy donor to the Ln^{3+} acceptor-emitter species. Both the direct and indirect excitation methods have been used in emission studies of Ln^{3+} -protein complexes.

In the indirect excitation method, in Ln^{3+} -protein systems, the Ln^{3+} ion may be excited by energy transfer from nearby aromatic side chain chromophores which are excited directly by near-ultraviolet radiation. The overall process is thus started by an absorption of an aromatic side chain of phenylalanine, tyrosine, or tryptophan in the 250-300 nm region; followed by a non-radiative energy transfer from an aromatic side chain to a nearby Ln^{3+} ; giving rise to a strongly enhanced (up to 10^5) Ln^{3+} emission in the visible region. The energy transfer

step probably occurs by a Förster dipole-dipole resonance transfer mechanism⁽⁹⁰⁾ with a r^{-6} dependence on the distance between the donor and acceptor sites. A semi-quantitative analysis suggests that 50% probability of energy transfer occurs at a donor to acceptor distance of 5-10 Å for tyrosine- Tb^{3+} and tryptophane- Tb^{3+} pairs⁽⁹¹⁾. Using Tb(III) or Eu(III) as an acceptor, Horrocks et al.⁽⁹¹⁾ measured the distance between tryptophane as an energy donor and the calcium-binding sites in parvalbumin from codfish. The 11.8 and 10.2 Å distances obtained using Tb^{3+} and Eu^{3+} as acceptor respectively, are in a good agreement with the 11.6 Å distance estimated from x-ray structural results.

Direct excitation of Eu^{3+} and Tb^{3+} emission using a pulsed laser source was employed in the study of luminescence lifetimes for a variety of complexes in aqueous solution⁽⁹²⁾. The lifetime and emission decay characteristics of Eu^{3+} and Tb^{3+} with a variety of ligands (including the protein thermolysin) were measured as a function of D_2O versus H_2O content of the water solvent. Such studies gave estimates of the number of water molecules bound to the Ln^{3+} in each complex⁽⁹²⁾. This follows from the somewhat different perturbative influences of D_2O versus H_2O upon the rate of radiative and radiationless processes of Eu^{3+} and Tb^{3+} excited states⁽⁹³⁾.

Eu^{3+} and Tb^{3+} are the most strongly emitting members of the Ln^{3+} series. Energy level diagram for Eu^{3+} and Tb^{3+} are shown in Figure (57)⁽¹¹⁾. The $^5\text{D}_0$ and $^5\text{D}_4$ emission levels of Eu^{3+} and Tb^{3+} can be excited by 579 and 488 nm light, respectively. The use of visible light for the excitation eliminates problems of protein-ultraviolet photosensitivity. The excited state lifetimes of these ions are environmentally sensitive and lies in the conveniently long 100-300 μs range. While ligand field splittings of f-electron levels are much smaller than for the d-electron levels of transition metal complexes, the absorption bands are generally much narrower, and small splittings can be readily detected. Individual emission bands can be examined under high resolution to yield

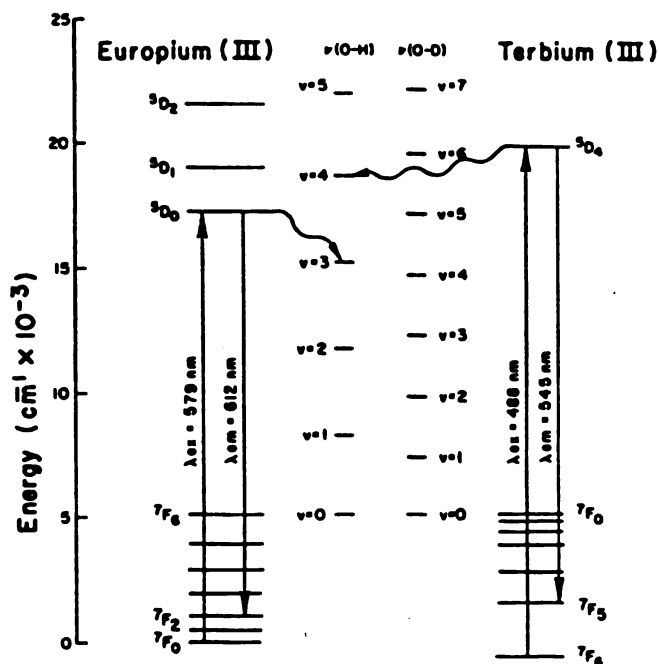


Figure 57. Electronic energy levels for europium(III) and terbium(III). The two upward-pointing arrows show the transitions which occur upon laser excitation at the wavelengths indicated. The two downward-pointing arrows label the most intense emissive transitions of the two ions. Radiationless energy transfer competes with the radiative processes through coupling of the emissive states to the O-H vibrational overtones of coordinated H_2O molecules. (The energy level diagram of Tb(III) has been displaced slightly to position the highest electronic acceptor state of the ground 7F term to coincide with the zero-point energies of the vibrational overtone ladders.)¹¹

information about the splitting of ground and excited states. Excitation spectroscopy using tunable lasers also yields information of this type.

A. Decay Lifetimes as a Measure of the Number of Metal Coordinated Water Molecules

The early observation that hydrated crystals show a much reduced fluorescence intensity in the middle of the series of rare earth ions (Sm, Eu, Gd, Tb, Dy) and practically no emission in those at the beginning and end of the series, led to the conjecture⁽⁹⁴⁾ that the highly energetic O-H vibrations in the crystal lattice act as energy sinks. The role of OH vibrations in the quenching of electronic f-f transitions in the rare earth transitions was demonstrated in crystals⁽⁹⁵⁾ by measuring fluorescence lifetimes of deuterated and protonated hydrous crystals of EuCl_3 and TbCl_3 . Quenching occurs if the energy gap between the lowest fluorescent and highest non-fluorescent level is matched by a single high energy (OH or OD) vibration of one solvent molecule. The decisive parameter is R, the ratio between the electronic energy gap (E) and the vibrational quantum energy ($h\omega$)⁽⁹⁶⁾.

$$R = E/h\omega$$

Of all the lanthanides Gd is in a class by itself with

$R \sim 10$ for H_2O and ~ 15 for D_2O .

There is a very low probability of radiationless transition to the very high vibrational quanta thus required. Accordingly⁽¹⁶⁾ addition of a single high-energy vibrational quantum due to deuterium substitution make no significant contribution to the radiationless dissipation of electronic energy. Hence, no isotopic effect is observed in the case of Gd. For Eu^{3+} ($E \sim 12,200 \text{ cm}^{-1}$), the isotope effect is the greatest of all Ln(III) series and is due to the requirement of $\nu = 4$ for OH and $\nu = 5$ for OD. Radiationless transition probability is not small and will differ greatly depending on whether H_2O or D_2O is interacting with Eu(III). For Tb^{3+} , ($E \sim 14,800 \text{ cm}^{-1}$), radiationless transition occurs to $\nu = 5$ for OH and to $\nu = 6$ or 7 for OD resulting in smaller probability for the transition compared to the case of Eu^{3+} and hence longer lifetime for Tb^{3+} is observed, and the isotopic effect is smaller.

The experimental reciprocal excited-state lifetime (exponential decay constant), τ_{obsd}^{-1} , consists of several terms

$$\tau_{\text{obsd}}^{-1} = \tau_{\text{nat}}^{-1} + \tau_{\text{nonrad}}^{-1} + \tau_{\text{OH}}^{-1}$$

where τ_{nat}^{-1} is the natural rate constant for the emission of photons, $\tau_{\text{nonrad}}^{-1}$ represents the rate constant for

nonradiative deexcitation which does not involve OH oscillators, and τ_{OH}^{-1} is the rate constant for nonradiative energy transfer to the OH vibrational manifold of OH oscillators in the first coordination sphere (e.g., coordinated water molecules); τ_{OH}^{-1} is very significant. For instance, for Eu^{3+} (aq), $\tau_{\text{OH}}^{-1} = 9.5 \text{ ms}^{-1}$, whereas, $\tau_{\text{nat}}^{-1} = 0.19 \text{ ms}^{-1}$, $\tau_{\text{nonrad}}^{-1} = 0.25 \text{ ms}^{-1}$ (93,97a). Replacement of OH oscillators by the OD variety causes the vibronic deexcitation pathway to become exceedingly inefficient (97a-c) because of the smaller orbital overlap as the vibronic quantum increases, and enables one to determine the number of OH oscillators in the first coordination sphere by carrying out experiments independently on H_2O and D_2O solutions. In D_2O solutions τ_{OH}^{-1} vanishes and $\tau_{\text{obsd}}^{-1} = \tau_{\text{nat}}^{-1} + \tau_{\text{nonrad}}^{-1}$, where the latter term includes any small deexcitation via DO oscillators. τ_{obsd}^{-1} varies linearly with the mole fraction of H_2O , $\chi_{\text{H}_2\text{O}}$, in H_2O - D_2O mixtures (92). Figure (58) (11), shows a plot of τ_{obsd}^{-1} vs $\chi_{\text{H}_2\text{O}}$ for EuCl_3 . In pure H_2O , nine water molecules are coordinated to Eu^{3+} . When 1 mole of EDTA (ethylenediaminetetracetate) was added the number of coordinated water molecules dropped to six. This is in agreement with the tridentate nature of EDTA which substitutes water molecules in the first coordination sphere. The same technique was used to estimate the number of coordinated water molecules in crystalline solids. (98a)

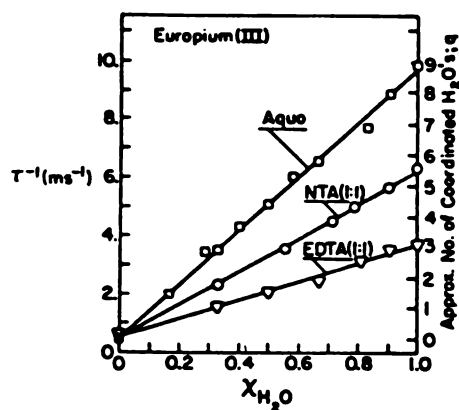


Figure 58. Plot of the observed reciprocal luminescence lifetimes, τ_{obs}^{-1} , vs. the mole fraction of H_2O , X_{H_2O} , in D_2O - H_2O mixtures of $Eu(III)$ solutions. The effect of the chelating ligands NTA and EDTA is to displace water molecules from the first coordination spheres of the aquametal ions to yield the approximate values indicated along the right-hand ordinate.¹¹

B. Characterization of Individual Binding Sites

Eu(III) ion is unique in that both the ground (7F_0) and the emissive excited (5D_0) states are nondegenerate. Since neither of these levels can be split by a ligand field, the absorption band corresponding to a transition between these levels must consist of a single, unsplit line for a given Eu(III) ion environment. Different ionic environments can, in principle, yield transitions at slightly different frequencies. Because ${}^5D_0 \leftarrow {}^7F_0$ transition is highly forbidden, study of this band by ordinary absorption spectroscopy on dilute solutions is not feasible. However, since 5D_0 is emissive, this transition can be studied via excitation spectroscopy by monitoring emitted photons (${}^5D_0 \rightarrow {}^7F_2$, 612 nm) while a tunable laser is continuously scanned through the ${}^5D_0 \leftarrow {}^7F_0$ transition region (578-580 nm). The position and shape of the excitation band will depend on the microenvironment around the Eu^{3+} ion.

Figure (59) shows the excitation spectra resulting from the titration of the Eu(III) aqua-ion with tridentate ligand, dipicolinate (DPA)^(98b). Individual narrow peaks characteristic of Eu^{3+} (aq), $[\text{Eu}(\text{DPA})]^+$, $[\text{Eu}(\text{DPA})_2]^-$, and $[\text{Eu}(\text{DPA})_3]^{3-}$ are apparent at the following respective frequencies: 17272, 17263, 17248, and 17231 cm^{-1} . Eu(III) excitation spectroscopy was used to characterize the individual metal ion binding sites in calcium-binding proteins such as thermolysin. These various Eu(III) coordination

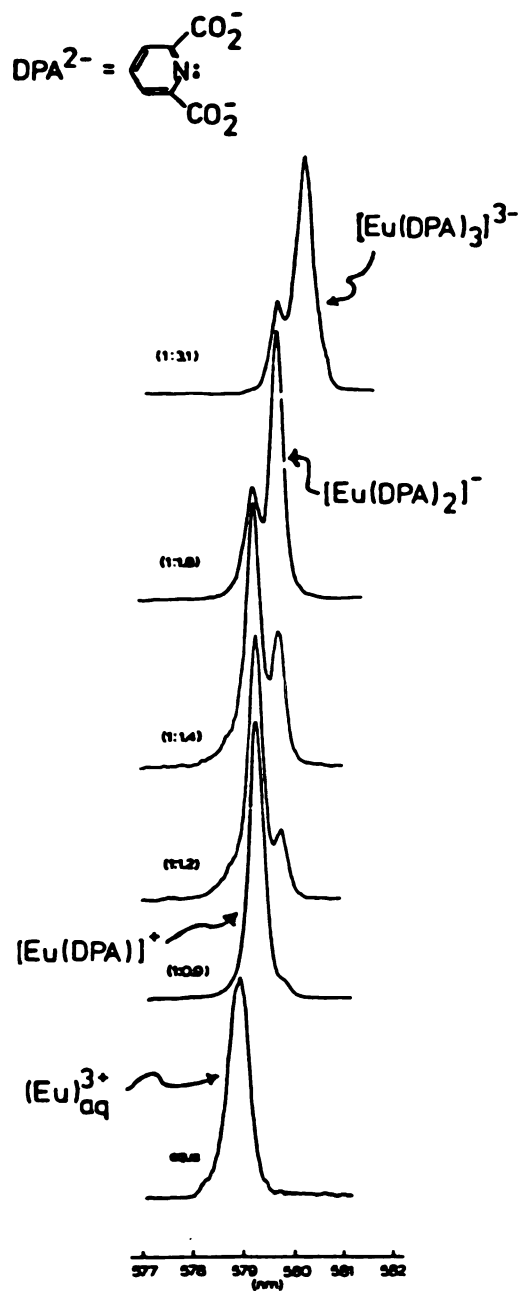


Figure 59. Excitation spectral profiles of the ${}^7F_0 + {}^5D_0$ transition obtained during the course of the titration of an aqueous EuCl_3 solution with the sodium salt of the dipicolinate anion (DPA). Eu(III) to ligand ratios are indicated to the left of each trace.^{98b}

environments were further characterized by their excited-state reciprocal lifetime which can be used to determine the number of coordinated water molecules in each site.

C. Inter Metal-Ion Energy-Transfer Distance Measurements

If there is a significant overlap between the emission spectrum of an energy donor D and the absorption spectrum of an energy acceptor A, energy transfer of a nonradiative kind can take place between D and A. Förster⁽⁹⁹⁾ showed that the efficiency of dipole-dipole energy transfer, E, is inversely proportional to the sixth power of the D-A separation, r, and is given by

$$E = \left(1 - \frac{\tau}{\tau_0}\right) = \left[\left(\frac{r}{R_0}\right)^6 + 1\right]^{-1}$$

τ and τ_0 are the excited-state lifetime of the donor in presence and absence of energy transfer.

r, is the actual donor-acceptor distance, R_0 , the critical distance for 50% energy transfer

$$(R_0)^6 = 8.78 \times 10^{-25} K^2 n^{-4} \phi_J \text{ cm}^6$$

8.78×10^{-25} is the product of fundamental constants K^2 , the orientation factor

n, the refractive index of the medium between the interacting ions

Φ , the quantum yield of the donor in the absence of the acceptor

J, the spectral overlap integral

$$J = \frac{\int F(\nu)\epsilon(\nu)\nu^{-4}d\nu}{\int F(\nu)d\nu}$$

$F(\nu)$ is the luminescence intensity of the donor at frequency (cm^{-1})

$\epsilon(\nu)$ is the molar extinction coefficient of the acceptor ($\text{M}^{-1} \text{cm}^{-1}$)

Ln(III)-transition metal ion and Ln(III)-Ln(III) energy transfer were applied in distance measurements. Recently, energy transfer involving Tb(III) to Fe(III) in transferrin⁽¹⁰⁰⁾ ($R_0 = 27.1 \text{ \AA}$, $r = 25 \pm 2 \text{ \AA}$) and Eu(III) to Co(II) in galactosyltransferase⁽¹⁰¹⁾ ($R_0 = 20 \text{ \AA}$, $r = 18 \pm 3 \text{ \AA}$) were reported. In neither case are confirmatory crystallographic studies available. Horrocks et al.⁽¹¹⁾ used the inter Ln(III) ion energy transfer to measure the distances between the calcium-binding sites in thermolysin. Thermolysin has four Ca^{2+} binding sites, S(1) to S(4), and one Zn^{2+} binding active site. The exchange-inert nature of Ln(III) ions occupying site S(1) of thermolysin makes it possible to substitute a luminescent ion (e.g., Tb(III) or Eu(III)) at this site and a different absorbing ion (e.g., Nd(III), Pr(III), Ho(III), or Er(III)) at sites S(2) and S(4). Nonradiative energy transfer can be

monitored by measuring the effect of the presence of energy acceptor ions on the excited-state reciprocal lifetime of the donor ion. The r values estimated from the energy transfer efficiencies are in good agreement with the X-ray distance of 11.7 Å between calcium sites S(1) and S(4), except for the $Tb^{3+} - Nd^{3+}$ results due to some contribution from a dipole-quadrupole mechanism of energy transfer.

II. Energy Transfer in Rare-Earth Metal Chelates

It was discovered by Weissman⁽¹⁰²⁾ in 1942 that β -diketone coordination compounds of trivalent europium, terbium, and samarium exhibit unusual luminescence properties when excited by near ultraviolet light. The compounds emit visible radiation characteristic of the rare-earth ions. Thus, intra-4f electronic transitions, which are known to originate from levels derived from the electrostatic and spin-orbit interactions among the 4f electrons within the rare-earth ions, occur whenever the excitation is carried out in the intense ligand absorption bands. These ligand bands (molar extinction coefficient $\sim 10^4$ to 10^5) are $\pi-\pi^*$ in nature and are characteristic of the coordinated ligands surrounding the central chelated ion. Weissman realized that the energy was being pumped into the electronic system of the complex characterized by the π -electronic levels of the ligands and was subsequently migrating to the central chelated rare-earth ion, from

whence characteristic luminescence (line emission) of the ion occurred. He designated this process intramolecular energy transfer.

A. Paths of Energy Migration

A schematic energy level diagram for rare earth chelate possessing low-lying 4f electronic state is given in Figure (60)⁽¹⁰³⁾. After excitation of a chelate to a vibrational level of the first excited singlet state ($S_0 \rightarrow S_1$), the molecule undergoes rapid internal conversion to the lower vibrational levels through interaction with the solvent matrix. The excited singlet state may be deactivated by combining radiatively with the ground state ($S_0 \leftarrow S_1$), resulting in molecular fluorescence, or the molecule may undergo radiationless intersystem crossing from the singlet to the triplet system. Again by internal conversion the molecule may reach the lowest triplet state, T_1 . From this state, it can then combine radiatively with the ground state by means of a spin-forbidden transition ($S_0 \leftarrow T_1$) giving rise to a typical long-lived molecular phosphorescence. Alternatively, the molecule may undergo a radiationless transition from the triplet system to a low-lying rare-earth ion state^(104a). The latter states are derived from the 4f electronic configuration of the coordinated trivalent rare-earth ion. After this indirect excitation by energy transfer, the

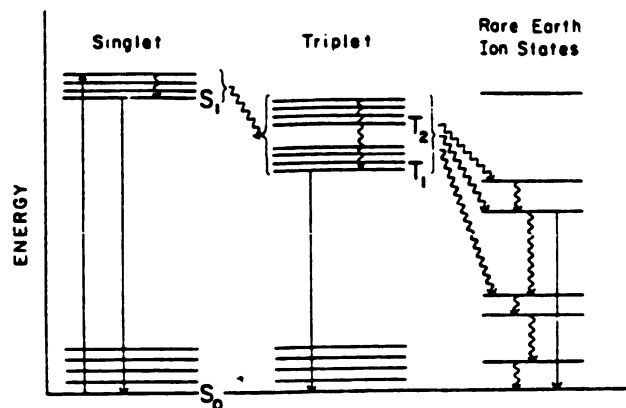


Figure 60. Schematic energy level diagram for a rare earth chelate possessing low-lying 4f electronic states: \rightarrow , radiative transitions; \rightsquigarrow , radiationless transitions.¹⁰³

metal ion may undergo radiative transition to a lower ion state resulting in a characteristic line emission, or it may be deactivated via radiationless processes. Direct transfer of energy from the excited singlet state to the low-lying rare-earth ion states has been shown to be unimportant^(104a).

Using emission spectroscopy, Crosby et al.^(104a-c) obtained a quantitative measurement of the positions of the excited singlet, triplet, and rare-earth ion levels present in rare-earth chelates. By correlating the relative positions of these levels with the observed emission, an empirical rule for the occurrence of line-like emission from these chelates was established. "The lowest triplet-state energy level of a complex must be nearly equal to or must lie above the resonance energy level 'the emitting level' of the rare-earth ion". Whenever a triplet state lies decidedly below a resonance level of a given ion, no emission from that ion level is observed. Figure (61)^(104d) shows the energy levels of several rare-earth ions, along with the measured triplet-state levels of various complexes. Eu(III) has two resonance lines, one at 17,257 cm^{-1} and a second at 19,020 cm^{-1} . Excitation of $\text{Eu}(\text{8HQ})_3$, tris(8-hydroxyquinolate)europium(III), with ultraviolet light results in an emission only from $^5\text{D}_0$ level and not from the upper $^5\text{D}_1$ level. Crosby et al.^(104a,e) interpreted this observation as a proof that the energy

traveled through the triplet manifold and then down to the 5D_0 and could not travel uphill to the 5D_1 .

Three paths have been proposed for the energy transfer process by which the excitation energy absorbed in the $\pi-\pi^*$ electronic bands of the ligands migrates to the resonance 4f electronic levels of the ions. They are:

- I. [singlet(S_1)] \rightsquigarrow [Triplet(T_1) or a triplet slightly higher than T_1] \rightsquigarrow [Rare earth ion (RE) level] \longrightarrow [Emission]^(104a)
- II. [Singlet(S_1)] \rightsquigarrow [Rare earth ion (RE) level] \longrightarrow [Emission]⁽¹⁰⁵⁾
- III. [Singlet(S_1)] \rightsquigarrow [Rare earth ion (RE) levels higher than (T_1)] \rightsquigarrow [Triplet (T_1)] \rightsquigarrow [Rare earth ion (RE) level lower than (T_1)] \longrightarrow [Emission]^(106a).

The weight of evidence in the literature is in favor of paths I and III and against path II.

B. Rate of Energy Transfer

Based upon experiments involving intermolecular energy transfer between benzophenone as a donor and rare-earth chelates as acceptors, a lower limit of 10^5 sec^{-1} for the rate was deduced by El-Sayed and Bhaumik^(106b). A maximum upper limit on the transfer would, of course, be 10^{12} to 10^{13} sec^{-1} which is the rate of vibrational

relaxation. If the energy transfer occurs from the singlet state, the transfer has to compete with the singlet-triplet intersystem crossing which is estimated to be $\sim 10^{11} \text{ sec}^{-1}$ in rare-earth complexes^(106c). If, as appears more probable, the mechanism is via the manifold of the triplet levels, a rate faster than 10^9 sec^{-1} is expected.

C. Mechanism of Transfer

The possibility of a pure Förster type mechanism seems doubtful because the necessary condition of spectral overlap of the emission of the complexed ligand and the absorption of the metal ion is not always fulfilled. The study of Eu(III) chelates, shows the efficiency of the energy transfer to be dependent on the nature of the ligand-metal bonds. A mechanism was suggested by Crosby et al.^(104a) in which a vibronic coupling of the electronic states of the rare-earth ion with those of the ligand passed through an exchange mechanism while preserving the total spin of the molecule. In the case of europium, as an example, $^5D + ^3T = ^7F + ^1S$.

Whenever the luminescence spectra observed from a series of lanthanide chelates are too weak or too complex to ensure accurate measurement of the phosphorescing (triplet) states, one can employ energy transfer as an aid in bracketing the energy of these states.

III. Europium Complex with Salicylidene-DL-Valinate Schiff Base

A. Introduction

In many enzymes a proton may assume a critical role in a chemical transformation at the active site, and a metal ion or metal complex may serve as a model enzyme by providing a positive center which promotes a similar function. Martell⁽¹⁰⁷⁾ called them model enzymes or "Artificial Enzymes". In the metal complex the metal ion may provide both the positive center and through its coordination requirements considerable stereospecificity. While the steric arrangements of donor groups around the metal ion as well as the intensity of metal-ligand interaction can be varied widely by changing the metal, one must expect the stereospecificity and adjacent group effects in the metal coordination sphere generally to differ widely from the stereospecificity of the enzymatic active site. Model studies have the advantage of allowing more complete study of structure-reactivity relationships and of achieving a better understanding of enzyme function than can be accomplished by studies of enzymes alone. The structure and reactivity of a model may be varied by the substitution of functional groups, charge of metal ion, and change in the structure of the substrates. Such variations are either not possible or limited when working with enzymes

themselves. The use of model systems in the study of complex enzymatic reactions is well known and particular interest has been shown in systems set up to explain the role of vitamin B₆ as a catalyst for some reactions involving amino-acid transformations. The reaction mechanisms of pyridoxal phosphate coenzymes have been the subject of intensive investigations^(108,109) and are now well documented as occurring through a Schiff base intermediate formed between the vitamin and the amine-containing substrate (normally an amino acid). It is also established that a metal is sometimes an additional cofactor in enzymatic catalysis by pyridoxal⁽¹¹⁰⁾ and that metals generally enhance the rate of some reactions even in the absence of enzyme⁽¹⁰⁷⁾. In this instance it has been proposed that the intermediate involves a coordination complex between the metal and the Schiff base. A general theory on the mechanism of these nonenzymatic reactions involves four stages:^(111,112) (1) Formation of a Schiff base with subsequent electron displacement from the α -carbon atom to the electronegative ring nitrogen through a conjugated system of double bonds, weakening of the bond to the α -carbon thus results. (2) Release of H⁺, COOH⁺ or R⁺ from the α -carbon to produce a transitional Schiff base. (3) Localization of the ring nitrogen lone pair of electrons onto the α -carbon for racemization and decarboxylation or onto the formyl carbon for transamination followed by protonation. (4) Hydrolysis of the

carbon-nitrogen bond to give products.

Pullman et al.⁽¹¹³⁾ showed that variation in resonance energy and electronic distribution among the possible transition states plays an important role in these catalytic reactions. Change in bond geometries is critical as well. x-ray-structure determination of two copper complexes with two Schiff bases (pyridoxal-valine and salicylaldehyde-valine) was studied⁽⁴¹⁾, Figure (62). In (pyridoxylidene-DL-valinato) copper(II) chelate, the molecule is centered on five-coordinate copper in square-pyramidal stereochemistry. The phenolic oxygen, imine nitrogen and carboxylate oxygen atoms of the tridentate Schiff base occupy three corners of the coordination square; the remaining in-plane positions being filled by the heterocyclic nitrogen of a neighboring molecule. Binding by the hydroxymethyl oxygen of yet another moiety in the fifth apical site completes the square-pyramid. In (salicylidene-DL-valinato) copper(II) chelate, the metal is four coordinated with planar geometry, one donor position being filled by a water molecule. The two chelate rings are somewhat more planar than in the pyridoxal complex although a tetrahedral distortion of about the same magnitude is still apparent in the arrangement of donors about the metal.

In aqueous media, Ln(III) ions form (1:2) complexes with N-hydroxyacetophenonevaline Schiff base⁽¹¹⁵⁾. The stability of these chelates follows the order: La(III) <

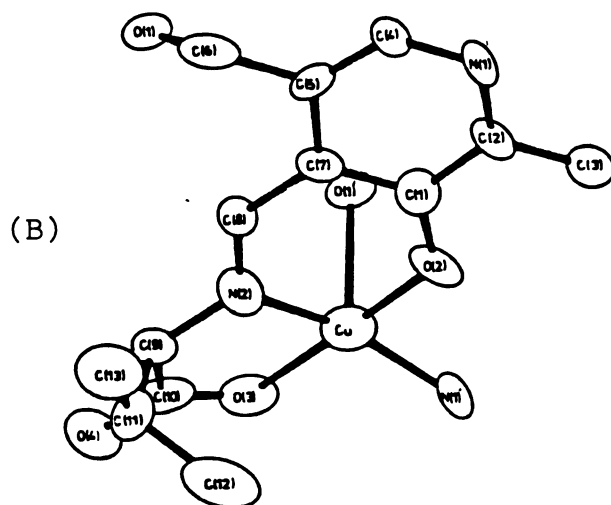
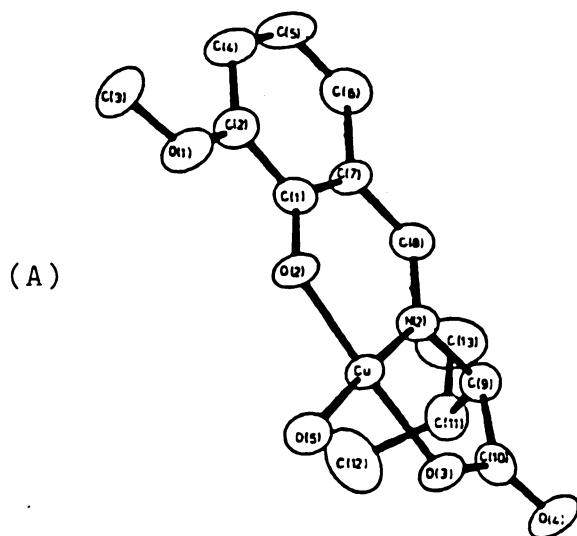


Figure 62. Diagram of Cu(II) complex with: (A) salicylaldehyde-valine Schiff base; (B) PLP-valine Schiff base.

Ce(III) < Pr(III) < Nd(III) < Sm(III) < Gd(III) < Tb(III) < Dy(III) < Ho(III), which is in agreement with lanthanide contraction.

We here prepared a solid europium chelate with salicylaldehyde Schiff base of DL-valine. The absorption and emission properties will be discussed in the following section.

B. Results and Discussion

Europium chelate with salicylidene-DL-valine Schiff base was characterized by elemental analysis, infrared and optical spectroscopy and its magnetic properties. Comparison of the infrared spectra of the complex with that of the pure ligand shows the following. The imine C=N (amide I) absorption which appears at 1635 cm^{-1} in the ligand⁽¹²⁾ was red shifted to 1600 cm^{-1} in the metal complex. The 1375 cm^{-1} symmetric stretching absorption band of the -COO^- group in the ligand was red shifted to 1350 cm^{-1} in the complex. The 1225 cm^{-1} phenolic C-O stretching of the ligand appears at 1215 cm^{-1} in the complex. The presence of broad water absorption bands prevented observation of bands in the neighborhood of 3000 cm^{-1} . In a recent study⁽¹¹⁴⁾ of the x-ray structure of a (1:1) complex of salicylene-DL-valine with Cu(II), it was shown that the Schiff base acts as a tridentate ligand through its phenolate and carboxylate oxygen atoms and

its azomethine nitrogen. The planar geometry of the complex with one water molecule filling the fourth position shows that the two chelating rings in the tridentate ligand are somewhat planar. Someone has to keep in mind that Cu(II) may force the planar configuration of the ligand through its complexation. We were not successful in preparing good crystals for x-ray measurements of the prepared chelate; however, according to our infrared and elemental analysis results as well as considering the chelating nature of our ligand, we can safely propose an octahedral structure, Figure (63) (meridian isomer) for our complex. The complex contains two water molecules. The magnetic behavior of the complex at low temperatures showed temperature-independent paramagnetism characteristic of Eu(III) rather than Eu(II)⁽¹¹⁶⁾. Figure (64) displays a plot of the reciprocal of the molar magnetic susceptibility ($1/\chi_M$) vs $T^\circ\text{K}$. At temperatures higher than 100°K , χ_M follows Curie-Weiss law ($\chi_M = C_M (T + \theta)^{-1}$); C_M and θ are constants. The slope of the obtained straight line equals $1/C_M$, accordingly $C_M = 2.375$. Since $\mu_{\text{eff}} = 2.837\sqrt{c}$; μ_{eff} for our complex equal to 4.37 B.M., a value of 3.53 B.M. is reported for Eu_2O_3 ⁽¹¹⁷⁾. Below 100°K , Van Vleck paramagnetism⁽¹¹⁶⁾, temperature-independent paramagnetism, was observed. Eu(III) has $4f^6$ configuration with 7F_0 ground state. Although the 7F multiplet width for Eu(III) is 5360 cm^{-1} ; the value of the interval between the two lowest components 7F_0 and 7F_1 is $5360/21 = 255\text{ cm}^{-1}$. At room temperature $kT \sim 200\text{ cm}^{-1}$,

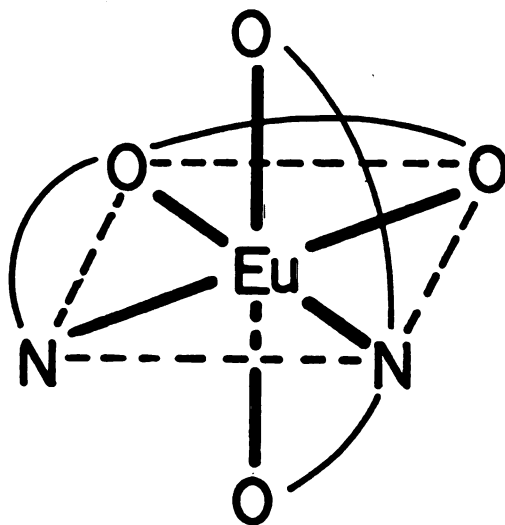
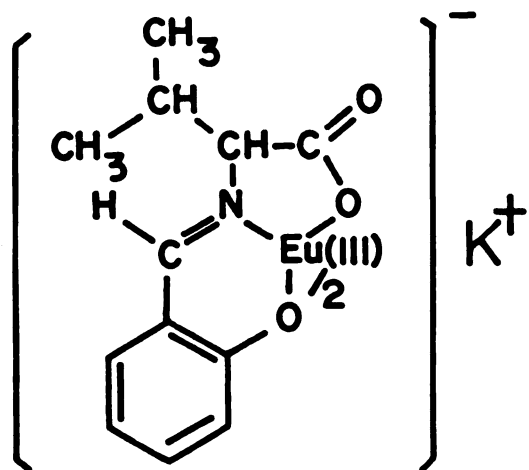


Figure 63. $K[Eu(C_{12}H_{13}NO_3)_2]$.

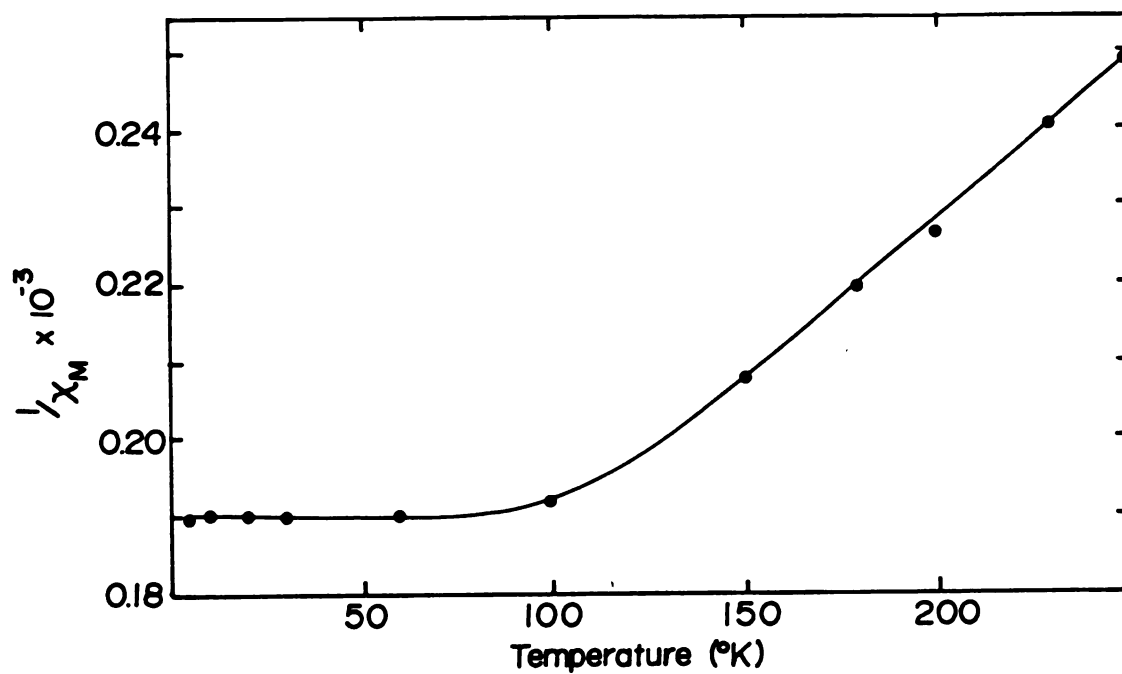


Figure 64. Magnetic behavior of $K[Eu(C_{12}H_{13}NO_3)_2]$ complex.

i.e., the transition (${}^7F_0 \rightarrow {}^7F_1$) $h\nu \approx kT$, resulting in an appreciable population of low-lying excited states which contribute to the paramagnetism at low temperatures.

Room temperature absorption spectra of the Eu-complex in ethanol and in DMSO are shown in Figure (65). The absorption band at ~ 350 nm ($28,500 \text{ cm}^{-1}$) with molar absorptivity ($\epsilon = 11,000$) corresponds to a transition to a charge-transfer state within the coordinated ligand. Similar absorption band at 350 nm was observed in the spectra of the ligand in acidic medium which is again a good clue for the involvement of the azomethine nitrogen in chelation. In metal chelates of these model Schiff bases, it is well known⁽¹¹⁸⁾, that coordination through the azomethine nitrogen produces an absorption band around 365 nm. No absorption bands due to f-f transitions were observed because of their very low molar absorptivity ($\epsilon \geq 3$)⁽¹¹⁹⁾.

Figure (66) shows the emission spectra of the Eu complex in ethanol and DMSO at room temperature and in ethanol at 77°K. The emission at 450 nm ($22,200 \text{ cm}^{-1}$) is assigned to a fluorescence from the coordinated ligand at room temperature in both solvents. The ≈ 610 nm ($16,400 \text{ cm}^{-1}$) narrow fluorescence is assigned to an f-f transition within the metal ion. Usually the transition ${}^5D_0 - {}^7F_2$ at $\approx 16,340 \text{ cm}^{-1}$ is very intense in europium chelates and its fine structure has received considerable attention^(120, 121). Salicylaldehyde Schiff bases chelate with Zn(II)

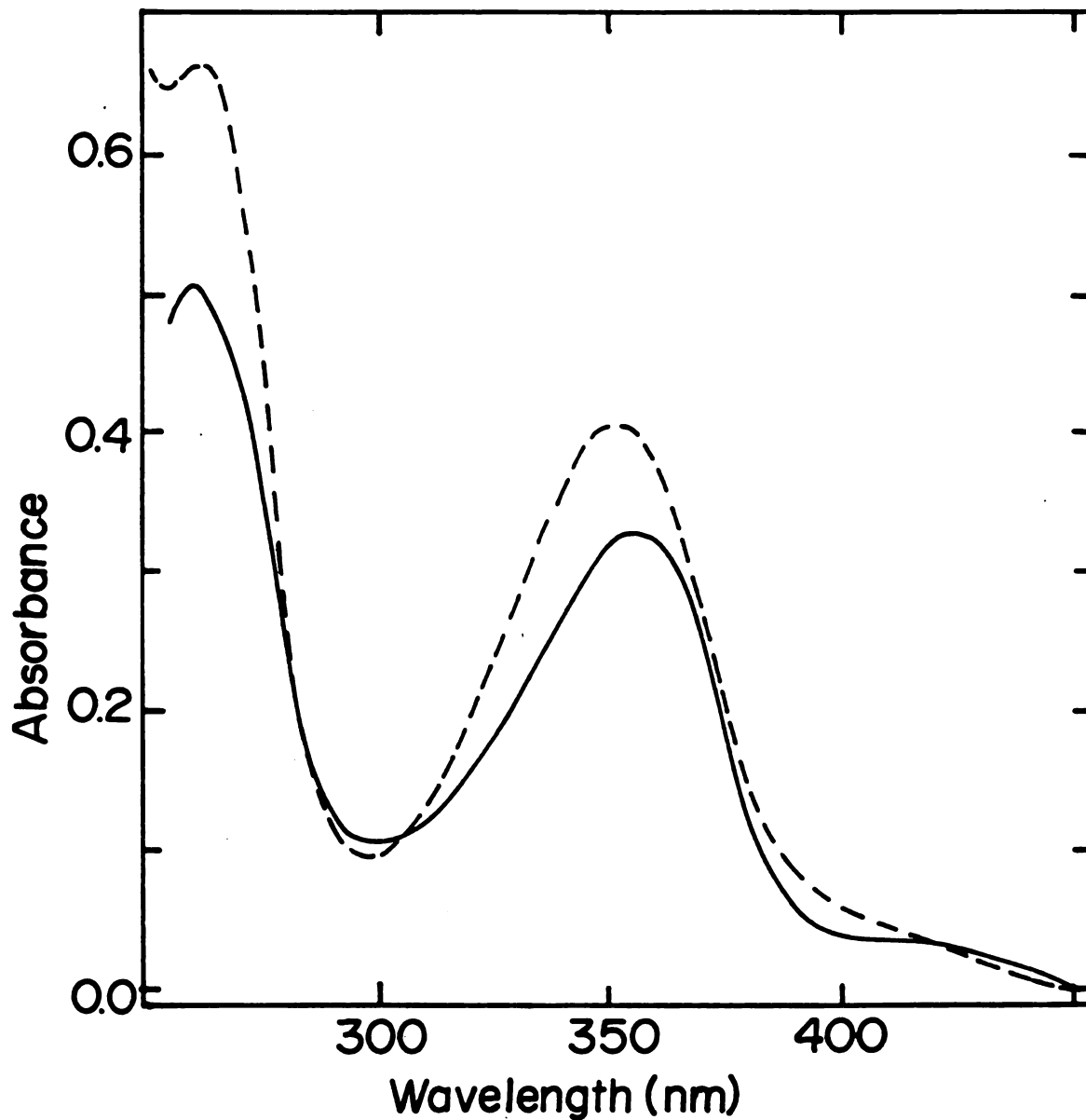


Figure 65. Absorption spectra of dilute solution (3×10^{-5} M) of $K[Eu(C_{12}H_{13}NO_3)_2]$ in ethanol (----) and DMSO (—).

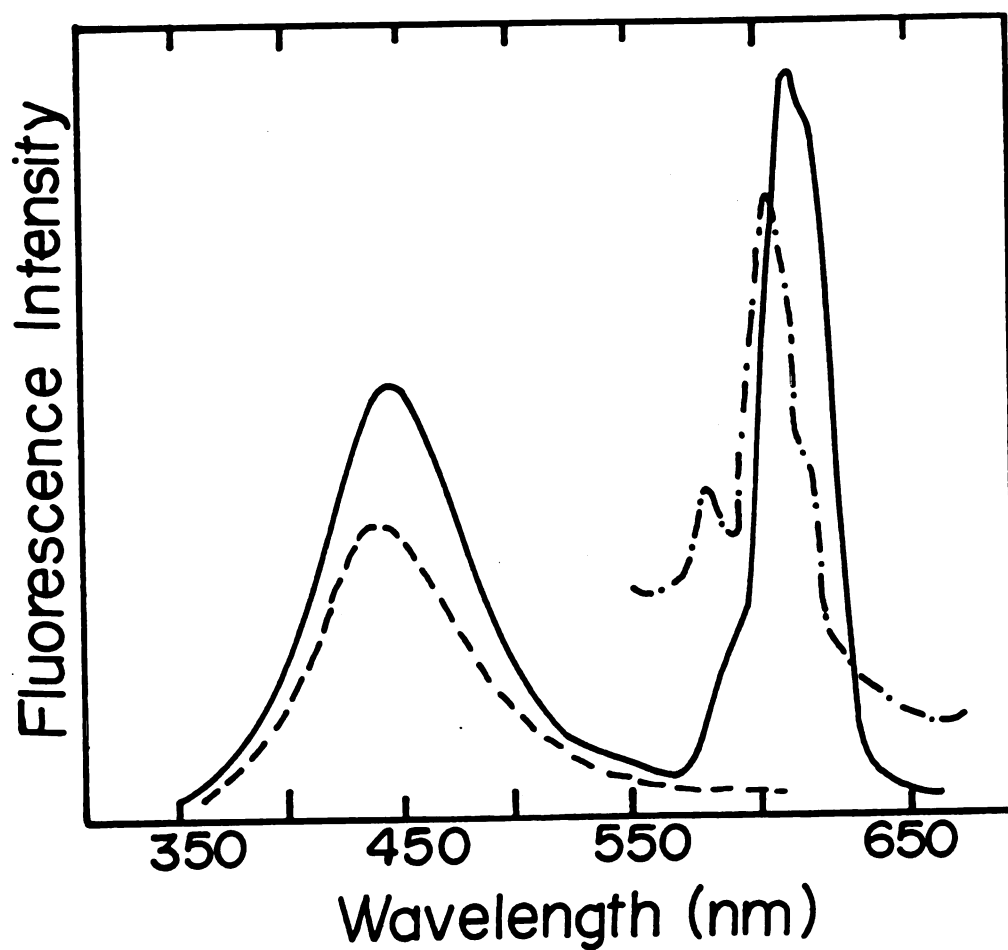


Figure 66. Emission spectra of dilute solutions (3×10^{-5} M) of $\text{K}[\text{Eu}(\text{C}_{12}\text{H}_{13}\text{NO}_3)_2]$ in ethanol at room temperature (----), ethanol at 77°C (-.-.-), and DMSO at room temperature (—).

and phosphoresces around ($20,500 \text{ cm}^{-1}$) which corresponds to the energy of the lowest triplet state⁽¹²²⁾ in these chelates. In Figure (67) we constructed an energy level diagram which shows the important radiative and radiationless transitions within the complex. Intramolecular energy transfer occurs from the ligand lowest triplet (as an energy donor) to the 5D_1 or 5D_0 of the metal (as an energy acceptor) followed by radiative transition (fluorescence) to the 7F . Two necessary conditions are required for sharp fluorescence from the rare-earth chelates through indirect excitation of the rare-earth ion via energy transfer mechanism: (1) at least one acceptor level should lie below the lowest triplet (donor) level of the isolated ligand, (2) the lifetime of triplet state should not be too short to achieve a good inversion and not too long to retain the inversion while waiting for the action to commence.

In water, the metal complex is completely hydrolyzed to give both absorption and emission spectra characteristic of the free ligand. In DMSO, DMF, and acetonitrile red emission from the metal ion was observed at room temperature; whereas, in ethanol this emission was only observed at 77°K . This can be due to the difference in the stability of the metal chelate in these solvents. In highly coordinating solvents DMSO, DMF, and acetonitrile, the complex is more stable, may be through solvent coordination which increases the coordination number to 8 or 9.

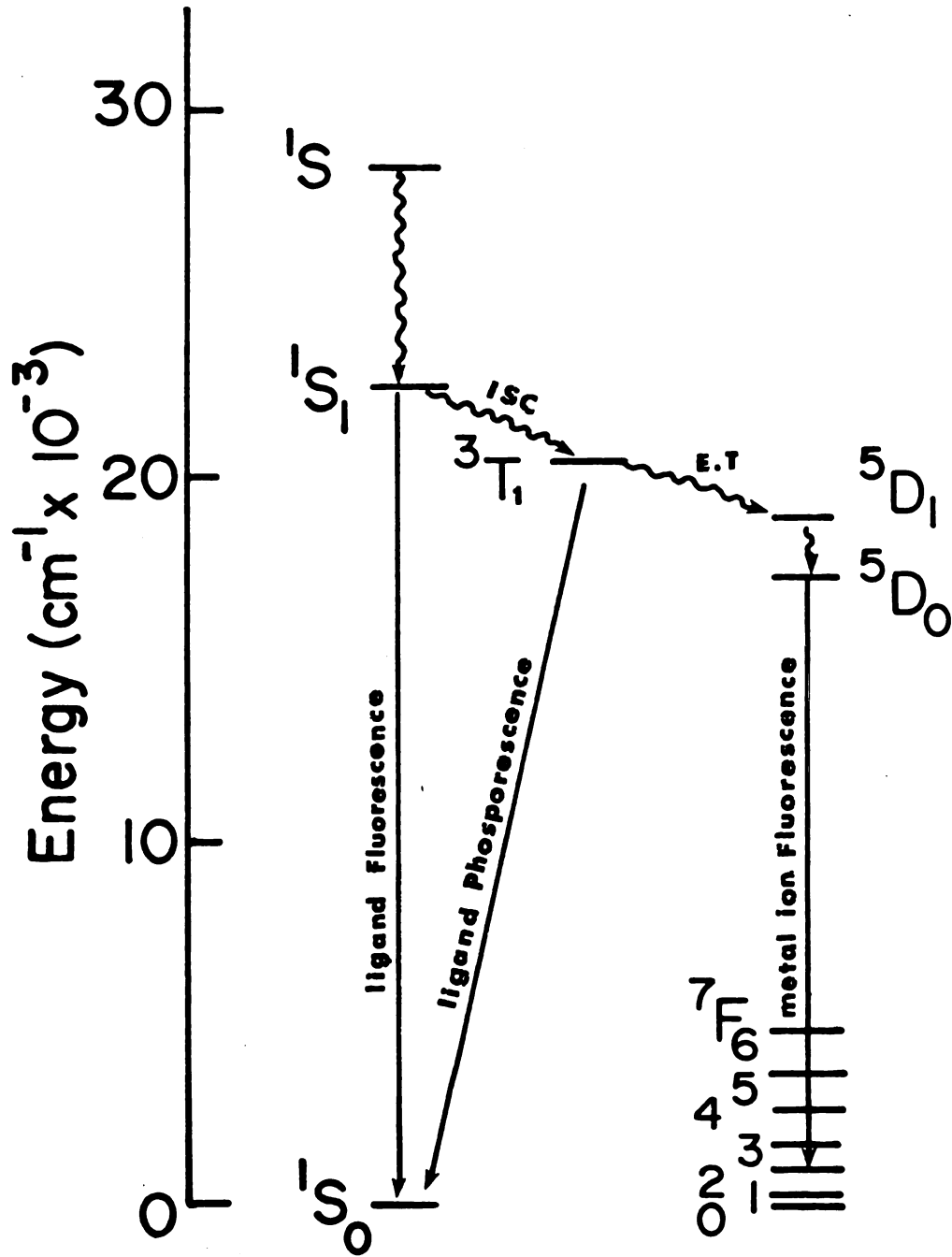


Figure 67. Energy level diagram for $K[Eu(C_{12}H_{13}NO_3)_2]$.

CHAPTER VI

CONCLUSION AND FUTURE WORK

In the carbonyl compounds, the emission spectra showed an excited state proton transfer. No ground state proton transfer occurs in these compounds as evidenced by their absorption spectra. Both ground-state and excited-state proton transfer were observed in salicylaldehyde Schiff base derivatives with n-butylamine and valine. Depending on the solvent, intramolecular or intermolecular proton transfer was observed. In nonpolar solvents, e.g., 3MP, intramolecular proton transfer occurred whereas, in polar solvents, intermolecular proton transfer to or from solvent molecules was observed. Such observation demonstrates the higher basicity of the azomethine nitrogen compared with the carbonyl oxygen in the ground state, and the enhanced basicity of both functional groups in the excited state.

Salicylaldehyde anion interacts strongly with some monovalent cations resulting in the formation of chelated-type complexes. Salts of para-substituted phenols form contact ion-pairs and solvent-separated pairs depending on the solvent and on the presence of crown ether molecules. The spectral blue shift observed by decreasing the cationic

radius indicate stronger interactions between the ions forming the ion pair and may be a factor in determining which cation is a better enzyme activator. Evidence for excited-state dissociation of ion pairs was given. The formation of these ion pairs may play a key role in the function of monovalent cations as activators of some PLP-enzymes.

The use of lanthanide ions as probes in biological systems is becoming increasingly important. Lanthanide ions, especially Eu(III) and Tb(III), are used extensively to probe the microenvironment at the active site and to measure the distances between the different binding sites in enzymes such as thermolysin. We have prepared a Eu(III) chelate with a Schiff base model compound. We have studied its magnetic and optical properties. The complex is more likely to have an octahedral configuration. Our demonstration of energy transfer resulting in a red emission at 610 nm offers new opportunities in probing the active site of PLP-enzymes.

Future work in this area is very important. Thus, time-resolved picosecond studies will undoubtedly help in identifying excited-state species resulting from proton transfer. The study of sterically hindered model compounds, which are expected to have slower rates of proton transfer (higher energy barrier), is particularly interesting. More attention should be given to the study of possible conformers that may exist in equilibrium in the ground state of a particular species.

The use of luminescence techniques offer a unique opportunity to study ion-pair association in the excited state. Our study opens the door for an extensive study of ion-association where one of the ions has convenient emission properties, e.g. fluorenyl anion. The study of time-resolved spectra of ion pairs is very interesting and important in order to obtain rate constants of excited-state sodium ion or potassium ion transfer.

Moreover, the study of the interaction of tryptophanase holoenzyme (tryptophanase-PLP) with Eu(III) is an obviously important experiment to measure distances between tryptophenyl residues and the active site. An experiment where a tunable dye laser is used as an exciting source to monitor the excitation spectrum of Eu(III) emission and lifetime measurements in the microsecond range of the holoenzyme in aqueous media and in the presence of D_2O provide unique information regarding the microscopic environment (water presence) at the active site. The use of other lanthanide ions such as Tb(III) should also be explored.

REFERENCES

REFERENCES

1. H. Sherman, et al. Pyridoxine and related compounds, in "The Vitamins," Vol. III, Chap. 14, W. H. Sebrell, Jr., and R. S. Harris (eds.), Academic, New York (1954).
2. S.A. Hoch and R.D. DeMoss, J. Bacteriol., 114, 341 (1973).
3. H. Wada, Tryptophan Metabolism, Vol. I, Sekai Hoken Tsushinsha (ed.), Ltd., Osaka, Japan (1964), p. 77-92.
4. F. C. Happold, and A. Struyvenberg, Biochem. J., 58, 379 (1954).
5. Y. Morino and E. E. Snell, J. Biol. Chem., 242, 2800 (1967).
6. D. S. June, et al., J. Am. Chem. Soc., 101, 2218 (1979).
7. D. S. June, C. H. Suelter, and J. L. Dye, Biochem., 20, 2707 (1981).
8. R. J. Johnson and D. E. Metzler "Methods in Enzymology", D. B. McCormick and L. D. Wright (eds.), Vol. 18, pt. A, p. 433-471, Academic Press, New York (1970).
9. H. C. Dunathan, Proc. Natl. Acad. Sci. U.S.A., 55, 712 (1966).
10. R. B. Martin and F. S. Richardson, Q. Rev. Biophys., 12, 181 (1979).
11. W. De W. Horrocks, Jr., and D. R. Sudnick, Acc. Chem. Res., 14, 384 (1981).
12. D. Heinert and A. E. Martell, J. Am. Chem. Soc., 84, 3257 (1962).
13. F. Maggio, T. Pizzino, V. Romano and R. Zingales, Inorg. Nucl. Chem. Lett., 14, 149 (1978).
14. H. E. Zaugg and A. D. Schaefer, J. Am. Chem. Soc., 87, 1857 (1965).

15. N. S. Potts, J. Chem. Phys., 20, 809 (1952).
16. Alberchet and W. T. Simpson, J. Chem. Phys., 23, 1480 (1955).
17. Watanabe, J. Chem. Phys., 22, 1564 (1954).
18. B. M. Wepster, Rev. Trav. Chim., 76, 333 (1957), 77, 491 (1958).
19. J. N. Murrell, The Theory of the Electronic Spectra of Organic Molecules (Methuen, London), (1963).
20. E. A. Braude and F. Sondheimer, J. Chem. Soc., 3754 (1955).
21. E. E. Snell, P. M. Fasella, A. E. Braunstein and Rossi-Fanelli (ed.), "Chemical and Biochemical Aspects of Pyridoxal Catalysis", MacMillan, New York, NY (1963).
22. D. Heinert and A. E. Martell, J. Am. Chem. Soc., 85, 188 (1963).
23. R. J. Johnson and D. E. Metzler, "Methods in Enzymology", Vol. 18, Pt. A, ed. by D. B. McCormick and L. D. Wright, Academic Press, New York, NY (1970) pp. 433-471.
24. W. Barton, P. J. Luechest and N. S. Snider, J. Am. Chem. Soc., 84, 1842 (1962).
25. A. Weller, Z. Physik. Chem. (Frankfurt), 17, 224 (1958).
26. Y. Matsushima and A. E. Martell, J. Am. Chem. Soc., 89, 1322 (1967).
27. J. Llor and M. Cortijo, J. Chem. Soc., Perkin Trans. II, 119, 1111 (1977).
28. S. Shaltiel and M. Cortijo, Biochem. Biophys. Res. Commun., 41, 594 (1970).
29. A. B. Kent, E. G. Krebs and E. H. Fischer, J. Biol. Chem., 232, 549 (1958).
30. M. Cortijo, I. Z. Steinberg and S. Shaltiel, J. Biol. Chem., 246, 933 (1971).
31. S. Shaltiel and E. H. Fischer, Isr. J. Chem., 5, 127 p (1967).

32. M. Arrio Duport, Biochem. Biophys. Res. Commun., 44, 653 (1971).
33. S. Veinberg, S. Shaltiel and I. Steinberg, Isr. J. Chem., 12, 421 (1974).
34. F. D. Dwyer and D. P. Mellor in "Chelating Agents and Metal Chelates, Academic Press, New York (1964) pp. 335.
35. E. E. Snell, Adv. Enzymol. Relat. Areas Mol. Biol., 42, 287 (1975).
36. W. A. Newton, Y. Morino and E. E. Snell, J. Biol. Chem., 240, 1211 (1965).
37. Y. Morino and E. Snell, J. Biol. Chem., 242, 5591 (1967).
38. N. Bjerrum, Kgt. danske Vidensk. Selsk., 7, 9 (1926).
39. R. M. Fuoss and C. A. Kraus, J. Am. Chem. Soc., 55, 476 (1933).
40. T. R. Griffiths and M. C. R. Symons, Mol. Phys., 3, 90 (1960).
41. H. V. Carter, B. J. McClelland, and E. Warhurst, Trans. Faraday Soc., 56, 455 (1960).
42. T. E. Hogen Esch and J. Smid, J. Am. Chem. Soc., 87, 669 (1965); 88, 307, 318 (1966).
43. R. Waack and M. A. Doran, J. Phys. Chem., 67, 148 (1963); J. Am. Chem. Soc., 85, 1651 (1963).
44. Ralph S. Becker, "Theory and Interpretation of Fluorescence and Phosphorescence", Wiley, New York, NY (1969), pp. 30.
45. E. M. Kosower and P. E. Klinedinst, Jr., J. Am. Chem. Soc., 78, 3493 (1956).
46. J. Smid in "Ions and Ion-Pairs in Organic Reactions", M. Szwarc ed. Wiley, New York, NY (1972).
47. T. L. Chan and J. Smid, J. Am. Chem. Soc. 90, 4654 (1968).
48. T. Shimomura, K. J. Tolle, J. Smid and M. Szwarc, J. Am. Chem. Soc., 89, 796 (1967).

49. T. Shimomura, J. Smid and M. Szwarc, J. Am. Chem. Soc., 89, 5743 (1967).
50. S. Claesson, B. Lundgren and M. Szwarc, Trans. Faraday Soc., 66, 3053 (1970).
51. W. S. LeNoble and A. R. Das, J. Phys. Chem., 74, 3429 (1970).
52. (a) M. Shinohara, J. Smid and M. Szwarc, J. Am. Chem. Soc., 90, 2175 (1968).
(b) M. Shinohara, J. Smid, and M. Szwarc, Chem. Comm., London, 1962, 1232.
53. (a) C. J. Pedersen, J. Am. Chem. Soc., 89, 7017 (1967).
(b) C. J. Pedersen, J. Am. Chem. Soc., 92, 391 (1970).
54. K. H. Wong, G. Konizer, and J. Smid, J. Am. Chem. Soc., 92, 666 (1970).
55. J. J. Christensen, D. J. Eatough and R. M. Izatt, Chem. Rev., 74, 351 (1974).
56. R. M. Izatt, R. E. Terry, B. L. Haymore, L. D. Hansen, N. Dalley, A. G. Avondet and J. J. Christensen, J. Am. Chem. Soc., 98, 7620 (1976).
57. (a) G. W. Liesegang, M. M. Farrow, N. Purdie and E. M. Eyring, J. Am. Chem. Soc., 98, 6905 (1976).
(b) G. W. Liesegang, M. M. Farrow, F. A. Vazquez, N. Purdie, and M. Eyring, J. Am. Chem. Soc., 99, 3240 (1977).
58. T. E. Hogen Esch and J. Smid, J. Am. Chem. Soc., 91, 4580 (1969).
59. J. P. Pascault, Thesis, l'Universite de Lyon, France, 1970.
60. (a) W. F. Edgell, A. T. Watts, J. Lyford and W. M. Risen, J. Am. Chem. Soc., 88, 1815 (1966).
(b) W. F. Edgell, J. Lyford, R. Wright, W. M. Risen and R. Watts, J. Am. Chem. Soc., 92, 2240 (1970).
61. J. C. Evans and G. Y-S. Lo, J. Phys. Chem., 69, 3223 (1965).

62. (a) B. W. Maxey and A. I. Popov, J. Am. Chem. Soc., 89, 2230 (1967).
(b) B. W. Maxey and A. I. Popov, J. Am. Chem. Soc. 91, 20 (1969).
63. (a) A. Tsatsas, W. M. Risen, J. Am. Chem. Soc., 92, 1789 (1970).
(b) A. Tsatsas, R. W. Stearns, and W. M. Risen, J. Am. Chem. Soc., 94, 5247 (1972).
64. M. C. R. Symons, Pure and Appl. Chem., 49, 13 (1977).
65. (a) M. C. R. Symons, J. Phys. Chem., 71, 172 (1967)
(b) H. Sharp and M. C. R. Symons, Ions and Ion-pairs in Organic Reactions, M. Szwarc, Ed., Wiley, New York, NY (1972).
(c) E. de Boer and E. Sommerdisk, Ions and Ion-pairs in Organic Reactions, M. Szwarc, Ed., Wiley, New York, NY (1972).
66. F. C. Adam and S. I. Weissman, J. Am. Chem. Soc., 80, 1518 (1958).
67. N. M. Atherton, and S. I. Weissman, J. Am. Chem. Soc., 83, 1330 (1961).
68. P. J. Zandstra, and S. I. Weissman, J. Am. Chem. Soc. 84, 4408 (1962).
69. W. G. Williams, P. J. Pritchett and G. K. Fraenkel, J. Chem. Phys., 52, 5584 (1970).
70. N. Hirota, J. Am. Chem. Soc., 90, 3603 (1968).
71. K. Nakamura and Y. Deguchi, Bull. Chem. Soc. Japan, 40, 705 (1967).
72. A. W. Rutter and E. Warhust, Trans. Faraday Soc., 66, 1866 (1970).
73. E. S. Amis and J. F. Hinton, "Solvent Effect on Chemical Phenomena", Vol. I, Academic Press, New York (1973) pp. 150-164.
74. E. G. Bloor and R. G. Kidd, Canad. J. Chem., 46, 3425 (1968).
75. R. H. Erlich, E. Roach and A. I. Popov, J. Am. Chem. Soc., 92, 4989 (1970).

76. R. H. Erlich and A. I. Popov, J. Am. Chem. Soc., 93, 5620 (1971).
77. M. S. Greenberg, R. L. Bender and A. I. Popov, J. Am. Chem. Soc., 77, 2449 (1973).
78. G. E. Maciel, J. K. Hancock, L. F. Lafferty, P. A. Mueller and W. K. Musker, Inorg. Chem., 5, 554 (1966).
79. J. W. Akitt and A. S. Downs in "The Alkali Metals Symposium", The Chemical Society London (1967) p. 199.
80. M. Y. Cahen, P. R. Handy, E. T. Roach and A. I. Popov, J. Chem. Phys., 79, 80 (1975).
81. H. J. Maria and S. P. McGlynn, J. Chem. Phys., 52, 3399 (1970).
82. T. P. Carter and G. D. Gillispie, Chem. Phys. Letters, 73, 75 (1980).
83. E. Nieboer, Struct. and Bond., 22, 1-47 (1975).
84. R. Prados, L. G. Stradtherr, H. Donato, Jr. and R. B. Martin, J. Inorg. Nucl. Chem., 36, 689 (1974).
85. R. D. Shannon, Acta Crystallogr., A32, 751 (1976).
86. (a) R. H. Kretsinger and C. E. Nockolds, J. Biol. Chem., 248, 3313 (1973).
(b) B. W. Matthews and L. H. Weaver, Biochemistry, 13, 1719 (1974).
87. K. Hermsmeyer and N. Sperelakis, Am. J. Physiol., 219, 1108 (1970).
88. N. Sperelakis, M. F. Schneider and E. J. Harris, J. Gen. Physiol., 50, 1563 (1967).
89. (a) F. Abbott, D. W. Darnall and E. R. Birnbaum, Biochem. Biophys. Res. Commun., 65, 241 (1975).
(b) F. Abbott, J. E. Gomez, E. R. Birnbaum and D. W. Darnall, Biochemistry, 14, 4935 (1975).
90. T. Forster, Disc. Farad. Soc., 27, 7 (1959).
91. De W. Williams, Horrocks, Jr. and W. E. Collier, J. Am. Chem. Soc., 103, 2856 (1981).

92. W. D. Horrocks, Jr., G. F. Schmidt, D. R. Sudnick, C. Kittrell and R. A. Bernhein, J. Am. Chem. Soc., 99, 2378 (1977).
93. G. Stein and E. Wurzburg, J. Chem. Phys., 62, 208 (1975).
94. J. L. Kropp and M. W. Windsor, J. Chem. Phys., 39, 2769 (1963).
95. J. P. Freeman, G. H. Crosby, and K. E. Lawson, J. Mol. Spectrosc., 13, 399 (1964).
96. Y. Haas, G. Stein, and E. Wurzburg, J. Chem. Phys., 58, 2777 (1973).
97. (a) J. L. Kropp and M. W. Windsor, J. Chem. Phys., 42, 1599 (1965).
(b) J. L. Kropp and M. W. Windsor, J. Chem. Phys., 39, 2769 (1963).
(c) J. L. Kropp and M. W. Windsor, J. Chem. Phys., 45, 761 (1966).
98. (a) W. De W. Horrocks, Jr., D. R. Sudnick, J. Am. Chem. Soc., 101, 334 (1979).
(b) W. De W. Horrocks, Jr., D. R. Sudnick, Science Washington, D.C.
99. T. Forster, Ann. Phys., 2, 55 (1948).
100. C. F. Meares and J. E. Ledbetter, Biochemistry, 16, 5178 (1977).
101. E. T. O'Keefe, R. L. Hill and J. E. Bell, Biochemistry, 19, 4954 (1980).
102. S. I. Weissman, J. Chem. Phys., 10, 214 (1942).
103. R. E. Whan and G. A. Crosby, J. Mol. Spectry., 8, 315 (1962).
104. (a) G. A. Crosby, R. E. Whan and R. M. Alire, J. Chem. Phys., 34, 743 (1961).
(b) G. A. Crosby and R. E. Whan, J. Chem. Phys., 32, 614 (1960).
(c) G. A. Crosby and R. E. Whan, Naturwiss., 47, 276 (1960).
(d) G. A. Crosby, Molecular Crystals, I, 37 (1966).

104. (e) G. A. Crosby, R. E. Whan and J. J. Freeman, J. Phys. Chem., 66, 2493 (1962).
105. M. Kleinerman, Bull. Am. Phys. Soc., 9, 265 (1964).
106. (a) M. L. Bhaumik and M. A. El-Sayed, J. Chem. Phys., 42, 787 (1965).
(b) M. A. El-Sayed and M. L. Bhaumik, J. Chem. Phys., 39, 2391 (1963).
(c) M. L. Bhaumik and M. A. El-Sayed, Appl. Opt. Supp. 2, 214 (1965).
107. A. E. Martell, "Metal Ions in Biological Systems", Vol. 2, H. Sigel, ed., M. Dekker, NY (1973), p. 207.
108. A. E. Braunstein, "The Enzymes", Vol. 2, P. Boyer, H. Lardy and K. Myrback (eds.), Academic Press, New York (1960).
109. W. H. Sebrell, Jr., and R. S. Harris (eds.), "The Vitamins", Vol. 2, Academic Press, New York (1968).
110. B. M. Guirard and E. E. Snell, J. Am. Chem. Soc., 76, 4745 (1954).
111. D. E. Metzler, M. Ikawa and E. E. Snell, J. Am. Chem. Soc., 76, 648 (1954).
112. M. Ikawa and E. E. Snell, J. Am. Chem. Soc., 76, 393 (1954).
113. A. Perault, B. Pullman and C. Valdemoro, Biochim. Biophys. Acta, 46, 555 (1961).
114. H. M. Dawes, J. M. Waters and T. N. Waters, Inorganic Chimica Acta, 66, 29 (1982).
115. R. S. Shekhawat, N. K. Sankhla and R. K. Metha, Polish Journal of Chemistry, 54, 391 (1980).
116. J. H. Van Vleck, "The Theory of Electric and Magnetic Susceptibilities", Oxford Univ. Press (1932), pp. 226-261.
117. Cabera and Duperier, Compets Rendus, 88, 1640 (1929).
118. S. Matsumoto and Y. Matsushima, J. Am. Chem. Soc., 96, 5228 (1974).
119. C. V. Banks and D. W. Klingman, Anal. Chim. Acta, 15, 356 (1956).

120. M. L. Bhaumik, J. Mol. Spectrus. 11, 323 (1963).
121. L. J. Nugent, M. L. Bhaumik, S. George and S. M. Lee, J. Chem. Phy., 41, 1305 (1964).
122. M. I. Knyazhanskii and P. v. Gilyanovskii, Opt. Spektrosk, 35, 1083 (1973).